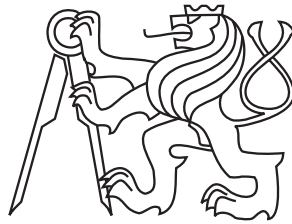


CZECH TECHNICAL UNIVERSITY IN PRAGUE

Faculty of Civil Engineering
Department of Mechanics



DOCTORAL THESIS

Dynamic Analysis of Grandstands

Author:

Ondřej ROKOŠ

Supervisor:

prof. Ing. Jiří MÁČA, CSc.

Supervisor specialist:

doc. RNDr. Petr KUČERA, CSc.

*A thesis submitted in fulfilment of the requirements
for the degree of Doctor of Philosophy*

May 2014

To my parents...

Declaration by Candidate

I, Ondřej ROKOŠ, declare that this thesis titled "Dynamic Analysis of Grandstands" and the work presented in it are my own. I confirm that:

- This work was done wholly or mainly while in candidature for a research degree at this University.
- Where any part of this thesis has previously been submitted for a degree or any other qualification at this University or any other institution, this has been clearly stated.
- Where I have quoted from the work of others, the source is always given.
- I have acknowledged all main sources of help.

In Prague, May 2014

Signature:

Contents

List of Figures	xi
List of Tables	xv
Acknowledgments	xvii
Abstract	xix
Notation	xxiii
Introduction	1
1 State of the Art	3
1.1 European and Czech standards	3
1.1.1 Load and structure assessment	3
1.1.2 Human exposure to vibrations	4
1.2 Other standards and recent research papers	6
1.2.1 Load models for human-induced vibrations	6
1.2.2 Passive crowd models	7
1.2.3 Measures of the structure response	8
2 Objectives of the thesis	9
3 Monte Carlo Simulation	13
3.1 Introduction	13
3.2 Forcing terms	14
3.3 Biodynamic models	15
3.4 Computational aspects	16
3.4.1 FEM discretization	16
3.4.2 Reduced-order modelling	19
3.4.2.1 Modal superposition	20
3.4.2.2 Krylov subspace projection	20
3.4.2.3 Proper orthogonal decomposition	21
3.4.2.4 Modal synthesis	21
3.5 Spatial crowd distribution	22
3.5.1 Random distribution of an active crowd	23
3.5.2 Mean-worst spatial distribution of an active crowd	23

3.6	MC convergence analysis	25
3.7	Conclusion	27
4	Deterministic system and stochastic input	29
4.1	Introduction	29
4.2	Gaussian input	29
4.2.1	Deterministic distribution of a crowd	30
4.2.1.1	Solution in the time domain	30
4.2.1.2	Solution in the frequency domain	32
4.2.1.3	Reduced-order modelling	32
4.2.1.4	Performance of the Gaussian processes	33
4.2.1.5	Applications to the response of grandstands	34
4.2.2	Random distribution of an active crowd	42
4.3	Non-Gaussian input	50
4.3.1	Translation processes	50
4.3.1.1	Approximation of the input	50
4.3.1.2	System response	54
4.3.1.3	Upcrossing estimates	56
4.3.2	Poisson white noise process	58
4.3.3	Frequency domain solution	60
4.3.4	Other non-Gaussian inputs	61
4.4	Conclusion	62
5	Random parameters of a passive crowd	65
5.1	Introduction	65
5.2	Sensitivity analysis	65
5.3	Deterministic distribution of a passive crowd	68
5.3.1	Taylor series method	68
5.4	Random distribution of a passive crowd	70
5.5	Conclusion	73
6	Stochastic system and input	75
6.1	Introduction	75
6.2	Random distribution of a crowd	75
6.3	Conclusion	79
7	Conclusion and future prospects	81
Appendix A Fractions of the probability theory		85
A.1	Basic concepts	85
A.2	Stochastic processes	85
A.3	Itô's formula and stochastic differential equations	87
Appendix B MATLAB implementation		89
B.1	General overview	89
B.2	MC simulation	90

B.3 Moment equations	90
Appendix C Description of toy structures used	91
C.1 Simply supported beam	91
C.2 Cantilever grandstand	92
C.3 Real grandstand	93
Bibliography	97
Index	101

List of Figures

1.1	Frequency weighting curves in ISO 2631-1	5
3.1	Flow-chart of MC simulation	13
3.2	Three characteristic pulse shapes after Sim [51], (a) double peaked, (b) merging, (c) single peaked	14
3.3	Typical realizations of single, weight normalized jumping processes according to Sim [51]	15
3.4	Scheme of a discrete uni-axial biodynamic model with physical meaning of individual parameters	16
3.5	Mass and stiffness matrices of the real grandstand in Appendix C.3, nz being a number of nonzero elements	19
3.6	Spectrum of the cantilever and real grandstand, the case of empty and fully occupied structures with a passive crowd; biodynamic models according to Coermann used	20
3.7	Response of the P_1 node and relative error as a function of the subspace dimension $\dim(\mathcal{V}) = k$	22
3.8	Bode plot of the FRF for $k = \dim(\mathcal{V}) = 50$ and relative error for example in Appendix C.3	23
3.9	Two mean-worst spatial distributions of an active crowd, Fourier coefficients after Ellis [15], with respect to peak displacement and acceleration	26
3.10	MC convergence for $n_x^+(T)$ and RMS; fixed and random spatial distribution of a crowd	26
4.1	Single time history and power spectral density of 10,000 realizations of forcing term $Y(t)$ generated according to [51]	34
4.2	Single centered time history of $\tilde{Y}(t)$ (a), the corresponding power spectral density of 10,000 realizations (b), a normalized histogram with standard normal density (c) and a normalized histogram of a non-unit process scaled with G [kN] $\sim \mathcal{N}(0.7709, 0.0167)$ (d), variance $\text{var}Y(t)$ (e) and mean value $\text{E}Y(t)$ (f)	36
4.3	Coefficient of skewness γ_3 and coefficient of kurtosis γ_4 for the normalized displacement and velocity of the harmonic oscillator forced by the jumping process as functions of eigenfrequency f_1 . Blue – viscous damping $\zeta = 0.001$; green – $\zeta = 0.07$; dashed line – corresponding values for the Gaussian random variable	37
4.4	Histograms of normalized displacement $\bar{Z}(t)$ with standard normal density based on 1,000 MC realizations assuming ergodicity	37

4.5	Spectral densities and spectral distribution functions of centered forcings $\tilde{Y}(t)$ and of their approximations $\sum_{i=1}^6 \hat{Y}_i(t)$, where $\hat{Y}_i(t)$ are independent AR(2) processes with the coefficients in Tab. 4.2 based on spectral optimization for $f_p = 2.0$ and 3.5 Hz	40
4.6	Normed histograms of the displacement assuming ergodicity, structures fully occupied by an active crowd only	41
4.7	Response mean displacement in comparison with an approximation based on the first four harmonics for a harmonic oscillator, $f_1 = 5$ Hz and $\zeta = 0.07$	41
4.8	Total mean upcrossings $n_x^+(T)$ and acceleration RMS values as functions of f_1 for a harmonic oscillator, distinct levels x and viscous damping ζ , $T = 160$ s	42
4.9	Total mean upcrossings $n_x^+(T)$ of a simply supported beam in Appendix C.1 as functions of x , $T = 160$ s, distribution of maxima $f_{\max}(x)$, single realization and mean responses for an active crowd and for a mixed crowd	43
4.10	Total mean upcrossings of a cantilever grandstand in Appendix C.2, distribution of maxima, single realization and mean responses for an active crowd and for a mixed crowd	44
4.11	Total mean upcrossings of a real grandstand in Appendix C.3, distribution of maxima, single realization and mean responses for an active crowd and for a mixed crowd; convergence of normalized variances with respect to $\dim(\mathcal{V})$	45
4.12	$q_{ij}(t, t)$ for $a = 1$, $\nu = 2\pi 5$, $\zeta = 0.05$, $\eta = 2\pi 4$, $\text{var}\chi = 0.25$ and $\sigma = 1$; red – exact, blue – stationary solution, green – time average	48
4.13	$c_{ii}^a(t, t)$ for the same data as in Fig. 4.12, $c_{11}^b = 8.063e-5$, $c_{22}^b = 7.958e-2$; red – exact, green – time average	49
4.14	Realization of uniform δ -correlated random crowd distribution, mean response and histogram assuming ergodicity for cantilever grandstand in Appendix C.2	50
4.15	Variance and RMS value as functions of p (a) and (b); variance and RMS value as functions of α (c) and (d); single trajectory of $\ddot{Z}_{P_1}(t)$, RMS, floating RMS for $\tau = 1$ resp. 10 s and the stationary estimate in Eq. (4.29) in (e)	51
4.16	Inverse of the marginal distribution \mathbb{F}_1 , Gaussian CDF Φ , translation function $g_1 = \mathbb{F}_1^{-1}\Phi$ and its approximations in Eqns. (4.61) and (4.66)	53
4.17	Relations between normalized covariance functions, $f_p = 2.7$ Hz; comparison of spectral densities for $\tilde{Y}(t)$ a linear combination of two AR(2) processes	54
4.18	Mean stationary x -upcrossing rates of centered response in P_1 point of example in Appendix C.1; ratios of exact to approximate upcrossing rates	58
4.19	Sample of the compound Poisson process $C(t)$ and its formal time derivative $W_P(t) = dC(t)/dt$	59
4.20	Resulting moments as functions of SDOF eigenfrequency f_1 for two relative dampings $\zeta = 0.001$ and $\zeta = 0.07$ and the case of Poisson white noise excitation	60
4.21	Bi-spectra of centered forcing process with jumping frequency $f_p = 3.5$ Hz based on MC according to [51], HOSA package used [54]	61

5.1	Behaviour of $\mathbf{Z}(t, \mathbf{E}\Theta)$ and $\mathbb{V}_i(t, \mathbf{E}\Theta)$ for the displacement of the structure (a); decomposed variance of the structure displacement $\text{var}Z_S(t)$ (b); $\gamma = 0.5$, $\zeta_S = 0.05$, $f_1 = 3.5$ Hz	67
5.2	$L^2(T_1, T_2)$ norms of members $c_{Z,11}^{ij}(t, t)$ constituting the variance of the structure displacement $c_{Z,11}(t, t) = \text{var}Z_S(t)$ as functions of the mass ratio γ and eigenfrequency f_1 of an empty structure, $T_1 = 10$ and $T_2 = 20$ s; for the legend <i>cf</i> Fig. 5.1b	67
5.3	Dependencies of the structure displacement variance $\text{var}Z_S$ on the mass ratio γ , on the empty grandstand eigenfrequency f_1 and on the probability p	72
5.4	Dependencies of the structure displacement and acceleration variances on the probability p ; mean value solutions and normalized histograms with standard normal density for $p = 0.5$, ergodicity in variance assumed	73
6.1	Simple example of harmonic oscillator with two positions for spectators, forced with two mutually independent white noise processes $W_i(t)$	76
6.2	Dependencies of the structure displacement and acceleration variances on the probability p ; relative errors in Eq. (6.15) as functions of f_1 and γ ; MC based on algebraic approach in Eq. (6.14)	79
6.3	Dependencies of the structure displacement and acceleration variances on the probability p ; mean value solutions and normalized response histograms with standard normal density for $p = 0.5$, ergodicity in variance assumed .	80
B.1	Implementation diagram	90
C.1	Geometry, labelled point of interest, positions for spectators and the first three bending modes of simply supported beam	91
C.2	Geometry, cross-sections, positions for spectators, labelled points of interest and the first two bending modes of cantilever grandstand	92
C.3	Geometry of the real grandstand kindly provided by Ing. David Jermoljev from Excon company, identification of particular elements, dimensions in [m], for specification <i>cf</i> Tab. C.2; seating deck L-beams are not included contrary to Fig. C.4	94
C.4	Geometry, positions for spectators, labelled points of interest and the two bending modes of the real grandstand	95

List of Tables

1.1	Characteristic magnitudes of imposed loads, ČSN EN 1991-1-1, part of Tab. 6.2	4
3.1	Parameters of the discrete biodynamic models, [47]	17
3.2	Mean values μ and standard deviations σ of undamped eigenfrequencies, relative dampings and masses of biodynamic models, [51]	18
3.3	The first two moments of physical parameters of SDOF model with a rigid mass for seated man, data published in [56]; upper square matrix is the covariance matrix, the last row is the mean vector; units t, kN/m and kNs/m	18
3.4	Time consumptions of ROMs in comparison with the full system, $k = 50$.	22
3.5	Peak vertical displacements and accelerations in P_1 node for various occupation by an active crowd; the case of real grandstand in Appendix C.3 . .	25
4.1	Coefficients $\hat{\alpha}$ for an approximation of the mean value in Eq. (4.30)	35
4.2	Coefficients $c_{k,i}$, $k = 1, 2, 3$ and $i = 1, \dots, 6$ of the six independent AR(2) members used for approximation of the centered forcing term $\tilde{Y}(t)$ in frequency range 0.5 – 10 Hz	39
4.3	Comparison of computational demands	46
4.4	Comparison of variances, RMS values and time consumptions for $p = 0.5$; ¹⁾ time for 100 realizations	49
4.5	Coefficients a_k in Eq. (4.61) for an arbitrary level n ; variance σ^2 , coefficient of skewness γ_3 and kurtosis γ_4 for centered unit processes of jumping frequencies f_p ; values based on 3,000 MC realizations	53
4.6	Coefficients $c_{k,i}$, $k = 1, 2, 3$ and $i = 1, 2$ of the two independent AR(2) members used for approximation of the centered unit variance forcing term $\tilde{Y}(t)$ in frequency range 0.5 – 10 Hz	54
4.7	Comparison of the first three moments of SDOF system based on moment equations and MC simulation	58
4.8	Comparison of the first three moments of simply supported beam in Appendix C.1 and in the point P_1 based on moment equations, MC simulation and higher order spectra	59
5.1	Stationary variances of structure response measured in P_1 point for random and deterministic mass of the SDOF biodynamic models, 36 active and 36 passive spectators, example in Appendix C.2; ¹⁾ time for 100 realizations	70
C.1	The first five eigenfrequencies of the cantilever grandstand corresponding to vertical bending modes [Hz]	93

- C.2 Table of cross-sections for the real grandstand, *cf* Fig. C.3; TR $A \times B$ represents a circular pipe with outer diameter A [mm] and wall thickness B [mm] 93
- C.3 The first eigenfrequencies of the real grandstand corresponding to vertical bending modes [Hz] 93

Acknowledgments

Before all other acknowledgments, I would like to express my sincere gratitude to my supervisor, Prof. Ing. Jiří Máca, CSc., who was always ready to help me with any difficulties or questions regarding topics of this thesis during the whole course of the work.

Special thanks belong to my supervisor specialist Doc. RNDr. Petr Kučera, CSc., for many discussions on mathematical subjects and for his special course on analysis conducted jointly with Doc. RNDr. Aleš Nekvinda, CSc. during early stages of my Ph.D. study; Doc. Ing. Jan Zeman, Ph.D. for his interest, encouragement and numerous fruitful discussions, Prof. Ing. Milan Jirásek, DrSc., whose great personality and all his lectures made an invaluable contribution to my education, Doc. RNDr. Jan Chleboun, CSc., Prof. RNDr. Daniela Jarušková, CSc., Prof. Ing. Jiří Šejnoha, DrSc., FEng., Prof. Ing. Michal Polák, CSc., Ing. Jiří Náprstek, DrSc., FEng., RNDr. Cyril Fischer, Ph.D. and Ing. David Jermoljev for their valuable comments, discussions, cooperation and recommendations which helped to develop overall direction of this thesis.

I would also like to thank Prof. RNDr. Viktor Beneš, CSc., Doc. RNDr. Zuzana Prášková, CSc., Doc. RNDr. Daniel Hlubinka, Ph.D., Prof. RNDr. Jiří Anděl, DrSc. and many others from the department of Probability and Mathematical Statistics at the Charles University in Prague who lead me through several courses on probability, stochastic calculus and stochastic differential equations, which I had the pleasure and the opportunity to attend.

Particularly, I am indebted to my parents, brother Roman and fiancée Tereza for their understanding, patience and endless encouragement during my study and completion of this dissertation.

The financial support of this work from the Czech Science Foundation under Projects No. GAP105/11/1529 and GA103/08/1642 is also gratefully acknowledged.

Since this version is a corrected edition of the original thesis, I would like to append here also a word of thanks to the opponents RNDr. Cyril Fischer, Ph.D. and Prof. Ing. Juraj Králik, CSc. for their critical review, comments, motivation and further suggestions.



CZECH TECHNICAL UNIVERSITY IN PRAGUE

Faculty of Civil Engineering
Department of Mechanics

Abstract

Dynamic Analysis of Grandstands

by Ondřej ROKOŠ

Nowadays, civil engineers are facing a lack of design suggestions in the field of grandstand problems mainly in the case of synchronized and lively crowds, when the resonance effects can occur. Some heuristic bounds restricting generally the spectrum of the structure are available; the question remains, however, how to tackle with the dynamic effects. Several procedures covering relatively wide variety of approaches were suggested ranging from simple static loads with dynamic coefficients, truncated Fourier series, approximations of the human-grandstand system with two-degree-of-freedom oscillators up to the Monte Carlo simulations based on recently developed algorithms reflecting the load most accurately. Clearly, based on the list given above, all procedures gradually try to reflect randomness such inevitably inherent to this type of structures. The question is, whether there is any possibility or benefit in employing analytical methods of stochastic calculus, random processes and the theory of probability. If the answer was affirmative, there would be a possibility of a systematic treatment of this kind of structures in order to estimate their performance and reliability, or just to test whether a particular structure is capable to withstand realistic load (the design load in standards is usually static or purely periodic as already mentioned). In the familiar context of the Finite Element Method together with well established Reduced Order Modelling, it would be moreover possible to employ numerical models developed in the previous design stages, supplemented with a specification of nodes where the spectators can possibly be situated. As will be shown later on in this text, in some cases, it is possible to estimate efficiently the response of the human-grandstand system by means of the Gaussian processes which cover the major source of the randomness—an active crowd—and to assess serviceability or reliability of the system. For the sake of completeness, the other sources of randomness are mainly random spatial distribution of a crowd and random parameters of the biodynamic models employed to reflect a passive crowd.

It would seem that the problem is not actual enough; hence, let us name several existing structures where the problems persist, *cf* also [9, 34] and references therein: at the Millennium stadium in Cardiff steel props are still added before concerts; Old Trafford stadium, where the third deck is used only during football matches excluding pop concerts; Anfield Stadium, where steel columns were additionally installed to newly constructed upper deck to raise its natural frequencies and stiffen the structure after the excessive vibrations were reported; Maracanã stadium, where excessive deflections led to the development of cracks in cantilever beams. Such situations would be avoided and more efficient structures with better sights, accommodating higher number of spectators, architecturally

of more interesting appearance would be projected if realistic and reliable design procedures were available, reflecting the loading scenarios and dynamic effects accurately. Hence, this thesis is interested in these procedures, and as was already mentioned, it approaches the problem mainly from the probabilistic point of view.

Abstrakt

Dynamická analýza konstrukcí tribun

Ondřej ROKOŠ

V současné době projektanti civilních staveb čelí jistému nedostatku v normách týkajícího se problematiky navrhování tribun, zejména v případě synchronizovaného temperamentního davu, kdy se mohou objevit rezonanční efekty. Některá heuristická doporučení omezující obecně frekvenční spektrum konstrukce jsou k dispozici, nicméně zbývá otázka, jak se vypořádat s dynamickými efekty. V literatuře bylo navrženo několik postupů pokrývajících relativně široké spektrum možností, jež sahají od jednoduchých statických zatížení s dynamickými koeficienty, zkrácené Fourierovy řady, jednoduché aproximace systémů divák-tribuna prostřednictvím oscilátorů se dvěma stupni volnosti až po simulace typu Monte Carlo, založených na nedávno navržených algoritmech zachycujících zatížení nejpřesněji. Na základě tohoto výčtu je zřejmé, že jednotlivé metody se snaží postupně zachycovat náhodnosti nevyhnutelně spojené s tímto typem konstrukcí. Otázkou zůstává, zda je možnost či nějaký přínos v použití analytických metod stochastického kalkulu, náhodných procesů a teorie pravděpodobnosti. Bude-li odpověď pozitivní, otevírají se možnosti systematického přístupu k tomuto typu konstrukcí sloužícího k odhadu jejich kvality a spolehlivosti, či pouze testujícího, zda konkrétní konstrukce vydrží realistické zatížení (normové návrhové zatížení je obvykle statické či čistě periodické, jak již bylo zmíněno). Ve velmi dobře známém kontextu konečných prvků společně s metodami redukujícími počet stupňů volnosti by pak bylo možné využít numerické modely vyvinuté v předchozích stádiích návrhu, doplněné pouze o specifikaci pozic pro diváky. Jak vyplyne dále z textu této práce, v některých případech je možné efektivně odhadnout odezvu systému divák-konstrukce prostřednictvím Gaussovských náhodných procesů pokrývajících hlavní zdroj náhodností, totiž aktivní dav, a k odhadnutí použitelnosti či únosnosti daného systému. Pro úplnost poznamenejme, že ostatní zdroje náhodností jsou zejména nahodilé rozmístění davu a nejisté parametry biodynamických modelů reprezentujících pasivní dav.

Mohlo by se zdát, že problematika není dostatečně aktuální; popišme tedy několik konstrukcí, u nichž problémy stále přetrvávají, porovnejte také s [9, 34] a referencemi tam uvedenými: stadion Millennium v Cardiffu, kde jsou před koncerty vždy přidány ocelové podpěry; stadion Old Trafford, kde je třetí tribuna využívána pouze pro fotbalové zápasy a nikoliv pro koncerty; stadion v Anfieldu, kde byly přidány ocelové sloupy u nově přistavěné horní tribuny z důvodu zvýšení vlastních frekvencí a celkového ztužení konstrukce poté, co byly zaznamenány nadměrné vibrace; Maracanã stadion, na němž došlo v důsledku nadměrných deformací k rozvoji trhlin u konzolových nosníků. Takovýmito situacím bychom se nicméně mohli vyhnout a realizovat konstrukce s lepšími výhledy, pojímající dostatečný počet diváků a zároveň architektonicky zajímavé, nicméně

za předpokladu znalosti realistických a spolehlivých návrhových postupů odrážejících veškeré dynamické efekty a způsoby zatížení. Tato práce se zabývá jedním z možných postupů, a jak již bylo zmíněno, k problematice přistupuje zejména z pravděpodobnostního hlediska.

Notation

Abbreviations

AR(p)	auto-regression process of the p -th order
CDF	cumulative distribution function
CF	crest factor
DLF	dynamic load factor
DOF	degree of freedom
FEM	finite element method
FRF	frequency response function
GB	gigabyte
GLF	generated load factor
HOSA	higher order spectral analysis
<i>iid</i>	independent, identically distributed
KS	Krylov subspace
MC	Monte Carlo
MDOF	multi-degree-of-freedom
MS	modal synthesis
MTVV	maximum transient vibration value
PDF	probability density function
POD	proper orthogonal decomposition
RAM	random-access memory
RMS	root mean square value
ROM	reduced-order model/modelling
SDE	stochastic differential equation
SDOF	single-degree-of-freedom
SOAR	second order Arnoldi algorithm
TMD	tuned mass damper
VDV	vibration dose value
2 DOF	two-degree-of-freedom

Symbols – coefficients and constants

a_i, b_i	constants in linear combination of artificial force generator
$C(n_s)$	coordination factor for n_s spectators
f_p	basic jumping frequency, [Hz], $f_p = 1/T_p$, typically $f_p \in (1, 3.5)$
f_{H_i}, ξ_{H_i}	modal parameters of a biodynamic model, [Hz], [-]
f_i	i -th eigenfrequency, [Hz]
F_{\max}	peak dynamic load, [kN], $F_{\max} = \max_{t \in T} F(t) $
$F_v(t)$	total load of an active crowd counting n_a spectators, [kN]

g	acceleration of gravity, [m/s ²]
G	static human weight, [kN]
G_v	total weight of an active crowd counting n_a spectators, [kN]
I_k	impulse size, [kJ], $I_k = \int_{-t_p/2}^{t_p/2} F(t) dt$
k_p	impact factor $k_p = F_{\max}/G$ (or number of physical parameters of a biodynamic model)
$k_{H_i}, m_{H_i}, c_{H_i}$	physical parameters of a biodynamic model, [kN/m], [kg], [kNs/m]
m_H	total mass of a passive crowd, [kg]
m_S	total mass of a grandstand, [kg]
N	number of MC simulations
n_a	number of active spectators
n_{DOF}	number of DOFs of a crowd-grandstand system
$n_{\text{DOF},H}$	number of DOFs of a passive crowd
$n_{\text{DOF},S}$	number of DOFs of the grandstand
n_p	number of passive spectators
n_s	number of spectators
n_{snap}	number of snapshots
P_i	i -th structure nodal point of interest
q_k	imposed surface load, [kN/m ²]
Q_k	imposed point load, [kN]
r_k	dynamic load factors
t_k	centroid of k -th jumping impulse, [s]
t_p	contact time, [s]
T_p	jumping period, [s]
α	contact ratio, $\alpha = t_p/T_p$
α, β	coefficients of the linear combination for the Rayleigh damping
α_k, β_k	Fourier series coefficients of the approximate mean jumping process
γ	mass ratio $\gamma = m_H/m_S$
ζ	damping ratio
ν	angular frequency of SDOF system, [rad ⁻¹]
ϕ_k	phase shifts according to dynamic load factors, [rad]
$\binom{n}{k}$	binomial coefficient, $\binom{n}{k} = \frac{n!}{k!(n-k)!}$

Symbols – vectors, matrices and algebra

\mathbf{A}, \mathbf{B}	real or complex matrices
$\mathbf{A} \circ \mathbf{B}$	Hadamard product, $(\mathbf{A} \circ \mathbf{B})_{ij} = A_{ij}B_{ij}$
$\mathbf{A} \otimes \mathbf{B}$	Kronecker product, $(\mathbf{A} \otimes \mathbf{B})_{ijkl} = A_{ij}B_{kl}$
$\mathbf{A} \oplus \mathbf{B}$	Kronecker sum, $\mathbf{A} \oplus \mathbf{B} = \mathbf{A} \otimes \mathbf{I}_{n_B \times n_B} + \mathbf{I}_{n_A \times n_A} \otimes \mathbf{B}$
$\mathbf{A}_{SS}, \mathbf{A}_{SH}, \mathbf{A}_{HH}$	submatrices of the crowd-grandstand system, \mathbf{A} represents stiffness, mass or damping
\mathbf{C}	crowd-structure system damping matrix
\mathbf{C}_H	passive crowd damping matrix
\mathbf{C}_r	reduced system damping matrix
\mathbf{C}_S	structure damping matrix
diag	diagonal matrix
$\mathbf{e}_i, \tilde{\mathbf{e}}_i$	i -th canonical basis vector

$\mathbf{f}(t)$	deterministic load vector
\mathbf{G}	load distribution matrix
$\mathcal{G}_n(\mathbf{A}, \mathbf{B}; \mathbf{u})$	second-order Krylov subspace
$\mathbf{I}_{n \times n}$	identity matrix of the size n
\mathbf{K}	crowd-structure system stiffness matrix
\mathbf{K}_H	passive crowd stiffness matrix
\mathbf{K}_r	reduced system stiffness matrix
\mathbf{K}_S	structure stiffness matrix
\mathbf{M}	crowd-structure system mass matrix
\mathbf{M}_H	passive crowd mass matrix
\mathbf{M}_r	reduced system mass matrix
\mathbf{M}_S	structure mass matrix
\mathbf{n}_a	set of code numbers where active spectators can be situated
\mathbf{n}_p	set of code numbers where passive spectators can be situated
\mathbf{n}_s	set of code numbers where spectators can be situated
nz	number of nonzero elements of a matrix
$\mathbf{r}(t)$	residual vector
$\text{span}[\bullet]$	linear hull of the vectors \bullet
\mathbf{u}, \mathbf{v}	real or complex vectors
$\mathbf{u} \cdot \mathbf{v}$	dot product, simple contraction, $\mathbf{u} \cdot \mathbf{v} = u_i v_i$
$\mathbf{v}_i, \boldsymbol{\psi}_i$	i -th eigenvector
\mathcal{V}, \mathcal{W}	vector spaces
$\mathbf{z}(t)$	deterministic crowd-grandstand system displacement vector
δ_{ij}	Kronecker delta, $\delta_{ij} = 0$ for $i \neq j$ and 1 for $i = j$
λ_i	i -th eigenvalue
$\boldsymbol{\Lambda}$	spectral matrix, $\boldsymbol{\Lambda} = \text{diag}[\lambda_1, \dots, \lambda_n]$
$\Pi_{\mathcal{V}, \mathcal{W}}$	projector onto \mathcal{V} parallel to \mathcal{W} , $\mathcal{V} = \text{span}[\mathbf{V}]$, $\mathcal{W} = \text{span}[\mathbf{W}]$
ρ_{ij}	horizontal distance between two active spectators
$\boldsymbol{\Psi}$	modal matrix, $\boldsymbol{\Psi} = [\boldsymbol{\psi}_1, \dots, \boldsymbol{\psi}_n]$
$\ \bullet\ _F$	Frobenius norm of a matrix \bullet
\bullet^T	transpose of a matrix \bullet
\bullet^\dagger	Hermitian transpose of a matrix \bullet

Symbols – analysis and functions

$a_w(t)$	weighted acceleration, $[\text{m/s}^2]$
\mathbb{C}	set of complex numbers
$e^{\mathbf{A}}$	matrix exponential, $e^{\mathbf{A}} = \sum_{k=0}^{\infty} \frac{1}{k!} \mathbf{A}^k$
$\mathcal{F}(f(\boldsymbol{\tau}))(\boldsymbol{\xi})$	Fourier transform of $f(\boldsymbol{\tau})$
$g_1(x)$	nonlinear, monotonic function of x
$\mathbf{H}(\xi)$	frequency response function
$\mathbf{H}(s)$	transfer function
H_k	Hermite polynomials
\mathbf{i}	imaginary unit, $\mathbf{i} = \sqrt{-1}$
$\text{Im}(z)$	imaginary part of a complex number z , $\text{Im}(z) = \frac{1}{2\mathbf{i}}(z - \bar{z})$
\mathbb{N}	set of natural numbers
\mathbb{R}	set of real numbers
\mathbb{R}^+	set of positive real numbers

$\Re(z)$	real part of a complex number z , $\Re(z) = \frac{1}{2}(z + \bar{z})$
t, τ	time domain parameters, [s]
w_i	integration weights
$X(t-)$	left limit, $X(t-) = \lim_{s \uparrow t} X(s)$
$\dot{X}(t)$	derivative with respect to time, $\dot{X}(t) = \frac{d}{dt}X(t)$
\bar{z}	complex conjugate of $z = x + iy$, $\bar{z} = x - iy$
Δt	time step, time increment
$\Delta X(t)$	jump discontinuity of X right continuous at t , $\Delta X(t) = X(t) - X(t-)$
$\theta(t)$	Green function or unit impulse response
ξ	frequency domain parameter, [Hz]
$\mathbb{1}_U$	indicator function of a set U , $\mathbb{1}_U(x) = 1$ for $x \in U$, $\mathbb{1}_U(x) = 0$ for $x \notin U$
$\ \bullet\ _{L^2}$	L^2 norm of \bullet

Symbols – probability, random variables and processes

a_i	coefficients of AR process
\mathbf{a}	drift matrix, possibly random
\mathcal{A}	σ -field of events
\mathbf{b}	diffusion matrix, possibly random
$b_{(p,q)}$	quasimoments of a random vector of order p and q
$\mathbf{B}(t)$	vector valued Brownian motion, Wiener process
\mathbf{c}	covariance matrix, function
c_v	coefficient of variation, $c_v = \sigma/\mu$
$C(t)$	compound Poisson process
cov	covariance of random variables, $\text{cov}(X, Y) = \mathbf{E}[(X - \mathbf{E}X)(Y - \mathbf{E}Y)]$
\mathbf{d}	load distribution matrix as a part of the drift matrix \mathbf{a}
$\mathbf{E}X(\omega)$	expectation operator, $\mathbf{E}X(\omega) = \int_{\Omega} X(\omega) \mathbf{P}(d\omega)$
$\mathbf{E}[X \mathcal{G}]$	conditional expectation with respect to σ -field \mathcal{G}
$f_{\max}(x)$	PDF of the local maxima of a random process
$\mathbf{F}(t)$	random load vector
\mathbb{F}_n	n -dimensional distribution function
$(\mathcal{F}_t)_{t \geq 0}$	filtration
$g(\xi)$	one-sided spectral density
\mathbf{h}	distribution matrix of the mean force
$I_T(\xi)$	periodogram
$K_{H_i}, M_{H_i}, C_{H_i}$	random physical parameters of a biodynamic model
\mathcal{L}	random differential operator
\mathbf{m}	mass matrix of the state space system, possibly random
$\mathcal{M}(dt, dy)$	Poisson random measure
$n_x^+(T)$	total number of x -upcrossings in the time interval $(0, T)$, $n_x^+(T) = \int_0^T \nu_x^+(t) dt$
$N(t)$	Poisson counting process
$\mathcal{N}(\mu, \sigma^2)$	normal distribution with mean μ and variance σ^2
\mathbf{P}	probability measure on \mathcal{A}
\mathbf{r}_X	correlation matrix, function, $\mathbf{r}_X = \mathbf{E}[\mathbf{X}\mathbf{X}^\top]$
$s(\xi)$	spectral density
$s_3(\boldsymbol{\xi})$	bi-spectra

$\hat{s}(\xi)$	spectral density estimate
$\mathcal{S}(\xi)$	spectral distribution function
T_k	stopping times
$\mathcal{U}(a, b)$	uniform distribution with support (a, b)
\mathbf{v}_i	derivative of the mass matrix, $\mathbf{v}_i = \frac{\partial}{\partial x_i} \mathbf{m}(\boldsymbol{\chi})$
\mathbb{V}_i	sensitivity factors
var	variance of a random variable X , $\text{E}[X - \text{E}(X)]^2$
\mathbf{w}_i	derivative of the drift matrix, $\mathbf{w}_i = \frac{\partial}{\partial x_i} \mathbf{a}(\boldsymbol{\chi})$
$\mathbf{W}(t)$	vector-valued Gaussian white noise process, formally $\mathbf{W}(t) = d\mathbf{B}(t)/dt$
$W_P(t)$	Poisson white noise process, formally $W_P(t) = dC(t)/dt$
\tilde{X}	centered, <i>i.e.</i> zero mean, random variable
$\mathbf{X}(t)$	state space variable of the system, a random vector process
$\bar{\mathbf{X}}$	mean value of a random vector \mathbf{X}
$\tilde{\mathbf{Y}}(t)$	autoregression approximation of a centered forcing
$\mathbf{Z}(t)$	crowd-structure system displacement vector
γ_3	coefficient of skewness
γ_4	coefficient of kurtosis
$\Theta = [\Theta_i, \dots, \Theta_n]$	random parameters
$\kappa_3(\boldsymbol{\tau})$	third order cumulant
λ	intensity of the Poisson process
λ_k	spectral moments $\lambda_k = \int_{-\infty}^{\infty} (2\pi\xi)^k s(\xi) d\xi$
$\boldsymbol{\mu}_\bullet$	mean value of a variable \bullet , possibly a function of time
$\nu_x^+(t)$	mean x -upcrossing rate at time t
$\nu_S(x), \nu_G(x), \nu_T(x)$	approximation of the x -upcrossing rate based on Gram-Charlier series, Gaussian process, translation process
$\rho(\tau)$	correlation coefficient function
ρ_{ij}	correlation coefficient
$\sigma_X^2, \dot{\sigma}_X^2, \ddot{\sigma}_X^2$	variances of stationary random processes $X(t), \dot{X}(t), \ddot{X}(t)$
$\phi(x)$	standard Gaussian PDF, $\phi(x) = \frac{1}{\sqrt{2\pi}} \exp(-x^2/2)$
$\phi(y_1, y_2; \rho)$	bivariate standard Gaussian PDF with correlation coefficient ρ
$\Phi(x)$	standard Gaussian CDF, $\Phi(x) = \int_{-\infty}^x \phi(y) dy$
χ_i	random indicator variables with state space 0 and 1
$\boldsymbol{\chi}$	matrix of indicator variables $\boldsymbol{\chi} = \text{diag}(\chi_1, \dots, \chi_n)$
$\boldsymbol{\chi}_n$	expanded diagonal matrix of the indicator variables
ω	sample point of a sample space Ω
Ω	sample space
$[X]$	quadratic variation process
$[X]^c$	continuous part of the quadratic variation process
$[X, Y]$	quadratic covariation process
$(\Omega, \mathcal{A}, \mathbf{P})$	probability space
$(\Omega, \mathcal{A}, (\mathcal{F}_t)_{t \geq 0}, \mathbf{P})$	filtered probability space

"As far as the laws of mathematics refer to reality, they are not certain; as far as they are certain, they do not refer to reality."

Albert Einstein

Introduction

In recent years, sport stadia found a multipurpose utilization and serve more as an entertainment centres hosting wide palette of events from sermons via sport matches to rock or pop concerts housing a large number of spectators. Great seating capacities and requirements on clear sight lines led to cantilever upper tiers, increasingly slender, lightweight and flexible. All these facts follow from the intentions of stadium owners to maximize a utilization of objects, economical aspects and requirements of the spectators.

Grandstand structures are of particular interest, since dense and lively crowds may cause serviceability or safety issues owing to highly synchronized movements. Although the question is actual (*e.g.* Millennium stadium in Cardiff, where steel props are added before pop concerts), the most advanced guidelines available [22, 25, 33] still indicate that the problem is not understood properly and further research is needed.

Difficulties of predicting stadia performance arise mainly from capability of the spectators to modify dynamic properties of the structural systems, ability to absorb a significant amount of vibrational kinetic energy and random nature of induced loading. Since all these effects depend on time, it is almost impossible to develop accurate or even exact models and approximations are needed. Contemporary approaches consider spectators as biodynamical spring-mass systems added to the structure and forced by Fourier series or time approximations of the human-induced loads.

Excluding simple methods such as equivalent static load with the dynamic magnification factor or bounds for eigenfrequencies of assembly structures, current state-of-the-art approaches prefer 3-DOF models [27], each DOF represents successively a structure, a passive crowd and an active crowd (in the case of bouncing). These models are capable to reflect vertical vibrations in dominant mode only, but no detailed information is available and the method can be viewed as oversimplified. Other possible approach relates to the modelling of individuals in complex FEM-based numerical system within a stochastic context using geometries, material properties and other parameters from the models for static analysis. No publications, however, on such an approach or even comparison indicating its accuracy and usability yet exist. *Filling this gap is the main objective of this thesis.*

Chapter 1

State of the Art

1.1 European and Czech standards

Standards are the first place where to look for general design principles, load and structure assessment. Nevertheless, in the case of European and hence Czech standards, no particular recommendations for the case of lively and synchronized crowds concerning load or serviceability limits are given.

1.1.1 Load and structure assessment

The list of Czech and European standards mentioning directly grandstands, spectator facilities or amusement structures include

- ČSN EN 1990, Eurocode: Basis of structural design
- ČSN EN 1991-1-1, Eurocode 1: Actions on structures – Part 1-1: General actions – Densities, self-weight, imposed loads for buildings
- ČSN EN 13200-5, Spectator facilities – Part 5: Telescopic grandstands
- ČSN EN 13200-6, Spectator facilities – Part 6: Demountable (temporary) stands
- ČSN EN 13814, Fairground and amusement park machinery and structures – Safety.

In subsequent paragraphs, a brief description of each standard from the above list will be given:

ČSN EN 1990 covers general principles of design, vibration and dynamic load. It suggests, basically, that the eigenfrequencies of a structure should be sufficiently above the loading spectrum. If this is not the case, in-depth dynamical analysis taking into account structural damping should be performed. No particular instructions, however, or design procedures are described. Grandstands are assigned into the RC3 class of high damage consequences.

ČSN EN 1991-1-1 lists primarily static loads acting on structures and the question of dynamic effects on grandstands answers with words: *”Where the danger of significant structural response to synchronized rhythmical movement of people, dancing or jumping exists, then in dynamic analysis the relevant load model should be considered, efficient for the verification of relevant structural response”*. Then, references to other sources,

Category of loaded areas	q_k [kN/m ²]	Q_k [kN]
C2	3 – 4	2.5 – 7
C5	5 – 7.5	3.5 – 4.5

Table 1.1: Characteristic magnitudes of imposed loads, ČSN EN 1991-1-1, part of Tab. 6.2

e.g. ČSN EN 1990, are listed. Further recommendations comprise only bridges and foot-bridges.

ČSN EN 13200, parts 5 and 6 determine horizontal and vertical imposed loads. Grandstands are of category C2 and C5, *cf* Tab. 1.1, where the static load is presented. In the case of dynamic effects, appropriate model should be developed for special analysis. Let us point out the load case where the orthogonal web of 1 kN point forces and 0.5 m spacing is used. Horizontal effects are considered as 6 % of the vertical load. Moreover, possible presence of lively crowd should be considered taking into account also the state of resonance. All mentioned levels of load are considered as lower bounds.

ČSN EN 13814 again specifies analogous values of imposed loads as ČSN EN 13200. Moreover, horizontal load of railing, barriers, *ect* are specified.

1.1.2 Human exposure to vibrations

From the serviceability point of view, an adverse impact of vibrations to human health and comfort should be considered. Such a question is quite satisfactorily treated in ČSN ISO 2631, Mechanical vibration and shock – Evaluation of human exposure to whole-body vibration. Here, basic factors are combined in order to asses an overall level of exposition. Frequency range is divided into two subintervals

- 0.1 – 0.5 Hz for motion sickness
- 0.5 – 80 Hz for health, comfort and perception.

Application excludes individual impacts with extreme magnitude, but is valid for whole-body vibrations transferred through the interfaces, *e.g.* feet of a standing person and back of a sitting person. Such a kind of vibrations occur in buildings with working machinery, vehicles, *etc.* Transferred vibrations are measured at the interface between the human body and the structure. Measured signal should be frequency-weighted. Human response to vibrations can be further influenced by many factors such as age, gender, physical fitness, experience and expectation. Vibration assessment comprises two following methods.

Basic evaluation method This method makes use of RMS [m/s²], an effective acceleration value, computed according to

$$\text{RMS} = \sqrt{\frac{1}{T} \int_0^T a_w(t)^2 dt}, \quad (1.1)$$

where $a_w(t)$ is weighted acceleration (translational or angular) as a function of time, and T denotes the integration time. Frequency weights corresponding to different directions can be found in Fig. 1.1. The basic method is suitable for crest factor $CF \leq 9$, where $CF = \max_{t \in [0, T]} |a_w(t)| / \text{RMS}$. Other criteria are to be found in Eq. (1.4).

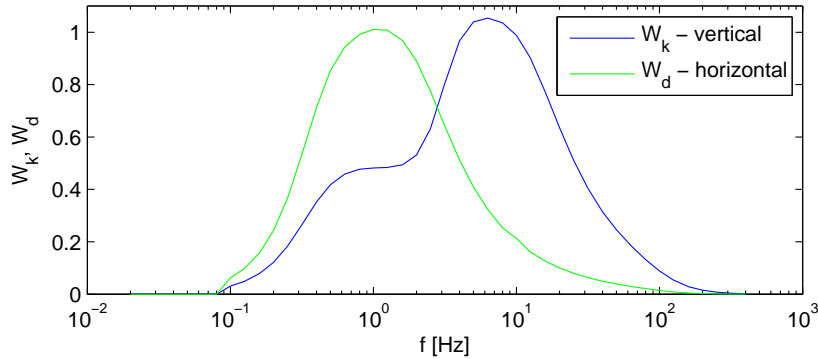


Figure 1.1: Frequency weighting curves in ISO 2631-1

Alternative additional methods These should be used when the basic method is insufficient, *i.e.* $CF > 9$ and in the case of impulsive or transient vibrations.

1. *Floating RMS method*

In this case, a short integration interval in Eq. (1.1) floating through $[0, T]$, is used. Level of vibrations is then defined as a peak value of moving average RMS (t_0), called maximum transient vibration value $\text{MTVV} = \max_{t_0 \in [0, T]} \text{RMS}(t_0)$, where

$$\text{RMS}(t_0) = \sqrt{\frac{1}{\tau} \int_{t_0 - \tau}^{t_0} a_w(t)^2 dt}, \quad (1.2)$$

and where τ denotes an integration period and t_0 an observation time. For MTVV, $\tau = 1$ is recommended.

2. *Fourth power vibration dose method*

Employing the fourth power instead of the second, the method becomes more sensitive to peaks and impulses. Vibration dose value (VDV [$\text{m/s}^{1.75}$]), is then defined according to

$$\text{VDV} = \sqrt[4]{\int_0^T a_w(t)^4 dt}. \quad (1.3)$$

Additional methods are appropriate for vibration assessment if the following criteria are fulfilled (depending on additional method)

$$\begin{aligned} \frac{\text{MTVV}}{\text{RMS}} &\geq 1.5 \\ \frac{\text{VDV}}{\text{RMS} \cdot T^{1/4}} &\geq 1.75, \end{aligned} \quad (1.4)$$

or together for $CF > 9$. Recommended thresholds for particular methods and various exposure durations are also listed in ISO 2631, but with rather ambiguous meaning in the context of grandstands and hence are not given here.

1.2 Other standards and recent research papers

Since further standards are regularly updated, in particular British and Canadian, they will be included in this section jointly with recent research papers. General overview of the present subject matter will be divided into three parts successively comprising the main cornerstones of the grandstand problem.

1.2.1 Load models for human-induced vibrations

Several types of human motion are considered to represent the dynamic effects induced by spectators on grandstands. After Jones *et al.* [27], these are namely

- walking and running
- jumping
- bouncing (bobbing, jouncing)
- swaying
- foot-stamping and hand-clapping
- abrupt rising
- rhythmic exercise loads.

The most significant vertical load that a human is capable to generate is often considered as jumping, and as such it is in the forefront of the interest. Original work by Parkhouse and Ewins [37] continued by Sim [51] and recently by Racic and Pavic [40, 41] address these effects and suggest advanced models for jumping individuals and small groups, namely using the MC (Monte Carlo) generators, *cf* also Chap. 3 of this thesis, which can be supplemented by human body weights, *e.g.* [21]. Nevertheless, elementary and mostly used estimates for individuals and groups are based on the time and frequency domain approximations. The former are described as half-sine pulses

$$F(t) = \begin{cases} k_p G \sin\left(\frac{\pi t}{t_p}\right), & 0 \leq t \leq t_p \\ 0, & t_p \leq t \leq T_p \end{cases} \quad (1.5)$$

where G denotes the static human weight, $k_p = F_{\max}/G$ the impact factor, F_{\max} the peak dynamic load, t_p the contact time, T_p the jumping period and $\alpha = t_p/T_p$ is the contact ratio. Several authors have suggested a number of contact ratio values specifying the type of the load. Frequency domain approach utilizes truncated Fourier series expansion in the form

$$F(t) = G \left[1 + \sum_{k=1}^n r_k \sin\left(\frac{2k\pi t}{T_p} + \phi_k\right) \right], \quad t \in \mathbb{R}, \quad (1.6)$$

where total of n harmonics are considered, usually set to $n = 3$. Fourier coefficients (known also as DLFs, dynamic load factors) are denoted by r_k , and phase shifts by ϕ_k . Different sets of values r_k , ϕ_k describe different types and intensities of human-induced effects (jumping, bouncing, *etc.*).

Expansion from individuals to crowds, *e.g.* in the ISO guidelines [22], is performed as a multiplication of individual load time history by a coordination factor $C(n_a)$ reflecting the inability of the crowd to synchronize perfectly, namely

$$F_v(t) = C(n_a) G_v \left[1 + \sum_{k=1}^n r_{k,v} \sin \left(\frac{2k\pi t}{T_p} + \phi_{k,v} \right) \right], \quad t \in \mathbb{R}, \quad (1.7)$$

where $F_v(t)$ denotes the total load of an active crowd counting n_a spectators, G_v its weight and the other quantities has analogous meaning to the quantities introduced in Eq. (1.6).

Jumping is typically characterized by an intermittent contact of the spectator with the structure described via contact ratio α and worse overall crowd synchronization. Ideally, this kind of load can be represented by forcing terms neglecting their influence to structure properties, *cf* [14]. On the other hand, bouncing or bobbing, considered as the second most onerous load, is specific with continuous contact of the spectators with the structure, better overall synchronization and higher loading frequencies. Induced forces are smaller in amplitudes compared to jumping, and loading scenario is considered as less intensive. Hence, bouncing spectators are represented as an internal force couple, or actuator, after Dougill et al [12], through an SDOF system attached to the structure. Accepting such a representation, DLFs are referred to as GLFs (generated load factors) for distinction.

Swaying and horizontal induced forces are still not addressed properly. Only recent works by Nhleko *et al.* [34, 36] focus on modelling horizontal front-to-back and side-to-side forces based on thorough measurements applying frequency domain fit, *cf* Eq. (1.6). Preceding works, *e.g.* [38], treat horizontal effects as equivalent to the fraction of the vertical induced loads, namely 6 – 10 %, *cf* [25].

It is worth mentioning that all types of the introduced contact forces are displacement and acceleration dependent, *i.e.* magnitudes and time histories of human-induced loads depend on the level of the structure excitation. The range of validity of given force approximations in Eqns. (1.5) – (1.7), is up to 0.8 g according to [27], where g denotes the acceleration of gravity.

1.2.2 Passive crowd models

Human body is a complex spatial nonlinear dynamical system with variable parameters depending on the posture, level of the excitation, physical condition, *etc.* Excluding rigid masses thought as unsatisfactory, simplest models reduce to linear and time invariant systems with lumped parameters attached to the structure, usually reproducing only the overall vertical response of a human body. Despite such simplifications, major effects are still preserved; *e.g.* changes in eigenfrequencies of the structural system, variations in system damping and dissipation of considerable amount of kinetic energy. Parameters of biodynamic models are given in available literature, *e.g.* [32, 46, 47, 49, 56, 58] and references therein, *cf* also Chap. 3 of this thesis.

1.2.3 Measures of the structure response

Discussion relating to appropriate measures of the serviceability limits is still going on among experts. Question is complex, since acceptable levels of vibration depend on many conditions such as duration, frequency of the vibration, human posture, physical condition, occupant attention, crowd density. It has been determined, however, that humans are able to detect acceleration as low as $0.005 g$ in vertical direction [28]. Upper comfort limits have been also established, *e.g.* [22–24] in terms of RMS or VDV acceleration values. Furthermore, two situations are to be treated separately: comfort and panic. Levels are determined as 10 % g of 10 s RMS, *cf* Eq. (1.2) where $\tau = 10$ s, for comfort and 20 % g of 1 s RMS for panic according to [22]. Recent thorough work performed by Browning [9], examine many variables which can be considered as the vibration serviceability limits. Regression analysis of statistical data collated on a group of people suggested two suitable single variable models: RMS acceleration for sitting spectators and RMS displacement for jumping spectators. Limit values are determined for accepted percentage of unsatisfied spectators spanning intervals $0.44 - 0.95 \text{ m/s}^2$ RMS for 5 – 20 % and high energy events (1.3 m/s^2 RMS being an extreme limit for 100 % unsatisfied spectators).

It is worth noting briefly also the reliability aspects. These are closely related to fatigue and fracture mechanics. Measures of the structure performance are mainly quantified in terms of stress amplitudes, number of cycles and in the field of stochastic structural dynamics it is the mean up-crossing rate, *cf* [6, 7].

Chapter 2

Objectives of the thesis

The main motivation for writing this thesis was a lack of design suggestions in European as well as in Czech standards, and non-existence of systematic FEM-based approaches concerning design of grandstands, or more generally concerning human-structure interaction. As presented in previous chapter, elaborate methods exist, but mainly of purely deterministic manner.

Present work attempts to approach the problem from stochastic point of view, of which nature the subject clearly is. The crowd-grandstand system and its parts are viewed as equivalent to the system with uncertain data. This approach is also supported with the fact that the serviceability limits obtained by means of the RMS values are actually the second order moment properties in context of the stochastic systems. In this specific case, several sources of randomness concerning mainly the right hand side of the system arise. The crowd on a structure is divided into two groups

- an active crowd
- a passive crowd.

An active crowd—throughout this thesis it is understood as a subset of all the spectators occupying the structure that are continuously and synchronously jumping, *cf* Sec. 3.5.1—acts as a forcing term which is characterized with a certain level of the overall synchronization if any stimulus is present, typically external audio-visual stimulus during pop and rock concerts or internal in the sense of various chants during sport events. Nevertheless, every forcing term is unique in some sense, which can be reflected through inherent randomness of the time loading history. Within the set of all possible positions for spectators, an active crowd can be distributed randomly, in groups, or can follow some other pattern. A passive crowd—understood as a subset of all the spectators (naturally disjoint with the set of an active crowd) that are at rest (standing or seated)—acts up to some extent as a TMD (tuned mass damper) and is again more or less of a random nature. Within many other effects, a passive crowd dissipates significant amount of kinetic energy, adjusts physical parameters of the structure such as mass and stiffness which leads to changes in the spectrum of the system and to changes in its overall behaviour. Again, spatial distribution can be random, in some groups, *etc.*

Note that a crowd—the union of an active and a passive crowd, but subset of all the possible positions for spectators over the structure—is assumed fixed within the experiment, meaning that an active spectator cannot become a passive during the time and vice versa; moreover, both subsets are uncertain in their cardinality.

For the purposes of the mathematical description, FEM (finite element method) is employed with advantage. The passive spectators are described through biodynamic models and discretized problem is written as a system of the second order stochastic differential equations

$$\mathbf{M}(\omega) \ddot{\mathbf{Z}}(t, \omega) + \mathbf{C}(\omega) \dot{\mathbf{Z}}(t, \omega) + \mathbf{K}(\omega) \mathbf{Z}(t, \omega) = \mathbf{GF}(t, \omega), \quad t \geq 0, \quad (2.1)$$

where $\omega \in \Omega$, $(\Omega, \mathcal{A}, \mathbb{P})$ being a product probability space of all random variables and functions for simplicity; $\mathbf{Z}(t, \omega)$ and $\mathbf{F}(t, \omega)$ are n_{DOF} and n_a -valued stochastic vector processes; $\mathbf{M}(\omega)$, $\mathbf{C}(\omega)$ and $\mathbf{K}(\omega)$ are $(d/2, d/2)$ matrices of structure mass, viscous damping and stiffness, \mathbf{G} being $(d/2, n_a)$ input distribution matrix. On the basis of the above discussion, the main uncertainties of the system include

- forcing terms resulting from active crowd movements, especially synchronized jumping,
- the uncertainties of the parameters in discrete biodynamic models—randomness of stiffness, mass and damping matrices,
- the size and spatial distribution of an active crowd and a passive crowd.

Further generalizations taking into account various kinds of nonlinearities, *e.g.* geometrical and material non-linearities and nonlinearities of biodynamic models, see [58], are in principle possible, nevertheless they cause superfluous complications with doubtful benefits and hence will be omitted. Moreover, the material parameters of the structure will be treated as deterministic, since their influence is negligible in comparison with the sources listed above and the scope of the overall response.

Ergo, the main objectives of submitted thesis can be summarized as follows:

1. Approach the grandstand problem from stochastic point of view reflecting at least the most relevant sources of randomness inherent to the system.
2. Measure the quality of the approximation based on analytical tools of the probability theory in comparison with direct MC simulation and compare the computational demands.
3. Demonstrate the approach on academic and real-world examples.

A more detailed description of all the chapters and partial objectives is following: after the introductory **Chapter 1**, leaving aside Chap. 2 and 3, the thesis is divided into three main parts of increasing model complexity taking into account different sources of randomness.

Chapter 3 summarizes again some input data of the model based on available literature, especially lists particular parameters of used biodynamic models and examines MC generators for an active crowd. Then, MC simulation comprising all kinds of randomness is described. For the case of efficiency, some methods reducing the order of the system are reviewed. A brief discussion of the spatial distribution of a crowd is given, finding also that one which yields the mean-worst response in preselected node. Eventually, a few MC convergence tests are performed in order to acquire a notion about their rate.

Chapter 4 treats the right hand side of the system in Eq. (2.1), *i.e.* the stochastic processes of an active crowd and its spatial distribution. Firstly, the Gaussian approximation in terms of a linear combination of AR(2) processes (continuous-time auto-regression

of the second order) is performed. Random distribution of an active crowd is realized via random indicator variables, with possible mutual interactions assumed by means of homogeneous isotropic covariance field. Secondly, non-Gaussian approximations are performed, namely by means of translation and Poisson white noise processes. Polyspectra and solution in frequency domain is also briefly reviewed.

Chapter 5 generalizes properties of the biodynamic models to being random, *i.e.* assumes the differential operator of Eq. (2.1) random, but independent of the right hand side. Referring to previous chapter, only the second-order moment properties are treated employing Taylor series method.

Chapter 6 encompass all the previously introduced sources of randomness into the final global model. Naturally, the resulting system comprises the stochastic differential operator and right hand side with large uncertainties, moreover with mutual dependencies. Hence, the second-order moment properties are obtained with more difficulties. An attempt was, however, made.

The last **Chapter 7** brings concluding summary with remarks, design recommendations and future prospects of the introduced method. Overall efficiency and performance is compared on the basis of MC simulation throughout the thesis and here is only briefly summarized.

In the first appendix, **Appendix A**, there it is given a short overview of the concepts from the theory of probability and stochastic processes employed widely throughout the thesis. Some references of the literature concerning these subjects are listed.

Since all the theoretical considerations were implemented in MATLAB environment with supporting `*.mex` files written and compiled in C++, **Appendix B** gives a short overview of implementation including also the MC simulation.

Finally, in **Appendix C** the list of toy structures employed throughout the thesis is presented. More detailed information about structure geometry, modal properties materials and possibilities for spectators is given.

Chapter 3

Monte Carlo Simulation

3.1 Introduction

Monte Carlo simulation provides a powerful tool for estimation of the response statistics. Generality and complexity are the main advantages of this robust method. Nevertheless, serious limitation is the computational overhead when highly complex systems or states with low probabilities are treated. Overall flow-chart in Fig. 3.1 shows the main parts of this method: first, N samples of random variables and functions in order to assess the system and its inputs are generated; then, N independent deterministic dynamic analysis are performed together with a statistical data processing of the calculated outputs; assessment of the structure safety and serviceability concludes the analysis. The only condition in order to employ the MC is the existence of computer algorithms for solving corresponding deterministic problems, appropriate generators of random variables and processes.

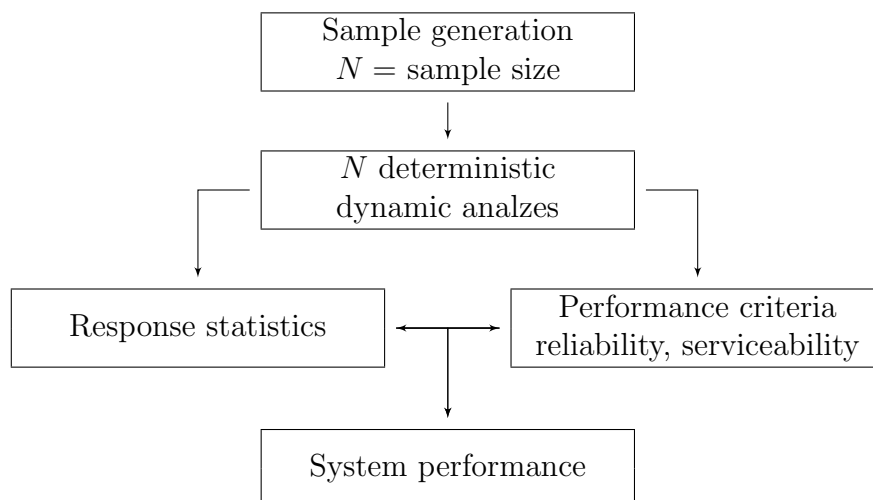


Figure 3.1: Flow-chart of MC simulation

In subsequent chapters, MC will be employed mainly for verification of the analytical or semi-analytical methods which will be introduced using the SDEs (stochastic differential equations). Let us note that total of N simulations require generation of Nn_a random forcing processes, n_a being the number of active spectators, and Nn_pk_p random variables

with prescribed distributions describing passive crowd models, n_p being the number of passive spectators and k_p the number of parameters describing a single biodynamic model. For more reliable representation of the output at least hundreds or rather thousands of realizations are needed, *cf* Sec. 3.6.

3.2 Forcing terms

In this section, more detailed description of a single realization of the force measured at the force plate and of two MC generators will be given, *i.e.* of the components of $\mathbf{F}(t, \omega)$ in Eq. (2.1). Particular realization comprise a sequence of pulses located on the time axis with jumping period equal to $T_p = 1/f_p$, up to some scatter, where f_p denotes the basic jumping frequency, typically $f_p \in (1, 3.5)$ Hz. Shapes of individual impulses are frequency-dependent, *cf* Fig. 3.2. Whereas for $f_p \geq 2$ the approximation based on segments of

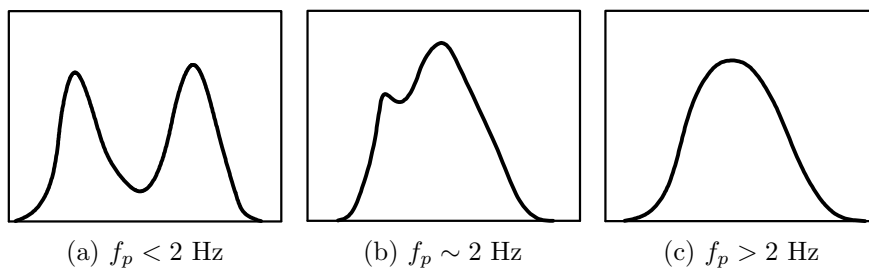


Figure 3.2: Three characteristic pulse shapes after Sim [51], (a) double peaked, (b) merging, (c) single peaked

trigonometric functions or their powers is sufficient, for lower jumping frequencies it is not. More sophisticated characterization can be based *e.g.* on linear combination of Gaussian bell-shaped functions [41], or on the analogy with time-dependent mass SDOF system [35].

For further purposes, procedure according to Sim [51] will be described and subsequently employed. Generator is capable to simulate only realizations of discrete jumping frequencies, $f_p = 1.5, 2.0, 2.67$ and 3.5 Hz. The main idea is to capture the lack of synchronization between the individual's timing subjected to some periodic audio-visual stimulus, *e.g.* metronome beep, $t_k - t_{\text{beep},k}$ where t_k denotes the centroid of k -th impulse. Mean delay, mostly positive and generally equal to 0.1 s for all jumping frequencies, its scatter and the relations between them are modelled through one or several random variables. As a matter of fact, the best coordination in terms of the mean delay is for $f_p = 2$ and 2.67 Hz, and in terms of the scatter it is for $f_p = 2.67$ Hz. Mean delay and its scatter are treated as independent, nevertheless in each realization the mean delay is fixed, and the delay scatter is treated as AR(1) time series having a short memory. For all jumping frequencies, the normalized impulse shapes are assumed in the form

$$F(t) = k_p \cos^2 \left(\frac{\pi t}{t_p} \right), \quad -\frac{t_p}{2} \leq t \leq \frac{t_p}{2}, \quad (3.1)$$

cf analogous Eq. (1.5). With the help of the conservation of linear momentum and assuming $t_p \rightarrow 0$ for ideally elastic collision, the relation between the impulse size $I_k = \int_{-t_p/2}^{t_p/2} F(t) dt = \frac{k_p t_p}{2}$ and its timing is derived as $I_k = (t_{k+1} - t_{k-1})/2$. Finally, the contact

ratio is described as a Gaussian random variable. Further details and implementation technicalities are given in [51]; several weight normalized realizations for particular f_p s are depicted in Fig. 3.3.

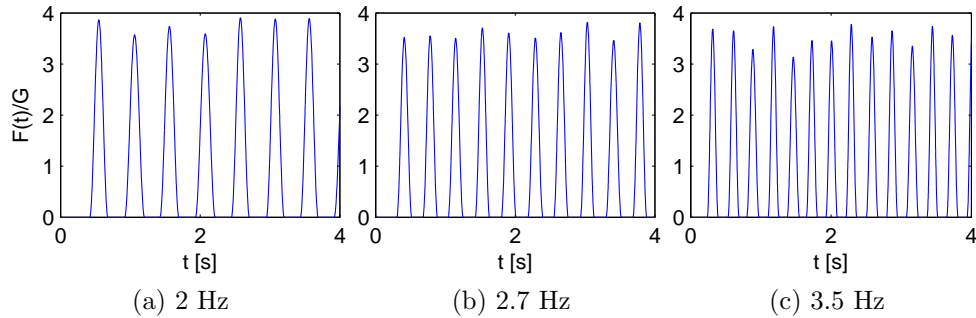


Figure 3.3: Typical realizations of single, weight normalized jumping processes according to Sim [51]

For completeness, let us briefly describe more recently developed approach due to Racic and Pavic [40], generalizing concepts introduced by Sim in several ways. Generator is capable to simulate individual processes with jumping frequencies in the whole range $f_p \in (1.4, 2.8)$ Hz employing electrocardiogram techniques. Sequence of the time differences $t_k - t_{k-1}$ is regarded as a random series with prescribed spectral density, t_k represents now the beginning of a k -th pulse, normalized impulse sizes are treated as AR(1) series. The method also captures asymmetry, pulse shapes being described as

$$F(t) = \sum_{i=1}^n a_i e^{-\frac{(t-t_i)^2}{2b_i}}, \quad 0 \leq t \leq t_p, \quad (3.2)$$

where a_i and b_i denote appropriate constants.

Phenomenon of synchronization is recognised when a group of spectators attempt to jump in phase with a given frequency. Degree of coordination is expressed as the ratio of the real to the ideally synchronized load. Model after Sim achieves group effect equal to 0.82 which is independent of a crowd size, while the measurements performed by Tuan and Ebrahimipour gives 0.65 and 0.53, *cf* [55].

3.3 Biodynamic models

The purpose of this section is to give a short overview of discrete biodynamic models available in the literature. Having on mind a reasonable degree of simplicity, we will restrict ourselves only to the case of discrete uni-axial models. These are with one or several DOFs in serial or parallel connection, possibly supplemented with attached rigid mass. Their parameters can be treated as deterministic, *cf* Tab. 3.1 and [47], or as random variables. In Tab. 3.2, mean values and standard deviations of modal and some physical characteristics published in [51] are given; Tab. 3.3 then gives the probabilistic characteristics of the physical quantities for SDOF model with a rigid mass based upon data published in [56]. The meaning of particular variables used for description is captured in Fig. 3.4. Let us note that in the case of MDOF models, the parameters do not reflect

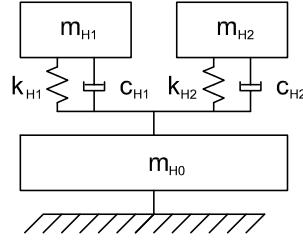


Figure 3.4: Scheme of a discrete uni-axial biodynamic model with physical meaning of individual parameters

the individual parts of a human body, but are derived rather on the basis of the best agreement of the model with the measured data, usually in terms of mechanical impedance or apparent mass. The modal characteristics specify several first eigenfrequencies of entire human body, corresponding eigenmodes are then typically caused by the longitudinal vibrations of human skeleton and shear vibrations of soft tissues together with internal organs. Generalizations to two or three-dimensional models are also available.

3.4 Computational aspects

As was mentioned in introductory Chap. 2, the continuous mechanical system representing a grandstand is discretized via FEM, yielding a large system of the second order differential equations with constant, sparse and generally random coefficient matrices. Active spectators are introduced as forcing terms and passive as added DOFs. The dynamic analysis is performed N times, and hence it is convenient to project the problem onto some subspace to be specified hereafter in order to lower the computational burden.

3.4.1 FEM discretization

Since the system is assumed linear, FEM discretization is employed in its standard, simplest and well known form, as is presented in many excellent theoretical books *e.g.* [10, 44] or in those more applied, such as [4, 5, 59, 60]. The output of the FEM discretization procedure consists of the system matrices $\mathbf{K}_S, \mathbf{M}_S, \mathbf{C}_S \in \mathbb{R}^{n_{\text{DOF},S} \times n_{\text{DOF},S}}$, $n_{\text{DOF},S} \sim 10^5$ or 10^6 , sparse, symmetric and positive definite. For computation, it is convenient to employ the Rayleigh damping which expresses the damping matrix as $\mathbf{C}_S = \alpha \mathbf{K}_S + \beta \mathbf{M}_S$, where α and β are coefficients acquired from measured, estimated or a priori known damping coefficients of any two given eigenfrequencies, *cf* [4]. $n_{\text{DOF},S}$ denotes the number of DOFs of the structure, *i.e.* generalized coordinates, numbered with code numbers; the subset of code numbers where the passive spectators are situated is denoted \mathbf{n}_p , for the full discussion please refer to Sec. 3.5.1. The system of biodynamic models is introduced through matrices $\mathbf{K}_{HH}, \mathbf{M}_{HH}, \mathbf{C}_{HH} \in \mathbb{R}^{n_{\text{DOF},H} \times n_{\text{DOF},H}}$, $n_{\text{DOF},H} \sim 10^3$ or 10^4 ; in the case of SDOF models, the matrices are diagonal with entries from Tab. 3.1, $n_{\text{DOF},H} = n_p$. Coupling with the structure is provided through $\mathbf{K}_{SH}, \mathbf{C}_{SH} \in \mathbb{R}^{n_{\text{DOF},S} \times n_{\text{DOF},H}}$, $\mathbf{K}_{HS}, \mathbf{C}_{HS} \in \mathbb{R}^{n_{\text{DOF},H} \times n_{\text{DOF},S}}$, $\mathbf{K}_{SH} = \mathbf{K}_{HS}^T$, $\mathbf{C}_{SH} = \mathbf{C}_{HS}^T$ matrices with nonzero entries in those rows taken from the set \mathbf{n}_p . Coupled human-grandstand system is described by \mathbf{K} ,

Damped SDOF system – seated spectator						
Model	Physical characteristics			Modal characteristics		
Coermann 1962 ¹	m_H	86.20	kg	f_H	5.00	Hz
	k_H	85.25	kN/m	ξ_H	0.32	
	c_H	1.72	kNs/m			
Damped two DOF system – seated spectator						
Wei and Griffin 1998 (parallel) ²	m_{H_1}	36.20	kg	f_{H_1}	4.90	Hz
	k_{H_1}	35.01	kN/m	ξ_{H_1}	0.36	
	c_{H_1}	0.82	kNs/m			
	m_{H_2}	8.90	kg	f_{H_2}	9.70	Hz
	k_{H_2}	33.25	kN/m	ξ_{H_2}	0.44	
	c_{H_2}	0.48	kNs/m			
	m_{H_0}	5.60	kg			
Suggs 1969 ³	m_{H_1}	36.30	kg	f_{H_1}	4.50	Hz
	k_{H_1}	28.45	kN/m	ξ_{H_1}	0.23	
	c_{H_1}	0.47	kNs/m			
	m_{H_2}	12.50	kg	f_{H_2}	5.50	Hz
	k_{H_2}	15.03	kN/m	ξ_{H_2}	0.31	
	c_{H_2}	0.27	kNs/m			
Damped SDOF system – standing spectator						
Brownjohn 1999	m_H	80.00	kg	f_H	4.90	Hz
	k_H	82.00	kN/m	ξ_H	0.37	
	c_H	1.95	kNs/m			
Damped 2 DOF system – standing spectator						
ISO 5982 (parallel)	m_{H_1}	62.00	kg	f_{H_1}	5.00	Hz
	k_{H_1}	62.00	kN/m	ξ_{H_1}	0.37	
	c_{H_1}	1.46	kNs/m			
	m_{H_2}	13.00	kg	f_{H_2}	12.50	Hz
	k_{H_2}	80.00	kN/m	ξ_{H_2}	0.46	
	c_{H_2}	0.93	kNs/m			

¹ Based on the mechanical impedances of 8 men² Based on apparent masses of 60 people³ Based on the mechanical impedances of 11 men

Table 3.1: Parameters of the discrete biodynamic models, [47]

Position / Parameters	Eigfrequency Hz				Relative damping			
	f_1		f_2		ξ_1		ξ_2	
	μ	σ	μ	σ	μ	σ	μ	σ
Seated man	5.1	0.58	9.3	2.01	0.311	0.1011	0.437	0.4341
Seated woman	5.3	1.06	9.2	2.85	0.385	0.1490	0.317	0.1163
Seated children	5.2	5.16	15.9	24.20	0.375	0.3923	0.312	0.3635
Standing men	5.8	0.54	12.6	2.34	0.331	0.0721	0.459	0.1721
Position / Parameters	Total mass kg				Partial mass kg			
	M_H		M_{H_0}		M_{H_1}		M_{H_2}	
	μ	σ	μ	σ	μ	σ	μ	σ
Seated man	58.2	14.00	7.6	3.01	37.4	10.36	13.7	7.01
Seated woman	50.8	6.70	7.3	1.75	32.0	6.02	11.1	5.45
Seated children	35.9	8.08	3.9	1.84	28.1	4.40	4.6	5.61
Standing men	73.9	7.57	—	—	43.1	16.90	28.5	19.07

Table 3.2: Mean values μ and standard deviations σ of undamped eigenfrequencies, relative dampings and masses of biodynamic models, [51]

	M_{H_0}	M_{H_1}	K_{H_1}	C_{H_1}
M_{H_0}	$4.470e - 5$	$-2.366e - 5$	$-1.159e - 2$	$-1.041e - 3$
M_{H_1}	$-2.366e - 5$	$2.292e - 4$	$1.570e - 1$	$4.956e - 3$
K_{H_1}	$-1.159e - 2$	$1.570e - 1$	225.110	4.390
C_{H_1}	$-1.041e - 3$	$4.956e - 3$	4.390	$1.468e - 1$
$\mathbf{E}(\bullet)$	$8.554e - 3$	$50.200e - 3$	51.904	1.367

Table 3.3: The first two moments of physical parameters of SDOF model with a rigid mass for seated man, data published in [56]; upper square matrix is the covariance matrix, the last row is the mean vector; units t, kN/m and kNs/m

\mathbf{M} and $\mathbf{C} \in \mathbb{R}^{n_{\text{DOF}} \times n_{\text{DOF}}}$ matrices, $n_{\text{DOF}} = n_{\text{DOF},S} + n_{\text{DOF},H}$, in Eq. (2.1),

$$\mathbf{A} = \begin{bmatrix} \mathbf{A}_{SS} & \mathbf{A}_{SH} \\ \mathbf{A}_{HS} & \mathbf{A}_{HH} \end{bmatrix} \quad (3.3)$$

where \mathbf{A} stands for mass, stiffness or damping matrix. \mathbf{A}_{SS} are derived from \mathbf{A}_S by adding constants of biodynamic models on i -th diagonal positions, $i \in \mathbf{n}_p$. Note also that biodynamic models are of nonproportional damping, hence \mathbf{C} eventually cannot be expressed as a linear combination of \mathbf{K} and \mathbf{M} .

Solution of the initial value problem, already discretized in space, is performed by discretization in the time domain and employing methods such as Newmark, Hilber-Hughes-Taylor and Central difference. Stability, accuracy, time step selection, and other issues are discussed in [4, 26, 30, 59]. All examples introduced in Appendix C and used throughout

this thesis are three-dimensional beam structures with Hermitian basis functions. Appropriate procedures are implemented in MATLAB[®] environment and described briefly in Appendix B. Any external FEM solver can be employed since only the matrices \mathbf{K}_{SS} , \mathbf{M}_{SS} and \mathbf{C}_{SS} are of interest.

Example 3.1. Assembly mass \mathbf{M} and stiffness \mathbf{K} matrices for the real grandstand in Appendix C.3 are depicted in Fig. 3.5 with indicated partition to particular submatrices and a total number of nonzero elements nz .

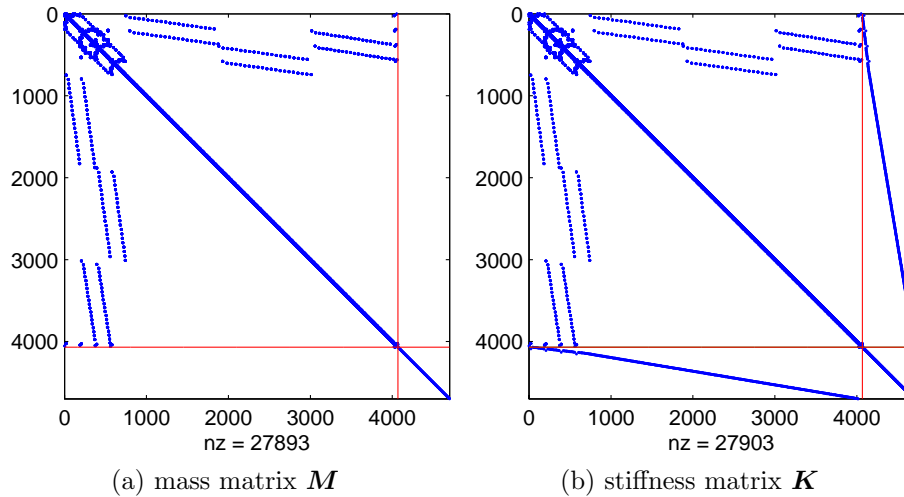


Figure 3.5: Mass and stiffness matrices of the real grandstand in Appendix C.3, nz being a number of nonzero elements

3.4.2 Reduced-order modelling

ROM (reduced-order model) plays an important role in the human-structure interaction as in many computational problems, and provides an efficient tool to replace the large-scale model by a smaller one, approximate, capable of capturing the dynamical behaviour while preserving essential properties of the larger one. Many reduced-order methods has been presented in the literature, nevertheless only some of them will be discussed further.

To describe briefly the general approach, for details see *e.g.* [16, 43], let us start with a deterministic counterpart of the full-order model in Eq. (2.1), where $\mathbf{z} \in \mathbb{R}^{n_{\text{DOF}}}$ and $\mathbf{f} \in \mathbb{R}^{n_a}$. The aim is to obtain a ROM

$$\mathbf{M}_r \ddot{\mathbf{z}}_r(t) + \mathbf{C}_r \dot{\mathbf{z}}_r(t) + \mathbf{K}_r \mathbf{z}_r(t) = \mathbf{G}_r \mathbf{f}(t), \quad t \in T, \quad (3.4)$$

where $\mathbf{z}_r \in \mathbb{R}^k$, $\mathbf{K}_r, \mathbf{M}_r, \mathbf{C}_r \in \mathbb{R}^{k \times k}$, $k \ll n_{\text{DOF}}$. Write

$$\mathbf{z}(t) \approx \tilde{\mathbf{z}}(t), \quad \tilde{\mathbf{z}}(t) = \mathbf{V} \mathbf{z}_r(t), \quad (3.5)$$

$\mathbf{V} \in \mathbb{R}^{n_{\text{DOF}} \times k}$ being a full-column rank matrix representing a time invariant basis of $\mathcal{V} = \text{span}[\mathbf{V}]$. The residual $\mathbf{r}(t) \in \mathbb{R}^{n_{\text{DOF}}}$, accounting for the fact that $\tilde{\mathbf{z}}(t)$ is not the exact solution, is constraint to be orthogonal to a subspace $\mathcal{W} = \text{span}[\mathbf{W}]$ defined by a test basis $\mathbf{W} \in \mathbb{R}^{n_{\text{DOF}} \times k}$, a full-column rank matrix, $\mathbf{W}^T \mathbf{r}(t) = \mathbf{0}$. Hence, left-multiplying

Eq. (2.1) after the insertion from Eq. (3.5) leads to the Petrov-Galerkin projection-based Eqns. (3.4), where

$$\begin{aligned} \mathbf{K}_r &= \mathbf{W}^\top \mathbf{K} \mathbf{V}, & \mathbf{M}_r &= \mathbf{W}^\top \mathbf{M} \mathbf{V} \\ \mathbf{C}_r &= \mathbf{W}^\top \mathbf{C} \mathbf{V}, & \mathbf{G}_r &= \mathbf{W}^\top \mathbf{G}. \end{aligned} \quad (3.6)$$

Hence, the solution $\tilde{\mathbf{z}}(t)$ is understood as a projection $\mathbf{\Pi}_{\mathbf{V}, \mathbf{W}} \mathbf{z}(t)$ onto \mathcal{V} parallel to \mathcal{W} , $\mathbf{\Pi}_{\mathbf{V}, \mathbf{W}}$ being a projector. If $\mathbf{W} = \mathbf{V}$, the method is called a Galerkin projection. The objective is to find an appropriate spaces with their bases capable to reproduce most accurately the behaviour of the system yielding so-called high-fidelity models.

3.4.2.1 Modal superposition

The first method, most common in structural dynamics, is the modal superposition, or singular value decomposition. In this case $\mathbf{W} = \mathbf{V} = [\mathbf{v}_1, \dots, \mathbf{v}_k]$, \mathbf{v}_i being the eigenvectors of the generalized eigenvalue problem $\mathbf{K} \mathbf{v}_i = \lambda_i \mathbf{M} \mathbf{v}_i$, under the assumption of a negligible damping. To reflect the behaviour of the system excited by an active crowd, the frequency interval at least of $[0, 10]$ Hz should be considered. Since the eigenfrequencies of all biodynamic models are about 5 Hz according to Tab. 3.1, the number of eigenmodes k in \mathbf{V} is significantly increased and the method is hence inappropriate.

Example 3.2. The spectrum with the effect of damping for cantilever and real grandstand, Appendices C.2 and C.3, for the case of empty and fully occupied structures with a passive crowd according to Coermann, Tab. 3.1, are depicted in Fig. 3.6 below in the complex plain. It is seen that in both cases the number of eigenfrequencies is increased by the number of biodynamic models, eigenvalues cumulate near $4.7 \cdot 2\pi \approx 30$ rad/s.

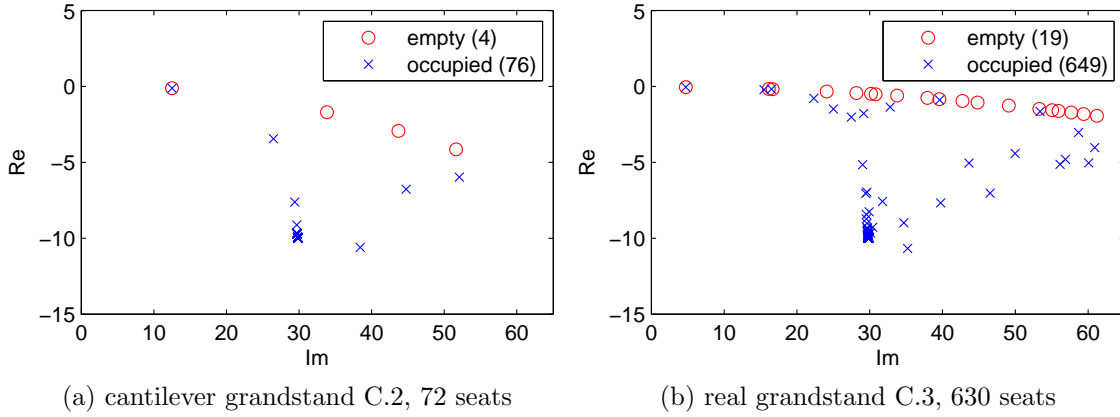


Figure 3.6: Spectrum of the cantilever and real grandstand, the case of empty and fully occupied structures with a passive crowd; biodynamic models according to Coermann used

3.4.2.2 Krylov subspace projection

KS (Krylov subspace) method comprises a projection onto a second-order Krylov subspace $\mathcal{G}_n(\mathbf{A}, \mathbf{B}; \mathbf{u})$, $\mathbf{A}, \mathbf{B} \in \mathbb{R}^{n_{\text{DOF}} \times n_{\text{DOF}}}$, $\mathbf{u} \in \mathbb{R}^{n_{\text{DOF}}}$, $\mathcal{G}_n(\mathbf{A}, \mathbf{B}; \mathbf{u}) = \text{span}[\mathbf{v}_0, \dots, \mathbf{v}_{k-1}]$,

cf [2], where

$$\begin{aligned} \mathbf{v}_0 &= \mathbf{u} \\ \mathbf{v}_1 &= \mathbf{A}\mathbf{v}_0 \\ \mathbf{v}_j &= \mathbf{A}\mathbf{v}_{j-1} + \mathbf{B}\mathbf{v}_{j-2}. \end{aligned} \quad (3.7)$$

It is known that the projection is equivalent to Padé approximation, matching the moments of the transfer function $\mathbf{H}(s)$, expressed as a Laplace transform of the differential operator in Eq. (2.1),

$$\mathbf{H}(s) = (s^2\mathbf{M} + s\mathbf{C} + \mathbf{K})^{-1}, \quad s \in \mathbb{C}. \quad (3.8)$$

To shift the expansion about the point s_0 , the following substitution is introduced

$$\begin{aligned} \mathbf{A} &= -(s_0^2\mathbf{M} + s_0\mathbf{C} + \mathbf{K})^{-1}(\mathbf{C} + 2s_0\mathbf{M}) \\ \mathbf{B} &= -(s_0^2\mathbf{M} + s_0\mathbf{C} + \mathbf{K})^{-1}\mathbf{M}. \end{aligned} \quad (3.9)$$

The appropriate basis is obtained with the SOAR (second-order Arnoldi algorithm), cf [3]. Under the symmetry assumptions of the \mathbf{K} , \mathbf{M} and \mathbf{C} matrices, the ROM matches the first $2k$ moments of the full system.

3.4.2.3 Proper orthogonal decomposition

POD (proper orthogonal decomposition) [16], also known as Karhunen-Loève decomposition, is a powerful tool for finding an orthogonal projector $\mathbf{\Pi}_{\mathbf{V},\mathcal{V}}$ of fixed rank k minimizing

$$J(\mathbf{\Pi}_{\mathbf{V},\mathcal{V}}) = \int_{t \in T} \|\mathbf{z}(t) - \mathbf{\Pi}_{\mathbf{V},\mathcal{V}}\mathbf{z}(t)\|_{L^2}^2 dt, \quad (3.10)$$

where $\|\bullet\|_{L^2}$ denotes the L^2 norm of \bullet . The subspace $\mathcal{V} = \text{span}[\mathbf{V}]$ minimizing $J(\bullet)$ is the invariant subspace of $\mathbf{K}_{\text{POD}} \in \mathbb{R}^{n_{\text{DOF}} \times n_{\text{DOF}}}$,

$$\mathbf{K}_{\text{POD}} = \int_{t \in T} \mathbf{z}(t) \mathbf{z}^\top(t) dt. \quad (3.11)$$

The data are usually discrete, so-called "snapshots", $\mathbf{z}(t_i)$, $i = 1, \dots, n_{\text{snap}}$. Hence, the integration is replaced with a sum, $\mathbf{K}_{\text{POD}} = \mathbf{Z}\mathbf{Z}^\top$, where $\mathbf{Z} \in \mathbb{R}^{n_{\text{DOF}} \times n_{\text{snap}}}$, $\mathbf{Z} = [\mathbf{z}(t_1)\sqrt{w_1}, \dots, \mathbf{z}(t_{n_{\text{snap}}})\sqrt{w_{n_{\text{snap}}}}]$, w_i being the integration weights. Since the non-zero eigenvalues of \mathbf{K}_{POD} are the same as of $\mathbf{R}_{\text{POD}} = \mathbf{Z}^\top\mathbf{Z}$, $\mathbf{R}_{\text{POD}} \in \mathbb{R}^{n_{\text{snap}} \times n_{\text{snap}}}$, $n_{\text{snap}} \ll n_{\text{DOF}}$, eigenproblem $\mathbf{R}_{\text{POD}}\boldsymbol{\psi}_i = \lambda_i\boldsymbol{\psi}_i$, is solved instead for \mathbf{K}_{POD} with the transformation $\mathbf{V} = \mathbf{Z}\boldsymbol{\Psi}\boldsymbol{\Lambda}^{-1/2}$, $\boldsymbol{\Psi} = [\boldsymbol{\psi}_1, \dots, \boldsymbol{\psi}_{n_{\text{snap}}}]$, $\boldsymbol{\Lambda} = \text{diag}[\lambda_1, \dots, \lambda_{n_{\text{snap}}}]$. Analogue to \mathbf{K}_{POD} in frequency domain, or Balanced POD can be also employed. Method consists in a training on quite short realizations with subsequent projection.

3.4.2.4 Modal synthesis

This last method, MS (modal synthesis), is based on rather heuristic considerations. Namely, the system is divided into two subsystems, a grandstand and a passive crowd. The

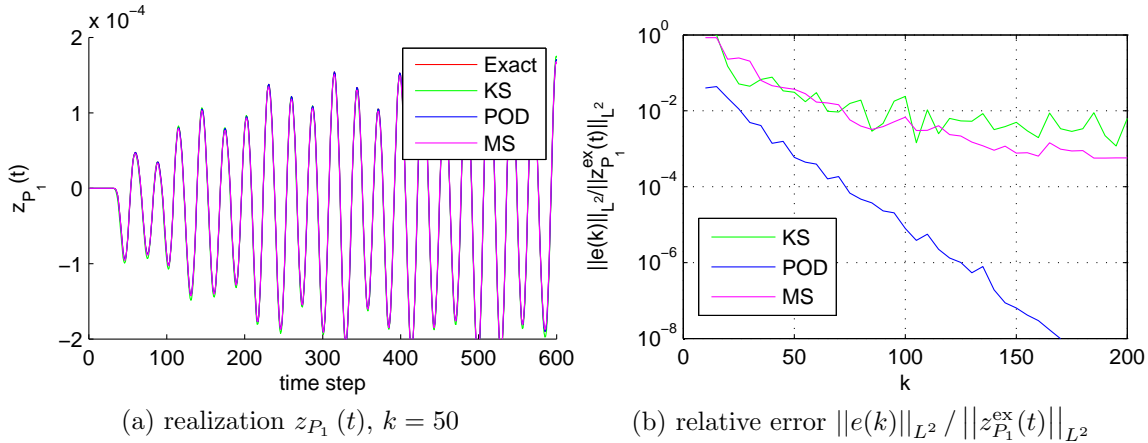
Model	Exact	KS	POD	MS
Time [s]	29.6	1.4	4.6	0.5

Table 3.4: Time consumptions of ROMs in comparison with the full system, $k = 50$

bases $\mathbf{V}_{SS} = [\mathbf{v}_{S,1}, \dots, \mathbf{v}_{S,n_{\text{eig},S}}]$ and $\mathbf{V}_{HH} = [\mathbf{v}_{H,1}, \dots, \mathbf{v}_{H,n_{\text{eig},H}}]$ are computed separately. In the case of the grandstand, the generalized eigenproblem $\mathbf{K}_{SS}\mathbf{v}_{S,i} = \lambda_{S,i}\mathbf{M}_{SS}\mathbf{v}_{S,i}$ in standard form is solved. Since the matrices \mathbf{K}_{HH} and \mathbf{M}_{HH} are diagonal for the SDOF biodynamic models, only one eigenvalue λ_H of multiplicity n_p with ambiguous, linearly independent basis in $\mathbb{R}^{n_{\text{DOF},H}}$ solve the problem. The simplest approach seems to be a projection of \mathbf{V}_{SS} onto \mathbb{R}^{n_p} , considering only the DOFs from the set \mathbf{n}_p . Any other basis, *e.g.* trigonometric is also possible. Eventually, the global basis is assembled as

$$\mathbf{W} = \mathbf{V} = \begin{bmatrix} \mathbf{V}_{SS} & \mathbf{0}_{n_{\text{DOF},S} \times n_{\text{eig},H}} \\ \mathbf{0}_{n_p \times n_{\text{eig},S}} & \mathbf{V}_{HH} \end{bmatrix}. \quad (3.12)$$

Example 3.3. The real grandstand in Appendix C.3 is fully occupied by a passive crowd. Vertical response is measured in P_1 node, an input is applied in P_3 node. Problem form a single-input single-output system, the comparison of time solutions is depicted in Fig. 3.7 together with the relative error, $e = z_{P_1}^{\text{ex}}(t) - z_{P_1}^{\bullet}(t)$, \bullet standing for any of ROM methods, $z_{P_1}^{\text{ex}}(t)$ for full order solution and $z_{P_1}^{\bullet}(t)$ for a ROM solution. Krylov subspace for $s_0 = 0$ used, comparison of the overall computational efficiency is summarized in Tab. 3.4, Fig. 3.8 then captures the Bode plots.

Figure 3.7: Response of the P_1 node and relative error as a function of the subspace dimension $\dim(\mathcal{V}) = k$

3.5 Spatial crowd distribution

This part of the MC simulation is quite intricate, since almost no relevant assumptions can be made about the spatial distribution of an active crowd. Some conclusions, however, concerning the number of jumping spectators can still be derived from the anticipated use of the structure or planned types of events, *e.g.* pop and rock concerts, sport events.

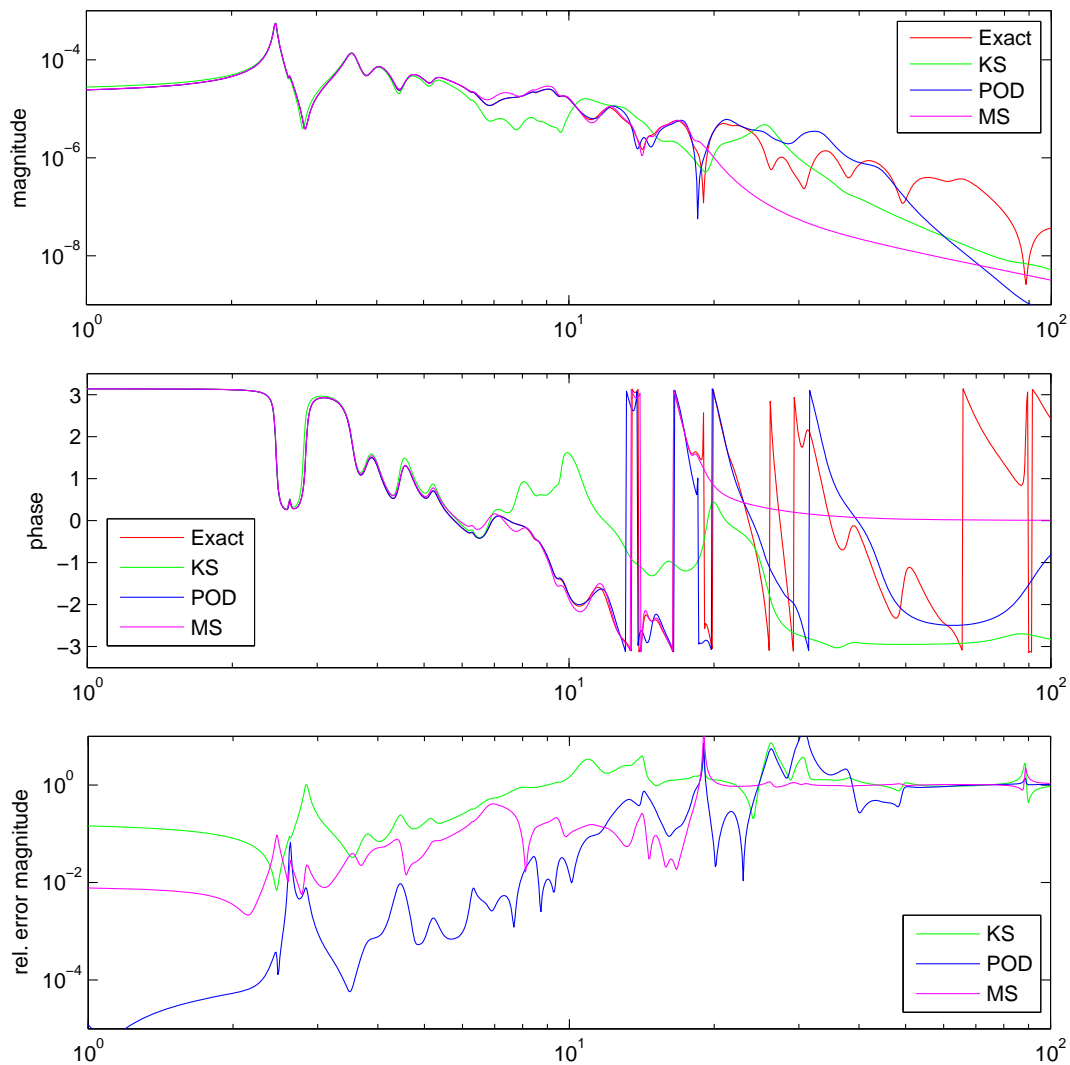


Figure 3.8: Bode plot of the FRF for $k = \dim(\mathcal{V}) = 50$ and relative error for example in Appendix C.3

3.5.1 Random distribution of an active crowd

The set of code numbers where the spectators can be situated is denoted \mathbf{n}_s having the cardinality $\#\mathbf{n}_s = n_s$. Assuming fully occupied structure, particular realization of the spatial crowd distribution consists in a disjoint decomposition of \mathbf{n}_s , $\mathbf{n}_s = \mathbf{n}_a \cup \mathbf{n}_p$, where $\mathbf{n}_a \cap \mathbf{n}_p = \emptyset$, $\#\mathbf{n}_a = n_a$ and $\#\mathbf{n}_p = n_p$. \mathbf{n}_a and \mathbf{n}_p are sets of those code numbers where the active and the passive spectators are situated. In the case of an active crowd only, it suffices to pick a subset \mathbf{n}_a of \mathbf{n}_s with $\mathbf{n}_p = \emptyset$. Knowing the loading scenario, which can be specified as the ratio n_a/n_s , the spatial distribution is realized. For further details see Sec. 4.2.2, where uncertain spatial distribution of an active crowd is realized through random indicator variables.

3.5.2 Mean-worst spatial distribution of an active crowd

Another approach consists in finding the worst response that the crowd is capable to excite. Clearly, such a distribution can be found in the mean sense for an active crowd

only, with no passive spectators damping the system and complicating unbearably the procedure. The occurrence of such a state is, however, questionable. Having n_s positions for spectators yields $\binom{n_s}{n_a}$ possibilities of their spatial distribution resulting in low probabilities. As will be shown later on in Chap. 4, the mean value of the forcing term can be satisfactorily approximated with a truncated Fourier series, *cf* also Eq. (1.6). Omitting G , this expression is rewritten as

$$\mu_F(t) = 1 + \sum_{k=1}^n r_k \sin(2k\pi f_p t + \phi_k) = \sum_{k=0}^n r_k \mathbb{I}m \left[e^{i(2k\pi f_p t + \phi_k)} \right], \quad (3.13)$$

where $r_0 = 1$, $\phi_0 = \pi/2$, $\mathbb{I}m$ denotes the imaginary part and i is the complex unit. The solution is then found using the FRF (frequency response function). Left hand side operator in Eq. (2.1) is now deterministic and no passive spectators occupy the structure, hence taking the expectation yields

$$\mathbf{M}\ddot{\boldsymbol{\mu}}_Z(t) + \mathbf{C}\dot{\boldsymbol{\mu}}_Z(t) + \mathbf{K}\boldsymbol{\mu}_Z(t) = \mathbf{G} \sum_{k=0}^n \mathbf{r}_k e^{i\phi_k} e^{i2k\pi f_p t}, \quad t \in \mathbb{R}, \quad (3.14)$$

$\mathbf{r}_k = [r_k, r_k, \dots]^\top$, $\mathbf{E}\mathbf{Z}(t) = \boldsymbol{\mu}_Z(t)$. Taking the unitary Fourier transform gives

$$\mathbf{H}^{-1}(\xi) \hat{\boldsymbol{\mu}}_Z(\xi) = \mathbf{G} \sum_{k=0}^n \mathbf{r}_k e^{i\phi_k} \delta(kf_p - \xi), \quad \xi \in \mathbb{R}, \quad (3.15)$$

where $\delta(\xi)$ is the Dirac delta distribution, $\hat{\boldsymbol{\mu}}_Z(\xi) = \mathcal{F}(\boldsymbol{\mu}_Z(t))(\xi)$, $\mathbf{H}(\xi)$ denotes the FRF with the analytical form

$$\mathbf{H}(\xi) = [-(2\pi\xi)^2 \mathbf{M} + i2\pi\xi \mathbf{C} + \mathbf{K}]^{-1}, \quad \xi \in \mathbb{R}, \quad (3.16)$$

$\mathbf{H}(\xi) = \mathbf{H}(s)|_{s=i2\pi\xi}$, ξ being an ordinary frequency. Taking the imaginary part of the inverse Fourier transform of Eq. (3.15) yields the solution

$$\boldsymbol{\mu}_Z(t) = \mathbb{I}m \left[\sum_{k=0}^n \mathbf{H}(kf_p) \mathbf{G} \mathbf{r}_k e^{i(2k\pi f_p t + \phi_k)} \right], \quad t \in \mathbb{R}. \quad (3.17)$$

Hence, it is necessary only to solve one real and n complex systems of linear equations.

Let us fix some particular code number, say m , with respect to which the worst spatial distribution of the crowd will be sought, $\mathbf{n}_s = [I_1, \dots, I_{n_s}]$. Then, an m -th row of Eq. (3.17) for a fully occupied structure by an active crowd is rewritten as

$$\mu_{Z,m}(t) = \sum_{i \in \mathbf{n}_s} \mathbb{I}m \left[\sum_{k=0}^n H_{mi}(kf_p) r_k e^{i(2k\pi f_p t + \phi_k)} \right] = \sum_{j=1}^{n_s} u_j(t), \quad t \in \mathbb{R}, \quad (3.18)$$

where $u_j(t)$ gives the displacement of an m -th code number owing to all harmonics of the load applied at j -th code number and time t . For a fixed time, each $u_j(t)$ can be considered whether contributes positively or negatively to $\mu_{Z,m}(t)$, and based on their signs such a subset of \mathbf{n}_s chosen to yield an extreme value. Repeating this procedure for

Occupancy	$\mu_{Z,P_1}^{\text{peak}}$ [m]	$\ddot{\mu}_{Z,P_1}^{\text{peak}}$ [m/s ²]
fully occupied	$1.852e - 2$	34.447
Fig. 3.9a	$4.014e - 2$	48.088
Fig. 3.9b	$3.370e - 2$	52.534

Table 3.5: Peak vertical displacements and accelerations in P_1 node for various occupation by an active crowd; the case of real grandstand in Appendix C.3

all $t \in [0, T_p]$ with a time step Δt gives the approximate global extreme and corresponding set of code numbers.

From computational point of view, it is convenient to rewrite $u_j(t)$ as element-by-element product of $\tilde{\mathbf{H}}, \mathbf{R}, \mathbf{E} \in \mathbb{R}^{n_s \times n}$ matrices,

$$u_j(t) = \text{Im} \left[\sum_{k=0}^n U_{jk}(t) \right], \quad U_{jk}(t) = \tilde{\mathbf{H}} \circ \mathbf{R} \circ \mathbf{E}(t), \quad (3.19)$$

where $U_{jk}(t)$ stores a contribution of the k -th harmonic of the load applied at code number I_j and at fixed time t . $(\mathbf{R} \circ \mathbf{E})_{ij} = R_{ij} E_{ij}$ with summation not implied over indices i and j is the Hadamard product, and

$$\tilde{\mathbf{H}} = [\mathbf{H}_{n_s m}(0f_p), \mathbf{H}_{n_s m}(1f_p), \dots, \mathbf{H}_{n_s m}(nf_p)], \quad (3.20)$$

$\mathbf{H}_{n_s m}(kf_p)$ being an n_s -subvector of the m -th column of the FRF computed as the solution of linear system obtained replacing the right hand side in Eq. (3.15) with \mathbf{e}_m , a column vector with 1 at m -th position,

$$\mathbf{R} = \begin{bmatrix} r_0 & r_1 & \dots & r_n \\ \vdots & \vdots & \ddots & \vdots \\ r_0 & r_1 & \dots & r_n \end{bmatrix}, \quad \mathbf{E} = \begin{bmatrix} e^{i(2 \cdot 0 \pi f_p t + \phi_0)} & e^{i(2 \cdot 1 \pi f_p t + \phi_1)} & \dots & e^{i(2 \cdot n \pi f_p t + \phi_n)} \\ \vdots & \vdots & \ddots & \vdots \\ e^{i(2 \cdot 0 \pi f_p t + \phi_0)} & e^{i(2 \cdot 1 \pi f_p t + \phi_0)} & \dots & e^{i(2 \cdot n \pi f_p t + \phi_n)} \end{bmatrix}. \quad (3.21)$$

Procedure is simply generalized to the set of code numbers m_1, m_2, \dots, m_q and when dynamic rather than peak displacement is of interest, it suffices to take $k = 1, \dots, n$ instead of $k = 0, \dots, n$. Spatial distribution in terms of peak acceleration is obtained twice differentiating Eqns. (3.18) and (3.19) with respect to time.

Example 3.4. Results for the real grandstand in Appendix C.3 are given in Fig. 3.9 where indicators yielding the extreme response in P_1 node are depicted. Fundamental harmonic $f_p = 2.7$ Hz, Fourier coefficients after [15] used, the first four amplitudes are $9/5, 9/7, 2/3, 9/55$ and phase shifts $-\pi/3, -2\pi/3, -\pi, 2\pi/3$. Tab. 3.5 compares particular displacements and accelerations.

3.6 MC convergence analysis

In this short paragraph we will give some convergence tests of the MC simulation on particular example to have an idea about the number of simulations N needed. Clearly,

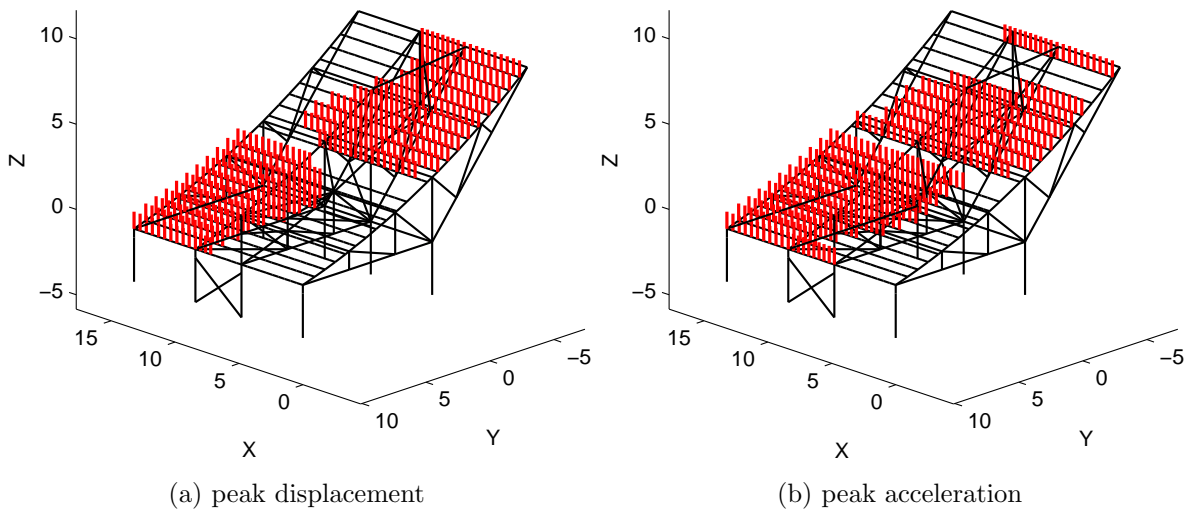


Figure 3.9: Two mean-worst spatial distributions of an active crowd, Fourier coefficients after Ellis [15], with respect to peak displacement and acceleration

in the case of the mean upcrossing rates the convergence strongly depends on the chosen level x , hence introduced example serves only as a demonstration.

Example 3.5. Convergence for the total mean upcrossings in the time interval $t \in [0, T]$ s, $n_x^+(T)$ for the cantilever grandstand in Appendix C.2 and the level x is depicted in Fig. 3.10. The response is measured in point P_1 , fixed and random spatial distribution of the mixed crowd assumed, structure is fully occupied. Corresponding measures are based on the interval of the stable response, excluding the transient part.

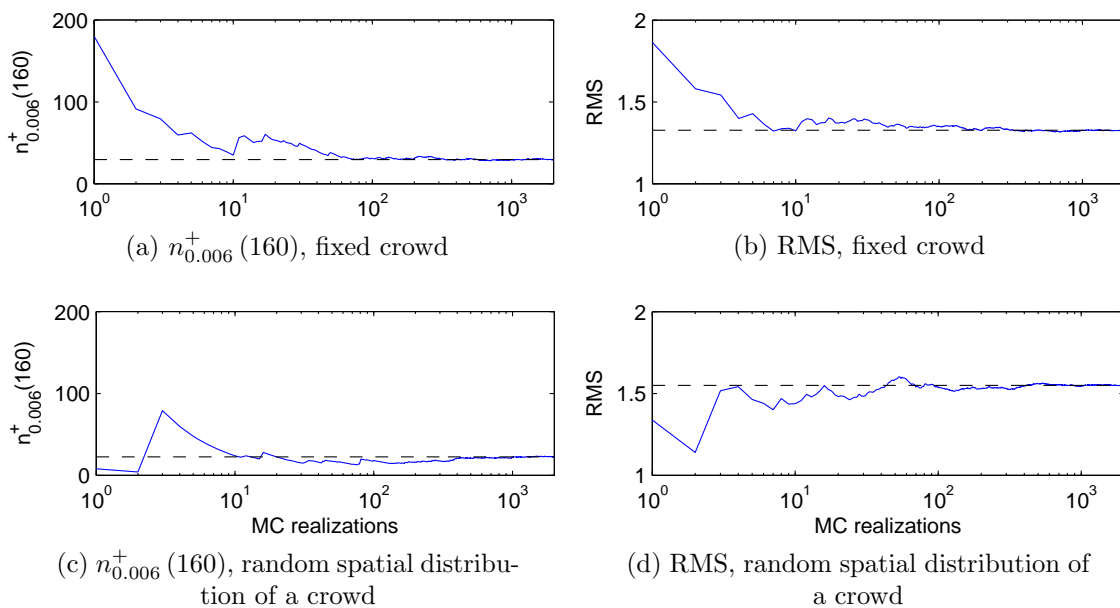


Figure 3.10: MC convergence for $n_x^+(T)$ and RMS; fixed and random spatial distribution of a crowd

3.7 Conclusion

In this chapter, an overview of the MC simulation has been given with emphasis laid upon the reduced modelling and the mean-worst spatial distribution of an active crowd. It has been shown that significant reduction of the model order is possible with several methods, however large errors were encountered when the model was oversimplified, including SDOF systems employed in some design approaches. For the purposes of the safety assessment, method for the mean-worst spatial distribution of an active crowd has been given. MC convergence analysis proved that at least hundreds, or better thousands of simulations have to be performed in order to obtain an accurate and reliable results.

Chapter 4

Deterministic system and stochastic input

4.1 Introduction

Our objective in this chapter is to give an overview of a possible approach to solution of the grandstand problem defined by Eq. (2.1) where only the vector processes $\mathbf{F}(t, \omega)$ and $\mathbf{Z}(t, \omega)$ are random, assuming the coefficient matrices deterministic and constant in time. From the physical point of view, this situation is equivalent to the fixed spatial distribution of a passive crowd with deterministic biodynamic models. Spatial distribution of an active crowd can possibly follow a random pattern.

Although the input forces are non-Gaussian, *cf* Fig. 3.3, the right hand side $\mathbf{F}(t, \omega)$ is assumed to be a Gaussian coloured vector process in the first approximation, *cf* also [45]. Such an approach can be justified in the first place by the fact that the RMS values, *i.e.* the second order moment properties, yield serviceability limits assessment, in the second place by the Central Limit and Rosenblatt theorems. Moreover, since only the quasi-stationary generators of an active crowd exist, the stationary probability distribution of the state vector is our principal objective.

Assessing the reliability limits of the structure, the Gaussian approximation can be considered as too coarse. Hence, the translation processes are employed to obtain a better agreement in the marginal distribution of the output displacements and upcrossing rates.

4.2 Gaussian input¹

To simplify subsequent expressions, let us apply expectation operator \mathbf{E} in Eq. (2.1) and subtract the result from it. We arrive at the set of two equations

$$\mathbf{M}\ddot{\boldsymbol{\mu}}_Z(t) + \mathbf{C}\dot{\boldsymbol{\mu}}_Z(t) + \mathbf{K}\boldsymbol{\mu}_Z(t) = \mathbf{G}\boldsymbol{\mu}_F(t), \quad t \geq 0, \quad (4.1)$$

$$\mathbf{M}\ddot{\tilde{\mathbf{Z}}}(t, \omega) + \mathbf{C}\dot{\tilde{\mathbf{Z}}}(t, \omega) + \mathbf{K}\tilde{\mathbf{Z}}(t, \omega) = \mathbf{G}\tilde{\mathbf{F}}(t, \omega), \quad t \geq 0, \quad (4.2)$$

for the mean value $\boldsymbol{\mu}_Z(t) = \mathbf{E}\mathbf{Z}(t)$ and centered process $\tilde{\mathbf{Z}}(t, \omega) = \mathbf{Z}(t, \omega) - \boldsymbol{\mu}_Z(t)$, forcing term is assumed in the form $\mathbf{F}(t, \omega) = \boldsymbol{\mu}_F(t) + \tilde{\mathbf{Y}}(t, \omega)$, $\mathbf{E}\tilde{\mathbf{Y}}(t, \omega) = \mathbf{0}$, $\boldsymbol{\mu}_F(t) =$

¹Partly reproduced from: O. Rokoš, J. Máca. The response of grandstands driven by filtered Gaussian white noise processes. *Advances in Engineering Software*, 72(0):85 – 94, 2014.

$\boldsymbol{\mu}_Y(t)$ and $\tilde{\mathbf{F}}(t) = \tilde{\mathbf{Y}}(t)$ in this particular case. Under certain conditions process $\tilde{\mathbf{Z}}(t)$ is approximately normal, and since SDE (4.2) is linear with deterministic coefficients, it is reasonable to accept Gaussian approximation also for $\tilde{\mathbf{Y}}(t)$. This consideration leads us to the Itô's calculus. Under Gaussian assumptions, the response will be completely specified by its mean $\boldsymbol{\mu}_Z(t)$ and covariance $\mathbf{c}_Z(t, s) = \mathbb{E} \left[\tilde{\mathbf{Z}}(t) \tilde{\mathbf{Z}}(s)^\top \right]$.

4.2.1 Deterministic distribution of a crowd

Assuming deterministic distribution of a crowd, the required quantities can be obtained from the time domain or from the frequency domain.

4.2.1.1 Solution in the time domain

Eq. (4.1) can be solved by direct integration or, more conveniently, by a Fourier series (or Fourier transform) assuming periodic mean $\boldsymbol{\mu}_Y(t)$, cf Sec. 3.5.2. Let us rewrite Eq. (4.2) as

$$\frac{d}{dt} \begin{bmatrix} \tilde{\mathbf{Z}}(t) \\ \dot{\tilde{\mathbf{Z}}}(t) \end{bmatrix} = \begin{bmatrix} \mathbf{0} & \mathbf{I} \\ -\mathbf{M}^{-1}\mathbf{K} & -\mathbf{M}^{-1}\mathbf{C} \end{bmatrix} \begin{bmatrix} \tilde{\mathbf{Z}}(t) \\ \dot{\tilde{\mathbf{Z}}}(t) \end{bmatrix} + \begin{bmatrix} \mathbf{0} \\ \mathbf{M}^{-1}\mathbf{G} \end{bmatrix} \tilde{\mathbf{Y}}(t), \quad t \geq 0, \quad (4.3)$$

or, in a more compact form,

$$\dot{\tilde{\mathbf{X}}}(t) = \mathbf{a}\tilde{\mathbf{X}}(t) + \mathbf{b}\tilde{\mathbf{Y}}(t), \quad t \geq 0, \quad (4.4)$$

where $\tilde{\mathbf{X}}$ is an \mathbb{R}^d -valued state-space vector stochastic process with zero mean, and \mathbf{a} and \mathbf{b} are (d, d) and (d, n_a) -matrices. The solution of this differential equation is given in the form

$$\tilde{\mathbf{X}}(t) = \boldsymbol{\theta}(t) \tilde{\mathbf{X}}(0) + \int_0^t \boldsymbol{\theta}(t-s) \mathbf{b}\tilde{\mathbf{Y}}(s) ds, \quad (4.5)$$

where $\boldsymbol{\theta}(t-s)$ denotes the Green function or the unit impulse response satisfying

$$\frac{\partial \boldsymbol{\theta}(t-s)}{\partial t} = \mathbf{a}\boldsymbol{\theta}(t-s), \quad t \geq s \geq 0, \quad (4.6)$$

$\boldsymbol{\theta}(0) = \mathbf{I}$ the identity and $\boldsymbol{\theta}(t-s) = \exp[\mathbf{a}(t-s)]$ can be expressed as a matrix exponential, cf [53]. Initial conditions $\tilde{\mathbf{X}}(0)$ will be set to zero for simplicity. Forcing term $\tilde{\mathbf{Y}}(t)$ can also satisfy its own SDE driven by Gaussian white noise $\mathbf{W}(t) = d\mathbf{B}(t)/dt$. For example, let $\hat{Y}_1(t)$ be a continuous-time Gaussian autoregression scalar process of order p , denoted as AR(p), cf [8]. Then $\hat{Y}_1(t) = \mathbf{e}_1^\top \mathbf{S}_1(t)$ where the state vector $\mathbf{S}_1(t) = [S_{1,1}(t), \dots, S_{1,p}(t)]^\top$ satisfies the Itô's equation

$$d\mathbf{S}_1(t) = \mathbf{A}_1 \mathbf{S}_1(t) dt + \mathbf{b}_1 dB(t), \quad (4.7)$$

$$\mathbf{A}_1 = \begin{bmatrix} 0 & 1 & 0 & \dots & 0 \\ 0 & 0 & 1 & \dots & 0 \\ \vdots & \vdots & \vdots & \ddots & \vdots \\ 0 & 0 & 0 & \dots & 1 \\ -a_p & -a_{p-1} & -a_{p-2} & \dots & -a_1 \end{bmatrix}, \quad \mathbf{e}_1 = \begin{bmatrix} 1 \\ 0 \\ \vdots \\ 0 \\ 0 \end{bmatrix} \quad \text{and} \quad \mathbf{b}_1 = \begin{bmatrix} 0 \\ 0 \\ \vdots \\ 0 \\ a_0 \end{bmatrix}.$$

Processes of this kind are also called filtered white noise processes or coloured processes, and they have a specific frequency content. Let us assume that $\tilde{Y}_i(t)$ of $\tilde{\mathbf{Y}}(t) = [\tilde{Y}_1(t), \dots, \tilde{Y}_{n_a}(t)]^\top$ are mutually independent AR(p_i) processes. Then we can merge Eqns. (4.3) and (4.7) to obtain one coupled system

$$d \begin{bmatrix} \tilde{\mathbf{Z}}(t) \\ \dot{\tilde{\mathbf{Z}}}(t) \\ \mathbf{S}_1(t) \\ \vdots \\ \mathbf{S}_{n_a}(t) \end{bmatrix} = \begin{bmatrix} \mathbf{0} & \mathbf{I} & \mathbf{0} & \dots & \mathbf{0} \\ -\mathbf{M}^{-1}\mathbf{K} & -\mathbf{M}^{-1}\mathbf{C} & \mathbf{M}^{-1}\mathbf{G}\mathbf{d}_1\mathbf{e}_1^\top & \dots & \mathbf{M}^{-1}\mathbf{G}\mathbf{d}_{n_a}\mathbf{e}_{n_a}^\top \\ \mathbf{0} & \mathbf{0} & \mathbf{A}_1 & \dots & \mathbf{0} \\ \mathbf{0} & \mathbf{0} & \mathbf{0} & \ddots & \mathbf{0} \\ \mathbf{0} & \mathbf{0} & \mathbf{0} & \dots & \mathbf{A}_{n_a} \end{bmatrix} \begin{bmatrix} \tilde{\mathbf{Z}}(t) \\ \dot{\tilde{\mathbf{Z}}}(t) \\ \mathbf{S}_1(t) \\ \vdots \\ \mathbf{S}_{n_a}(t) \end{bmatrix} dt + \begin{bmatrix} \mathbf{0} & \dots & \mathbf{0} \\ \mathbf{0} & \dots & \mathbf{0} \\ \mathbf{b}_1 & \dots & \mathbf{0} \\ \mathbf{0} & \ddots & \mathbf{0} \\ \mathbf{0} & \dots & \mathbf{b}_{n_a} \end{bmatrix} d\mathbf{B}(t), \quad (4.8)$$

where \mathbf{d}_i are column vectors with the unit in i -th position, and $\mathbf{B}(t)$ is an \mathbb{R}^{n_a} -valued Brownian motion. This approach is called a state augmentation method [19]. An extension to the case $\tilde{Y}_i(t) = \sum_{k=1}^n \hat{Y}_k(t)$, where $\hat{Y}_k(t)$ are mutually independent AR(p) processes, is carried out in an obvious manner. Eq. (4.8) can again be rewritten in compact form

$$d\mathbf{X}(t) = \mathbf{a}\mathbf{X}(t) dt + \mathbf{b}d\mathbf{B}(t), \quad t \geq 0, \quad (4.9)$$

and employing the Itô's formula, cf Appendix A, we arrive at the system of evolutionary equations for the response mean $\boldsymbol{\mu}_X(t)$ and covariance $\mathbf{c}_X(t, s)$

$$\dot{\boldsymbol{\mu}}_X(t) = \mathbf{a}\boldsymbol{\mu}_X(t), \quad t \geq 0, \quad (4.10)$$

$$\dot{\mathbf{c}}_X(t, t) = \mathbf{a}\mathbf{c}_X(t, t) + \mathbf{c}_X(t, t)\mathbf{a}^\top + \mathbf{b}\mathbf{b}^\top, \quad t \geq 0, \quad (4.11)$$

$$\frac{\partial \mathbf{c}_X(t, s)}{\partial t} = \mathbf{a}\mathbf{c}_X(t, s), \quad t > s \geq 0. \quad (4.12)$$

Since the driving forces $d\mathbf{B}(t)$ are Gaussian white noise and the coefficients are constant in time, the solution is an Ornstein-Uhlenbeck process with an existing stationary solution. In our case, stationary mean $\boldsymbol{\mu}_X = \mathbf{0}$ and covariance $\dot{\mathbf{c}}_X(t, t) = \dot{\mathbf{c}}_X(t - t) = \dot{\mathbf{c}}_X = \mathbf{0}$ which leads to the so-called continuous Lyapunov equation

$$\mathbf{0} = \mathbf{a}\mathbf{c}_X + \mathbf{c}_X\mathbf{a}^\top + \mathbf{b}\mathbf{b}^\top. \quad (4.13)$$

For details and further developments, see [19]. Since the stationary matrix \mathbf{c}_X contains only response displacements and velocities, the variances of the acceleration have to be computed through the following formula which is valid for weakly stationary processes

$$\mathbf{c}_{\dot{X}} = -\left. \frac{d^2 \mathbf{c}_X(t)}{dt^2} \right|_{t=0} = -\mathbf{a}^2 \mathbf{c}_X, \quad (4.14)$$

where \mathbf{a}^2 denotes matrix power and \mathbf{c}_X denotes the stationary covariance matrix of velocities and accelerations. Equation (4.14) is evaluated employing (4.12), which in our special case simplifies to

$$\mathbf{c}_X(t) = \boldsymbol{\theta}(t) \mathbf{c}_X = \exp[\mathbf{a}t] \mathbf{c}_X. \quad (4.15)$$

4.2.1.2 Solution in the frequency domain

Employing spectral decomposition of stationary random processes, the response variances are acquired through spectral density matrices $\mathbf{S}_{\tilde{Y}\tilde{Y}}$ and $\mathbf{S}_{\tilde{Z}\tilde{Z}}$, $(S_{\tilde{Y}\tilde{Y}}(\xi))_{ii} = \hat{s}_{\tilde{Y}}(\xi)$, $i = 1, \dots, n_a$, where $\hat{s}_{\tilde{Y}}(\xi)$ is a spectral density estimate of the centered forcing term,

$$\hat{s}_{\tilde{Y}}(\xi) = \mathbf{E} \int_{-\infty}^{\infty} b(x - \xi) I_T(\xi) dx, \quad (4.16)$$

$b(x)$ being some weight function, *cf* [1], and $I_T(\xi)$ denotes the corresponding periodogram

$$I_T(\xi) = \left| \int_0^T \tilde{Y}(t) e^{-i2\pi t \xi} dt \right|^2, \quad -\infty < \xi < \infty. \quad (4.17)$$

The diagonal form of $\mathbf{S}_{\tilde{Y}\tilde{Y}}$ suggests that we treat all input processes as independent. Knowing the spectral density matrix of the input, we obtain the spectral density matrix of the output process according to [53]

$$\mathbf{S}_{\tilde{Z}\tilde{Z}}(\xi) = \mathbf{H}(\xi) \mathbf{G} \mathbf{S}_{\tilde{Y}\tilde{Y}}(\xi) \mathbf{G}^T \mathbf{H}^\dagger(\xi) \quad (4.18)$$

where $\mathbf{H}^\dagger(\xi)$ denotes a Hermitian transpose to $\mathbf{H}(\xi)$, to the FRF. The variance of the stationary scalar process $\tilde{Z}(t)$ with two-sided spectral density $s_{\tilde{Z}}(\xi)$ or with one-sided spectral density $g_{\tilde{Z}}(\xi)$ is evaluated as

$$\sigma_{\tilde{Z}}^2 = \int_{-\infty}^{\infty} s_{\tilde{Z}}(\xi) d\xi = \int_0^{\infty} g_{\tilde{Z}}(\xi) d\xi \quad (4.19)$$

and the variance of time derivative $\dot{\tilde{Z}}(t)$

$$\sigma_{\dot{\tilde{Z}}}^2 = \dot{\sigma}_{\tilde{Z}}^2 = \int_{-\infty}^{\infty} (2\pi\xi)^2 s_{\tilde{Z}}(\xi) d\xi = \int_0^{\infty} (2\pi\xi)^2 g_{\tilde{Z}}(\xi) d\xi. \quad (4.20)$$

By analogy for higher time derivatives, applying higher powers of angular frequency $2\pi\xi$, we compute so-called spectral moments $\lambda_k = \int_0^{\infty} (2\pi\xi)^k g_{\tilde{Z}}(\xi) d\xi$.

Solution in frequency domain can be performed also through linearized FRF (in ξ) based on Eq. (4.4) instead of Eq. (4.2), now having the form

$$\mathbf{H}(\xi) = (i2\pi\xi \mathbf{I}_{d \times d} - \mathbf{a})^{-1}, \quad (4.21)$$

where $\mathbf{I}_{d \times d} \in \mathbb{R}^{d \times d}$ is an identity matrix.

4.2.1.3 Reduced-order modelling

All matrices in Eq. (4.3) are transformed according to Eq. (3.6) to obtain a ROM of Eq. (4.13). It is also possible to apply ROM techniques directly on Eq. (4.3), *cf* Eq. (4.21),

using KS, POD, *etc.* We will pursue further, however, only the firstly mentioned approach.

Concerning the Lyapunov equation (4.13) of the reduced system, we can decrease the computational effort by some prior information. Let us assume that the system response is described through Eq. (4.8) with $p_i = 2$. Splitting all matrices leads to

$$\begin{bmatrix} \mathbf{a}_{11} & \mathbf{a}_{12} \\ \mathbf{a}_{21} & \mathbf{a}_{22} \end{bmatrix} \begin{bmatrix} \mathbf{c}_{11} & \mathbf{c}_{12} \\ \mathbf{c}_{21} & \mathbf{c}_{22} \end{bmatrix} + \begin{bmatrix} \mathbf{c}_{11} & \mathbf{c}_{12} \\ \mathbf{c}_{21} & \mathbf{c}_{22} \end{bmatrix} \begin{bmatrix} \mathbf{a}_{11}^\top & \mathbf{a}_{21}^\top \\ \mathbf{a}_{12}^\top & \mathbf{a}_{22}^\top \end{bmatrix} + \begin{bmatrix} \mathbf{0}_{2k \times 2k} & \mathbf{0}_{2k \times l} \\ \mathbf{0}_{l \times 2k} & \mathbf{b}\mathbf{b}^\top_{22} \end{bmatrix} = \mathbf{0}, \quad (4.22)$$

where

$$\mathbf{a}_{11} = \begin{bmatrix} \mathbf{0}_{k \times k} & \mathbf{I}_{k \times k} \\ -\mathbf{M}_r^{-1} \mathbf{K}_r & -\mathbf{M}_r \mathbf{K}_r \end{bmatrix}, \quad (4.23)$$

$k = \dim(\mathcal{V})$, $l = \sum_{i=1}^{n_a} p_i$, $\mathbf{a}_{21} = \mathbf{0}$ and remaining submatrices have obvious structure. Dropped subscript X at covariance matrix \mathbf{c} emphasizes a projection onto some subspace. Since $\mathbf{b}\mathbf{b}^\top$ is symmetric, in fact diagonal, the solution will be also symmetric, $\mathbf{c}_{12} = \mathbf{c}_{21}^\top$. In the case of AR(2) processes, submatrix \mathbf{c}_{22} can be computed explicitly; single AR(2) process has uncorrelated state variables S_1 , S_2 and $\text{var}S_1 = a_0^2 / (2a_1a_2)$, $\text{var}S_2 = a_0^2 / (2a_1)$, *cf* Eq. (4.7), based on moment equations, thus \mathbf{c}_{22} is a diagonal matrix. Introduced considerations reduce the system of four equations in Eq. (4.22) in expanded form, to the set of two coupled equations

$$\mathbf{a}_{11} \mathbf{c}_{12} + \mathbf{c}_{12} \mathbf{a}_{22}^\top + \mathbf{a}_{12} \mathbf{c}_{22} = \mathbf{0} \quad (4.24)$$

$$\mathbf{a}_{11} \mathbf{c}_{11} + \mathbf{c}_{11} \mathbf{a}_{11}^\top + \mathbf{c}_{12} \mathbf{a}_{12}^\top + \mathbf{a}_{12} \mathbf{c}_{12}^\top = \mathbf{0} \quad (4.25)$$

for unknowns \mathbf{c}_{12} and \mathbf{c}_{11} . The set resembles Sylvester and Lyapunov equations respectively with reduced size. Backward transformation $\bar{\mathbf{c}}_X = \mathbf{V} \bar{\mathbf{c}} \mathbf{W}^\top$ gives covariance matrix for displacement or velocity vector, where $\bar{\mathbf{c}}$ denotes an appropriate submatrix.

4.2.1.4 Performance of the Gaussian processes

As was mentioned in introductory Chap. 1, for grandstand serviceability and reliability assessment, properties such as RMS values and the mean upcrossing rates have to be computed. Together with the distribution of the maxima, they represent the content of this short section.

Level Crossings One of the measures of system performance is level crossing. Under some circumstances, it can be shown that upcrossing is directly connected with the reliability of the system. Employing Rice formula (A.1), the x -upcrossing rate of a Gaussian process $X(t)$ with non-stationary mean value $\mu(t)$ and stationary variance σ^2 is estimated as [53]

$$\nu_x^+(t) = \frac{\dot{\sigma}}{\sigma} \left[\phi \left(\frac{\dot{\mu}(t)}{\dot{\sigma}} \right) + \frac{\dot{\mu}(t)}{\dot{\sigma}} \Phi \left(\frac{\dot{\mu}(t)}{\dot{\sigma}} \right) \right] \phi \left(\frac{x - \mu(t)}{\sigma} \right), \quad (4.26)$$

where $\nu_x^+(t)$ is the x -upcrossing rate of level x at time t , $\phi(\alpha) = 1/\sqrt{2\pi} \exp(-\alpha^2/2)$, $\Phi(u) = \int_{-\infty}^u \phi(\alpha) d\alpha$, $\sigma^2 = \text{var}X(t)$, $\dot{\sigma}^2 = \text{var}\dot{X}(t)$. The total mean number of upcrossings in time interval $[0, T]$ is computed according to

$$n_x^+(T) = \int_0^T \nu_x^+(t) dt. \quad (4.27)$$

The relations can be generalized to D -outcrossings of a d -valued stochastic process, where D is some set in \mathbb{R}^d .

Distribution of maxima The probability density function of the local maxima is expressed as, [53]

$$f_{\max}(x) = \frac{\sqrt{1-\nu^2}}{\sigma} \phi\left(\frac{x}{\sqrt{1-\nu^2}}\right) + \frac{\nu x \sqrt{2\pi}}{\sigma} \phi\left(\frac{x}{\sigma}\right) \Phi\left(\frac{\nu x}{\sqrt{\sigma(1-\nu^2)}}\right), \quad (4.28)$$

where $\nu = \dot{\sigma}^2 / (\sigma \ddot{\sigma})$, and $\phi(\alpha)$, $\Phi(u)$, σ , $\dot{\sigma}$ have the same meaning as in Eq. (4.26), $\ddot{\sigma}^2 = \text{var}\ddot{X}(t)$.

RMS values Another measure of the system performance from the point of view of serviceability is the root mean square value. Since 1) the shortest integration time in the floating RMS value is $\tau = 1$ s for the case of panic, *cf* [27], 2) the jumping frequencies are roughly within the interval $f_p \in (1.4, 3.5)$ Hz and the mean value is a function of higher harmonics, 3) superposed noise is also frequency limited from below at least with 1 Hz and 4) available generators simulate "stationary" signals, it results that except for the initial transient part at the onset of loading, the response of the system is "stationary", the floating RMS averages are "constant", and can be approximated by

$$\text{RMS} = \sqrt{\frac{1}{T} \int_0^T X(t)^2 dt} = \sqrt{\frac{1}{T} \int_0^T \mu_X(t)^2 dt + \sigma^2}, \quad (4.29)$$

where $\mu_X(t) = \text{E}X(t)$. Then, the limit stationary solution is viewed as an approximate averaged value providing an estimate. Analogous formulas are valid for velocity and acceleration.

4.2.1.5 Applications to the response of grandstands

As was noted in introductory Chap. 1, an active spectator can be treated as a time-dependent forcing process. Figure 4.1 shows a single realization and corresponding spectral density of a unit process, *i.e.* of the process with $G = 1$, where G denotes the weight of a spectator, jumping frequency $f_p = 2.7$ Hz. Spectral densities were computed from (4.16) with Parzen weight. The realization was generated according to [51]. Since this function

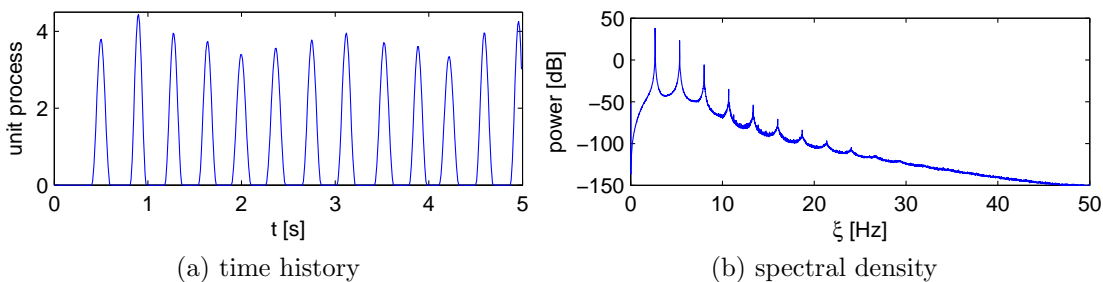


Figure 4.1: Single time history and power spectral density of 10,000 realizations of forcing term $Y(t)$ generated according to [51]

is highly periodic, we will search the mean value in the form

$$\mu_Y(t) = \alpha_0 + \sum_{k=1}^p \alpha_k \cos(2k\pi f_p t) + \beta_k \sin(2k\pi f_p t). \quad (4.30)$$

Then vector $\hat{\boldsymbol{\alpha}}$ of the estimated parameters $\hat{\alpha}_0, \hat{\alpha}_1, \hat{\beta}_1, \dots, \hat{\alpha}_p, \hat{\beta}_p$ can be found by the linear Least Squares Method as

$$\hat{\boldsymbol{\alpha}} = (\boldsymbol{\Phi}^\top \boldsymbol{\Phi})^{-1} \boldsymbol{\Phi}^\top \bar{\boldsymbol{\mu}}_Y, \quad (4.31)$$

where

$$\boldsymbol{\Phi} = \begin{bmatrix} 1 & \cos(2\pi \bar{f} t_1) & \sin(2\pi \bar{f} t_1) & \dots & \cos(p \cdot 2\pi \bar{f} t_1) & \sin(p \cdot 2\pi \bar{f} t_1) \\ 1 & \cos(2\pi \bar{f} t_2) & \sin(2\pi \bar{f} t_2) & \dots & \cos(p \cdot 2\pi \bar{f} t_2) & \sin(p \cdot 2\pi \bar{f} t_2) \\ \vdots & \vdots & \vdots & \ddots & \vdots & \vdots \\ 1 & \cos(2\pi \bar{f} t_n) & \sin(2\pi \bar{f} t_n) & \dots & \cos(p \cdot 2\pi \bar{f} t_n) & \sin(p \cdot 2\pi \bar{f} t_n) \end{bmatrix},$$

t_1, \dots, t_n is a fine enough and equidistant partition of the time interval, $\bar{\boldsymbol{\mu}}_Y = [\bar{\mu}_Y(t_1), \dots, \bar{\mu}_Y(t_n)]^\top$ with

$$\bar{\mu}_Y(t_i) = \frac{1}{N} \sum_{k=1}^N Y_k(t_i), \quad (4.32)$$

are means over N realizations $Y_k(t_i)$ in time instants t_i . Generating 10,000 trajectories provides the coefficients given in Tab. 4.1. Realization centered with the mean value ac-

$f_p = 1.5$ Hz				$f_p = 2.0$ Hz			
$\hat{\alpha}_0$	0.9940			$\hat{\alpha}_0$	0.9944		
$\hat{\alpha}_1$	0.7559	$\hat{\beta}_1$	0.7068	$\hat{\alpha}_1$	0.8009	$\hat{\beta}_1$	1.0233
$\hat{\alpha}_2$	-0.0056	$\hat{\beta}_2$	0.1471	$\hat{\alpha}_2$	-0.0930	$\hat{\beta}_2$	0.3415
$\hat{\alpha}_3$	-0.0044	$\hat{\beta}_3$	0.0008	$\hat{\alpha}_3$	-0.0304	$\hat{\beta}_3$	0.0102
$\hat{\alpha}_4$	0.0003	$\hat{\beta}_4$	-0.0001	$\hat{\alpha}_4$	0.0005	$\hat{\beta}_4$	0.0002
$f_p = 2.7$ Hz				$f_p = 3.5$ Hz			
$\hat{\alpha}_0$	0.9958			$\hat{\alpha}_0$	0.9966		
$\hat{\alpha}_1$	0.2939	$\hat{\beta}_1$	1.1170	$\hat{\alpha}_1$	-0.3197	$\hat{\beta}_1$	0.9566
$\hat{\alpha}_2$	-0.2471	$\hat{\beta}_2$	0.0984	$\hat{\alpha}_2$	-0.0916	$\hat{\beta}_2$	-0.0997
$\hat{\alpha}_3$	-0.0037	$\hat{\beta}_3$	-0.0153	$\hat{\alpha}_3$	-0.0003	$\hat{\beta}_3$	0.0004
$\hat{\alpha}_4$	-0.0008	$\hat{\beta}_4$	-0.0001	$\hat{\alpha}_4$	0.0007	$\hat{\beta}_4$	-0.0003

Table 4.1: Coefficients $\hat{\boldsymbol{\alpha}}$ for an approximation of the mean value in Eq. (4.30)

ording to Eq. (4.30) and the coefficients from Tab. 4.1 is depicted in Fig. 4.2 together with the spectral density and a normalized histogram, *i.e.* a histogram of the process $\bar{Y}(t) = [Y(t) - \mu(t)] / \sigma_Y = \tilde{Y}(t) / \sigma_Y$ where $\sigma_Y = \sqrt{\text{var}Y(t)} = \sqrt{0.7486}$ for $f_p = 2.7$ Hz is the stationary standard deviation. The centered process resembles non-Gaussian coloured noise and within approximations will be treated in further considerations as stationary

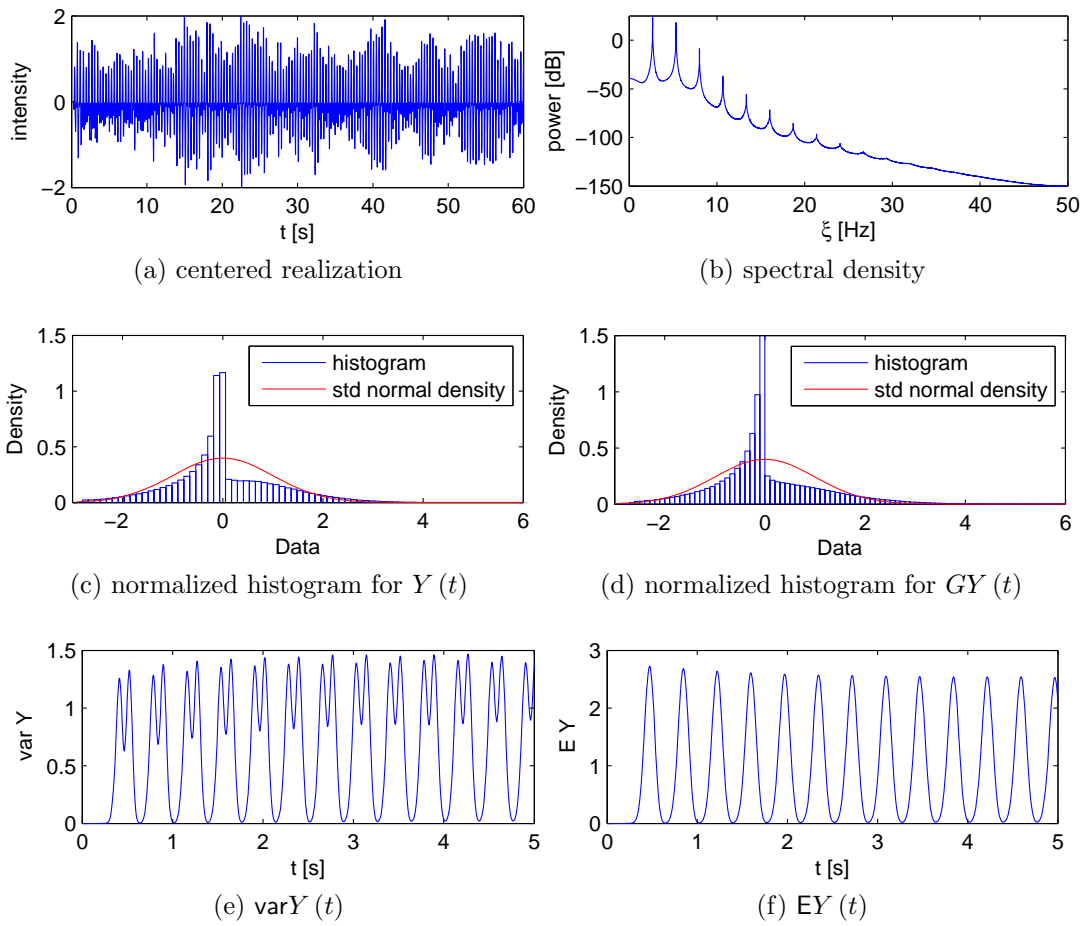


Figure 4.2: Single centered time history of $\tilde{Y}(t)$ (a), the corresponding power spectral density of 10,000 realizations (b), a normalized histogram with standard normal density (c) and a normalized histogram of a non-unit process scaled with G [kN] $\sim \mathcal{N}(0.7709, 0.0167)$ (d), variance $\text{var}Y(t)$ (e) and mean value $EY(t)$ (f)

and ergodic, *cf* Fig. 4.2e and 4.2f where the true nonstationary variance and the mean value as functions of time are depicted. To quantify the stationary difference, for $\bar{Y}(t)$ we have $\mu_{\bar{Y}} = 0$ for the mean, $\text{var}\bar{Y} = 1$ for the variance, $\gamma_{3,\bar{Y}} = 0.424$ for the coefficient of skewness, and $\gamma_{4,\bar{Y}} = 4.076$ for the coefficient of kurtosis, *cf* also Tab. 4.5. For comparison, the standard Gaussian process has coefficients 0, 1, 0 and 3.

Example 4.1. Let us briefly analyze the response of a harmonic oscillator with unit mass forced by jumping process $Y(t)$ with $f_p = 2.7$ Hz, employing MC to justify the normality assumptions. The coefficients of skewness and kurtosis of the state vector $\mathbf{X}(t) = [Z(t), \dot{Z}(t)]^T$ as functions of the oscillator eigenfrequency f_1 for two different values of viscous damping ζ are depicted in Fig. 4.3. Note that for frequency range 0.5 – 7 Hz the response is approximately Gaussian. As was expected, worse convergence is achieved for higher damping values, *cf* the Rosenblatt theorem [18]. Normalized histograms of displacement for eigenfrequencies $f_1 = 4$ and 12 Hz and both damping values are depicted in Fig. 4.4. Other techniques can be applied for approximations of the response outside this frequency range, *e.g.* memoryless transformations of Brownian coloured white noise, *cf* also Sec. 4.3.1. Based on heuristic arguments and the Central Limit Theorem, we

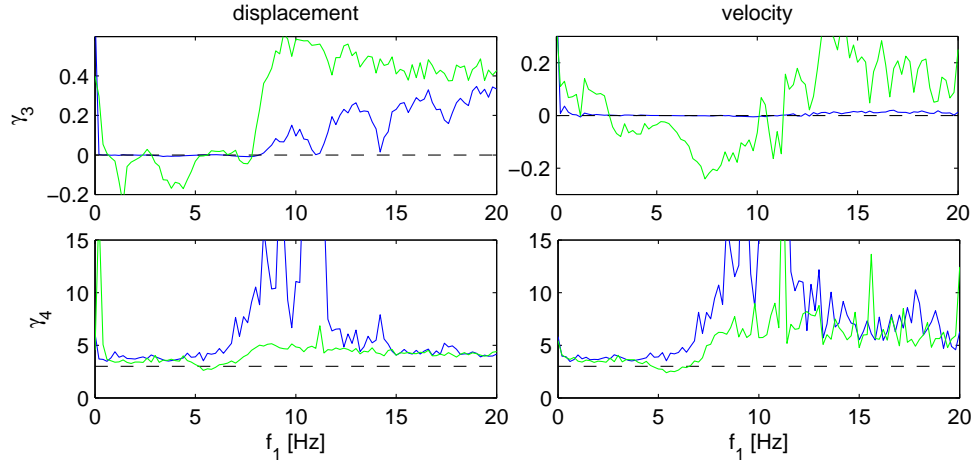


Figure 4.3: Coefficient of skewness γ_3 and coefficient of kurtosis γ_4 for the normalized displacement and velocity of the harmonic oscillator forced by the jumping process as functions of eigenfrequency f_1 . Blue – viscous damping $\zeta = 0.001$; green – $\zeta = 0.07$; dashed line – corresponding values for the Gaussian random variable

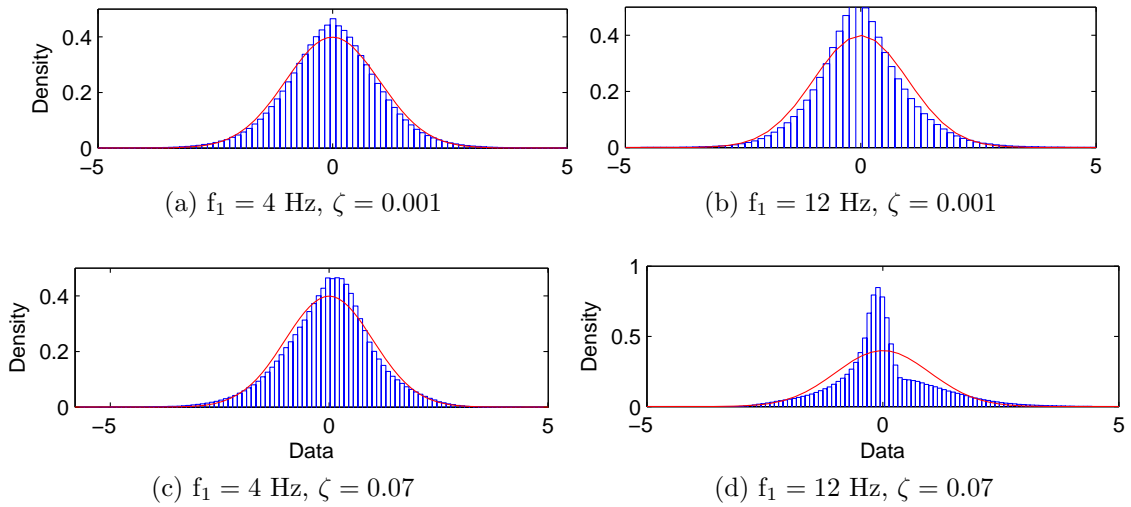


Figure 4.4: Histograms of normalized displacement $\bar{Z}(t)$ with standard normal density based on 1,000 MC realizations assuming ergodicity

can assume that the higher the number of active spectators, and the more complex the grandstand geometry is, the more Gaussian the response will be.

A spectral density approximation of the forcing process for the frequency domain solution, Fig. 4.2b, cannot be further simplified. This is because the FRF of the structure has sharp peaks, and thus exact function values are needed. Any approximation employing indicator functions in the vicinities of significant harmonics preserving variance would be inaccurate.

We can employ, however, filtered white noise processes AR(2), which arise as solutions of the second order equations

$$c_{2,i}\ddot{\hat{Y}}_i(t) + c_{3,i}\dot{\hat{Y}}_i(t) + c_{1,i}\hat{Y}_i(t) = W(t), \quad t \geq 0, \quad (4.33)$$

with spectral densities

$$s_i(\xi, \mathbf{c}) = \frac{1}{[c_{1,i} - c_{2,i}(2\pi\xi)^2]^2 + (2\pi\xi c_{3,i})^2}, \quad (4.34)$$

where $\{c_{1,i}, c_{2,i}, c_{3,i}\}$ correspond to the stiffness, mass and damping of a harmonic oscillator. This function has a sharp peak positioned at $f_1 = \sqrt{c_1/c_2}/2\pi$ if we neglect shifts caused by damping effects. For a closer approximation, we assume $\tilde{Y}(t) \approx \sum_{i=1}^n \hat{Y}_i(t)$, where $\hat{Y}_i(t)$ are mutually independent AR(2) processes. Identification leads to a nonlinear optimization problem: find such $c_{k,i}$, $k = 1, 2, 3$ and $i = 1, \dots, n$, that minimize L^2 norm of the difference

$$e(\xi, \mathbf{c}) = \hat{s}_{\tilde{Y}}(\xi) - \sum_{i=1}^n s_i(\xi, \mathbf{c}), \quad (4.35)$$

$$\min_{\mathbf{c}=\{c_{1,1}, \dots, c_{3,n}\}} \|e(\xi, \mathbf{c})\|_{L^2}, \quad \xi \in A \subset \mathbb{R}^+ \text{ connected}, \quad (4.36)$$

where $\hat{s}_{\tilde{Y}}$ denotes a spectral density estimate of the centered force term $\tilde{Y}(t)$. The problem can be solved by the Nonlinear Least Squares method, by Simulated Annealing *etc*, with easily estimated initial vector \mathbf{c}_0 . Optimized coefficients for $n = 6$ of the centered process $\tilde{Y}(t)$ are presented in Tab. 4.2, and the corresponding spectral density and spectral distribution function are presented in Fig. 4.5 for $f_p = 2.0$ and 3.5 Hz. Note that the spectral density is two-sided, and only one half was integrated in the spectral distribution function, thus the variance indicated is $0.7486/2 = 0.3743$ for $f_p = 2.0$ Hz, and $0.6824/2 = 0.3412$ for $f_p = 3.5$ Hz.

Let us briefly note the situation when the forcing process $Y(t)$ is not a unit process, *i.e.* $G \neq 1$. Since we are limiting our considerations to Gaussian approximation, only the first two moments of G will apply. The deterministic weight corresponds to a singular case $\text{var}G = 0$. Then the forcing term has the form $Y_G(t) = GY(t)$ and alter its mean value by multiplication with EG and its spectral density by multiplication with EG^2 . Then the mean response reads $\mu_{Z,G}(t) = E[G]\mu_Z(t)$ and stationary response variance $\sigma_{Z,G}^2 = E[G^2]\sigma_Z^2$, where $\mu_Z(t)$ and σ_Z^2 are the response mean and the variance of the structure loaded by the unit forcing term $Y(t)$. Nevertheless, we should be aware that even when process $F(t)$ was a Gaussian, process $F_G(t)$ as a product of a random variable with a stochastic process, is not Gaussian. To quantify the influence of such scaling, compare the histograms in Fig. 4.2c and 4.2d, where G has normal distribution with mean value 0.7709 and variance 0.0167.

In the rest of this section, the quality of the approximation in the time or frequency domain will be compared with MC simulation. A total of four mechanical systems will be tested: a harmonic oscillator, a simply supported beam, a simple cantilever grandstand, and a realistic grandstand with 1, 4, 72 and 630 positions for spectators respectively, *cf* Appendix C. Centered normed response histograms for an active crowd only, based on MC simulation, are depicted in Fig. 4.6. Note also that assumptions on convergence to normal distribution are approximately fulfilled. All examples are artificial, not realistic, so the measured responses would be unacceptable. Remind also that the forcing is scaled such that $G = 1$.

$f_p = 1.5$ Hz					$f_p = 2.0$ Hz				
i	$c_{1,i}$	$c_{2,i}$	$c_{3,i}$	f_i	i	$c_{1,i}$	$c_{2,i}$	$c_{3,i}$	f_i
1	32.1868	0.3740	0.0926	1.48	1	35.9984	0.2313	0.0639	1.99
2	28.4744	0.3206	0.0755	1.50	2	35.4762	0.2214	0.0624	2.02
3	32.1054	0.3503	0.0885	1.52	3	85.4862	0.1363	0.0426	3.99
4	56.5951	0.1603	0.0655	3.00	4	90.3709	0.1420	0.0431	4.02
5	107.2460	0.2981	0.0903	3.02	5	203.8343	0.1434	0.0677	6.00
6	165.2705	0.2069	0.1449	4.50	6	753.2156	0.2982	0.1909	8.00
$f_p = 2.7$ Hz					$f_p = 3.5$ Hz				
i	$c_{1,i}$	$c_{2,i}$	$c_{3,i}$	f_i	i	$c_{1,i}$	$c_{2,i}$	$c_{3,i}$	f_i
1	43.0323	0.1546	0.0450	2.66	1	60.8293	0.1258	0.0349	3.50
2	42.8054	0.1504	0.0442	2.69	2	74.0274	0.1510	0.0432	3.52
3	106.3256	0.0949	0.0343	5.33	3	71.5957	0.1501	0.0434	3.58
4	132.7502	0.1172	0.0380	5.36	4	104.3139	0.0585	0.2817	6.72
5	370.5087	0.1463	0.0794	8.01	5	131.9751	0.0682	0.0340	7.00
6	1641.3390	0.3646	0.2983	10.68	6	1709.7792	0.3931	0.3047	10.50

Table 4.2: Coefficients $c_{k,i}$, $k = 1, 2, 3$ and $i = 1, \dots, 6$ of the six independent AR(2) members used for approximation of the centered forcing term $\tilde{Y}(t)$ in frequency range 0.5 – 10 Hz

Example 4.2. Let us assume a harmonic oscillator with unit mass, two values of viscous damping ζ_i , $i = 1, 2$, and variable stiffness. The mean value response is presented in Fig. 4.7. The response was acquired by direct integration of (4.1), starting at $t = 0.5$ s. The approximation utilizes Eq. (4.30) and the coefficients in Tab. 4.1. A comparison of the total mean upcrossings $n_x^+(T)$ in the time interval $[0, T]$, $T = 160$ s, as functions of oscillator eigenfrequency f_1 for two values of viscous damping $\zeta = 0.001$ and $\zeta = 0.07$ and for two fixed levels $x = 0.002$ and $x = 0.005$ m are depicted in Fig. 4.8, employing formulas (4.26) and (4.27). The size of time interval T is based on heuristic considerations about the average length of the musical compositions. The time domain solution is based on the sum of six independent AR(2) processes with the coefficients in Tab. 4.2. The stationary response variances are computed according to formulas (4.24), (4.25) and (4.14). The frequency domain approximation employs Eqns. (4.18) – (4.20). The spectral density estimate $\hat{s}_{\tilde{Y}}(\xi)$ of the centered input process has 307 values over the frequency range 0 – 10 Hz, using variable partition. Fig. 4.8 shows that the results are roughly in agreement with MC in the frequency range 0.2 – 10 Hz. Note that the total number of mean zero-upcrossings for a deterministic periodic function with frequency 2.7 Hz is $160 \cdot 2.7 \approx 432$, cf Fig. 4.8c and 4.8d, where distinct plateaux are found. The results for MC are based on 1,000 realizations 160 s in length.

Example 4.3. The next example is a simply supported beam in Appendix C.1. Poor approximations are anticipated, since the structure is quite stiff with high eigenfrequencies, see the results for the harmonic oscillator. Two cases are studied: a structure occupied

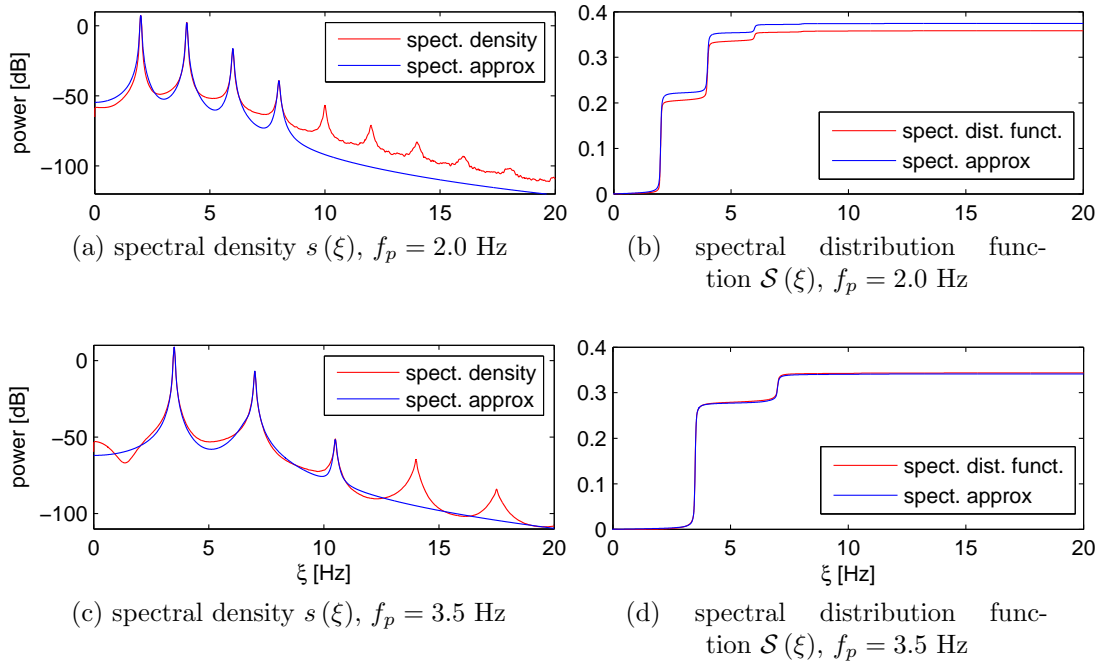


Figure 4.5: Spectral densities and spectral distribution functions of centered forcings $\tilde{Y}(t)$ and of their approximations $\sum_{i=1}^6 \hat{Y}_i(t)$, where $\hat{Y}_i(t)$ are independent AR(2) processes with the coefficients in Tab. 4.2 based on spectral optimization for $f_p = 2.0$ and 3.5 Hz

by an active crowd only; and a structure occupied by a mixed crowd. In the second case, the two left hand side positions are loaded by forces and the two right hand side positions are occupied by passive spectators. Deterministic biodynamic models according to Coermann [11] are used, *cf* Tab. 3.1. Results are presented for the point P_1 . The total mean upcrossings for the first case n_x^+ (160) as a function of level x are depicted in Fig. 4.9a. The RMS values for acceleration are 1.947 m/s² for the MC solution, 2.135 m/s² for the frequency domain solution, and 1.914 m/s² for the time domain solution. All input processes are treated as independent, so matrix $\mathbf{S}_{\tilde{Y}\tilde{Y}}$ in Eq. (4.18) has nonzero only diagonal entries. The mean value response is depicted in Fig. 4.9f with a single realization 4.9e. PDFs of local maxima $f_{\max}(x)$ for the centered response are compared in Figs. 4.9c and 4.9d. The total upcrossings for a mixed crowd are depicted in Fig. 4.9b, and the RMS values are 1.048 m/s² for the MC solution, 1.094 m/s² for the frequency domain solution, and 0.990 m/s² for the time domain solution. Let us also recall our assumption of fixed spatial distribution of the crowd, mass coefficient $\gamma = m_H/m_S = 0.1$. Results for MC are based on 2,000 realizations. The approximate shape of the total upcrossings, especially for a mixed crowd, differ from the MC simulation because of the non-Gaussian response owing to high structure eigenfrequencies.

Example 4.4. This system is the cantilever grandstand described in Appendix C.2. The total upcrossings of the response displacement for the point P_1 and fully occupied structure by active spectators are depicted in Fig. 4.10a, single realization and the mean response are depicted in subfigures 4.10e and 4.10f, RMS accelerations 5.583 m/s² for the MC solution, 5.682 m/s² for the frequency domain solution, and 5.616 m/s² for the time domain solution. For 36 spectators chosen to be passive according to Coermann with uniformly

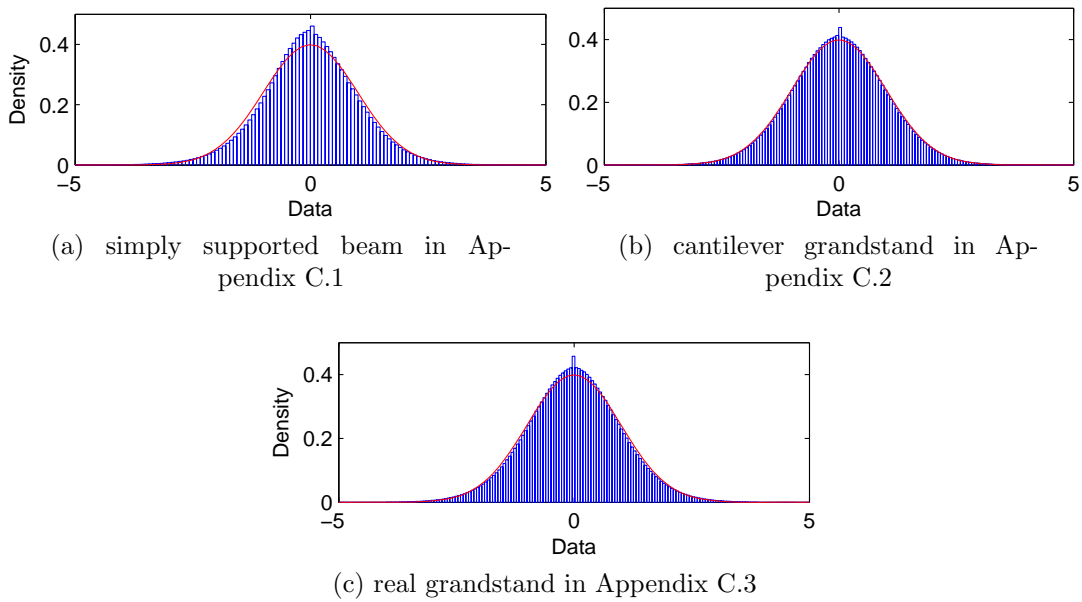


Figure 4.6: Normed histograms of the displacement assuming ergodicity, structures fully occupied by an active crowd only

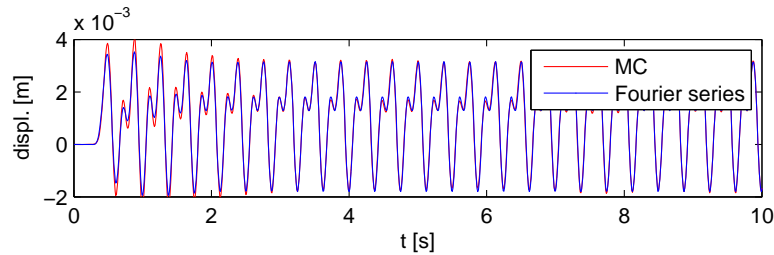


Figure 4.7: Response mean displacement in comparison with an approximation based on the first four harmonics for a harmonic oscillator, $f_1 = 5$ Hz and $\zeta = 0.07$

random but fixed positions, the resulting upcrossings are depicted in subfigure 4.10b, mass coefficient $\gamma = 0.17$. The acceleration RMS values in this case appear to be 1.327 m/s^2 for the MC solution, 1.347 m/s^2 for the frequency domain solution, and 1.309 m/s^2 for the time domain solution. Comparison of the PDFs for local maxima of centered response are depicted in Figs. 4.10c and 4.10d showing a good agreement. The results for MC are again based on 2,000 realizations 160 s in length.

Example 4.5. In this concluding example, let us briefly examine the response for a real grandstand in Appendix C.3 and the point P_1 . Results for the structure loaded by an active crowd only are depicted in Figs. 4.11a, 4.11c, 4.11e and 4.11f. The acceleration RMS values appear to be 5.546 m/s^2 for the MC solution, 5.565 m/s^2 for the frequency domain solution, and 5.597 m/s^2 for the time domain solution. In the second case, 315 positions are occupied by passive spectators according to Coermann, mass coefficient $\gamma = 0.18$. The results for this case are presented in Figs. 4.11b and 4.11d, RMS accelerations 1.905 m/s^2 for the MC solution, 1.904 m/s^2 for the frequency domain solution, and 1.919 m/s^2 for the time domain solution. MC simulation was again based on 2,000 realizations. For comparison, Fig. 4.11g captures a convergence of the normalized variances $\text{var}Z_{P_1}$, $\text{var}\dot{Z}_{P_1}$

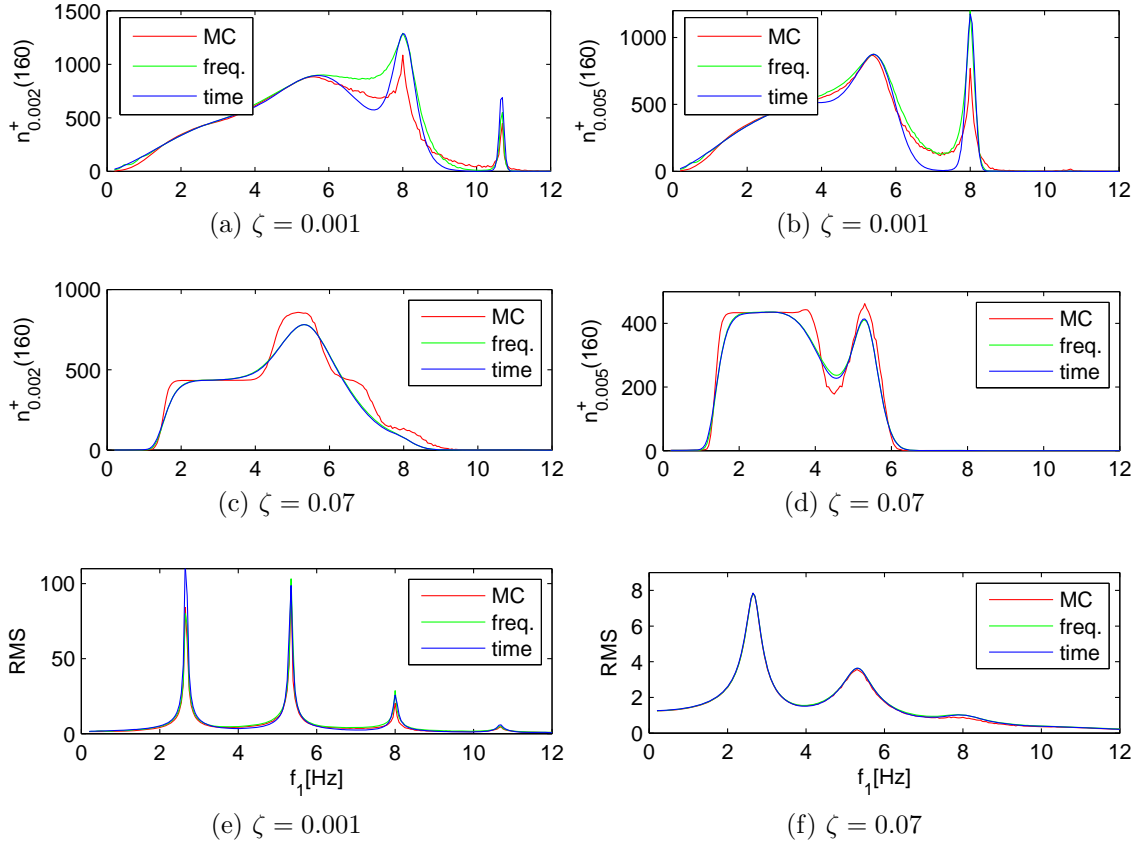


Figure 4.8: Total mean upcrossings $n_x^+(T)$ and acceleration RMS values as functions of f_1 for a harmonic oscillator, distinct levels x and viscous damping ζ , $T = 160$ s

and $\text{var} \ddot{Z}_{P_1}$ for MS ROM with respect to $\dim(\mathcal{V})$ where $\dim(\mathcal{V}) = \dim(\mathcal{V}_S) + \dim(\mathcal{V}_H)$ and $\dim(\mathcal{V}_H) = \dim(\mathcal{V}_S)/3$ rounded to nearest lower integer value.

The time consumption for the different solution techniques is summarized in Tab. 4.3, where the demands of MC simulation are presented for 100 realizations only. This value is based on the convergence tests of total upcrossings, *cf* Sec. 3.6, clearly highly sensitive to level x . Hence, the value used can be considered as a lower bound. The size of the time integration step was chosen to be $h = 0.005 \sim 0.01$ s depending on the structure; Newmark integration scheme used. The number of DOFs of each system is also mentioned. For the purposes of comparison, the time consumptions for MS ROM technique are also summarized together with the size of the projection subspace $\dim(\mathcal{V})$. All simulations were performed on core i7 with a 16 GB RAM computer, MATLAB[®] parallel implementation.

4.2.2 Random distribution of an active crowd

In this section, a brief generalization to the case where only an active crowd with a random spatial distribution occupies the structure will be given. Possibly some passive spectators can occupy the structure, but in that case, \mathbf{n}_p is assumed fixed. Let us accept the following

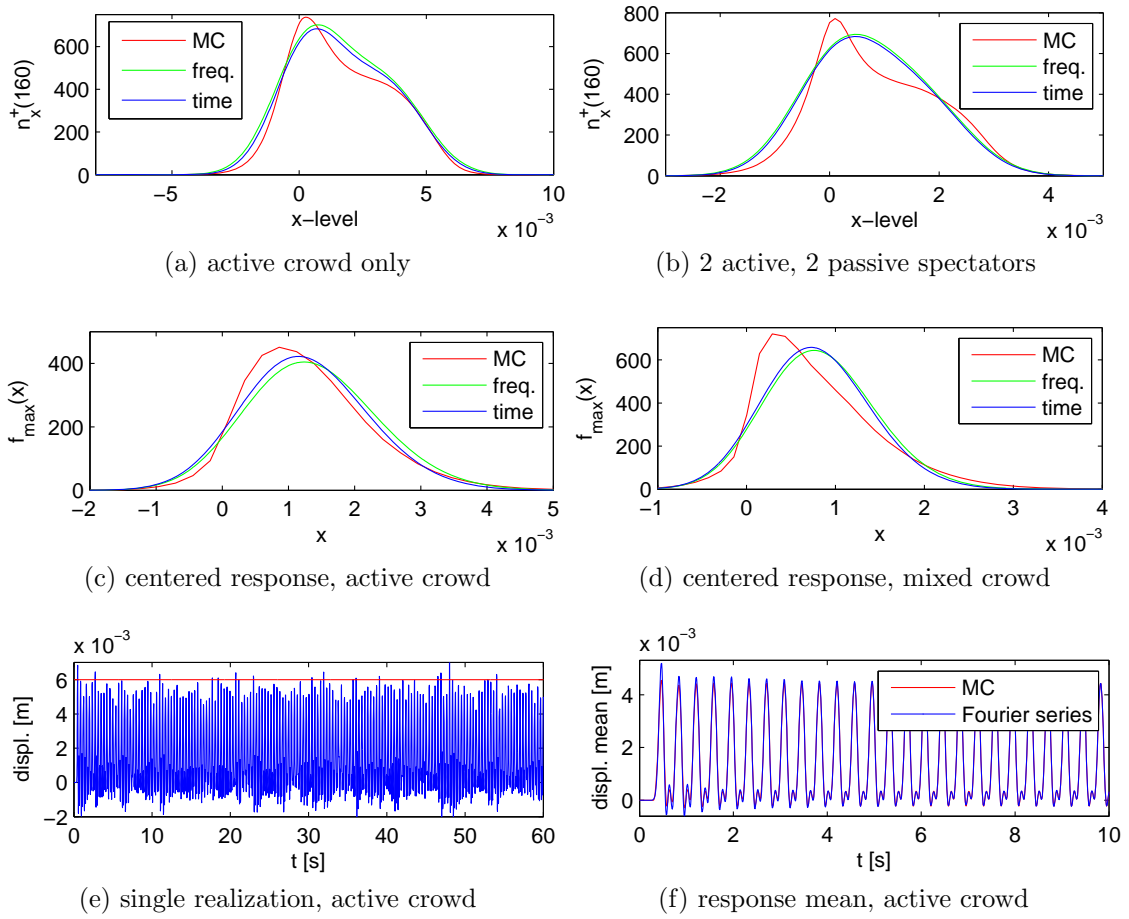


Figure 4.9: Total mean upcrossings $n_x^+(T)$ of a simply supported beam in Appendix C.1 as functions of x , $T = 160$ s, distribution of maxima $f_{\max}(x)$, single realization and mean responses for an active crowd and for a mixed crowd

form of the forcing term in Eq. (2.1),

$$\mathbf{F}(t, \omega) = \boldsymbol{\chi}(\omega) \left[\boldsymbol{\mu}_Y(t) + \tilde{\mathbf{Y}}(t, \omega) \right], \quad t \geq 0, \quad (4.37)$$

where $\boldsymbol{\mu}_Y(t)$ and $\tilde{\mathbf{Y}}(t, \omega)$ were introduced earlier. A square, diagonal random matrix $\boldsymbol{\chi} \in \mathbb{R}^{n_a \times n_a}$, $\boldsymbol{\chi} = \text{diag}(\chi_1, \dots, \chi_{n_a})$, where χ_i are identically distributed random indicator variables, or Bernoulli trials

$$\chi_i = \begin{cases} 1, & \text{P}[\chi_i = 1] = p \\ 0, & \text{P}[\chi_i = 0] = 1 - p \end{cases} \quad (4.38)$$

for $p \in [0, 1]$ with moments $\text{E}\chi_i^k = p$, $k = 1, 2, \dots$. In this context, the probability p can be interpreted as an intensity factor describing an overall loading scenario. Hence, $\mathbf{F}(t, \omega) = \boldsymbol{\mu}_F(t) + \tilde{\mathbf{F}}(t, \omega)$, where $\boldsymbol{\mu}_F(t) = \text{E}\boldsymbol{\chi}(\omega) \boldsymbol{\mu}_Y(t)$ and $\tilde{\mathbf{F}}(t, \omega) = \tilde{\boldsymbol{\chi}}(\omega) \boldsymbol{\mu}_Y(t) + \boldsymbol{\chi}(\omega) \tilde{\mathbf{Y}}(t, \omega)$, $\tilde{\boldsymbol{\chi}}(\omega) = \boldsymbol{\chi}(\omega) - \text{E}\boldsymbol{\chi}(\omega)$. Mean response can be obtained directly from Eq. (4.1) taking $\mathbf{G}\boldsymbol{\mu}_F(t)$ for the right hand side leading simply to $p\boldsymbol{\mu}_Z(t)$, where $\boldsymbol{\mu}_Z(t)$ is the mean response of the system forced by $\boldsymbol{\mu}_Y(t)$. Eq. (4.11) holds in this case

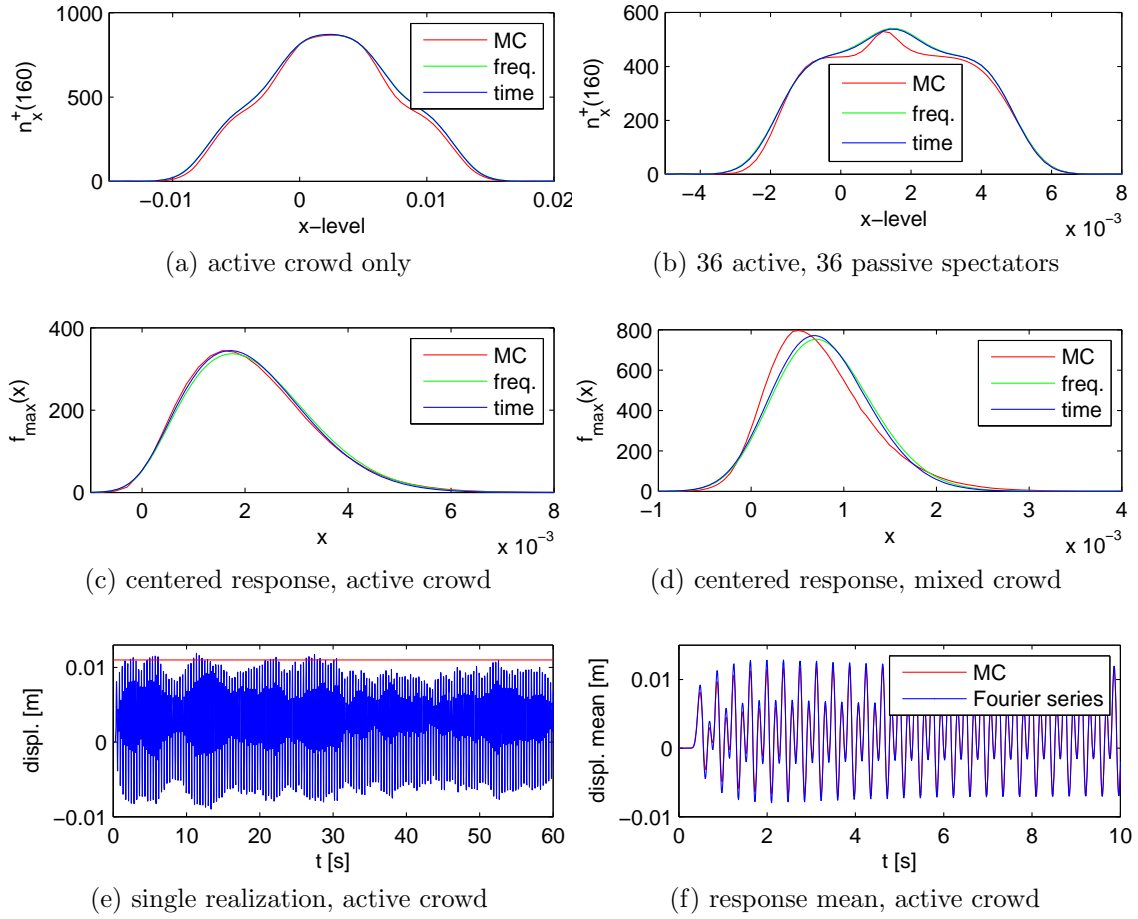


Figure 4.10: Total mean upcrossings of a cantilever grandstand in Appendix C.2, distribution of maxima, single realization and mean responses for an active crowd and for a mixed crowd

too, but with slight adjustments. Assume again the zero mean forcing $\tilde{\mathbf{Y}}(t, \omega)$ approximated as a linear combination of an n AR(2) processes as usual, and denote $\chi_n = \text{diag}[\chi_{1,1}, \dots, \chi_{1,n}, \dots, \chi_{n_a,1}, \dots, \chi_{n_a,n}]$. Then, Eq. (4.9) reads

$$d\mathbf{X}(t) = \mathbf{a}\mathbf{X}(t)dt + \mathbf{h}\tilde{\chi}\mu_Y(t)dt + \mathbf{b}\chi_n d\mathbf{B}(t), \quad t \geq 0, \quad (4.39)$$

with \mathbf{b} in analogy to Eq. (4.8), $d\mathbf{B}(t) \in \mathbb{R}^{n_a n}$, and

$$\mathbf{h} = \begin{bmatrix} \mathbf{0}_{k \times n_a} \\ \mathbf{M}^{-1}\mathbf{G} \\ \mathbf{0}_{l \times n_a} \end{bmatrix} \quad (4.40)$$

where $k = n_{DOF}$ for brevity, $l = \dim(\mathbf{S}) = 2n_a n$. It is also possible, even more conveniently, to introduce the indicator variables χ into the drift matrix \mathbf{a} ; nevertheless, in order to emphasize the fact that the random spatial distribution of an active crowd is just a matter of the forcing term, we have chosen the representation in Eq. (4.39), *cf* also Chaps. 5 and 6 where the randomness of the operator and of the right hand side are strictly

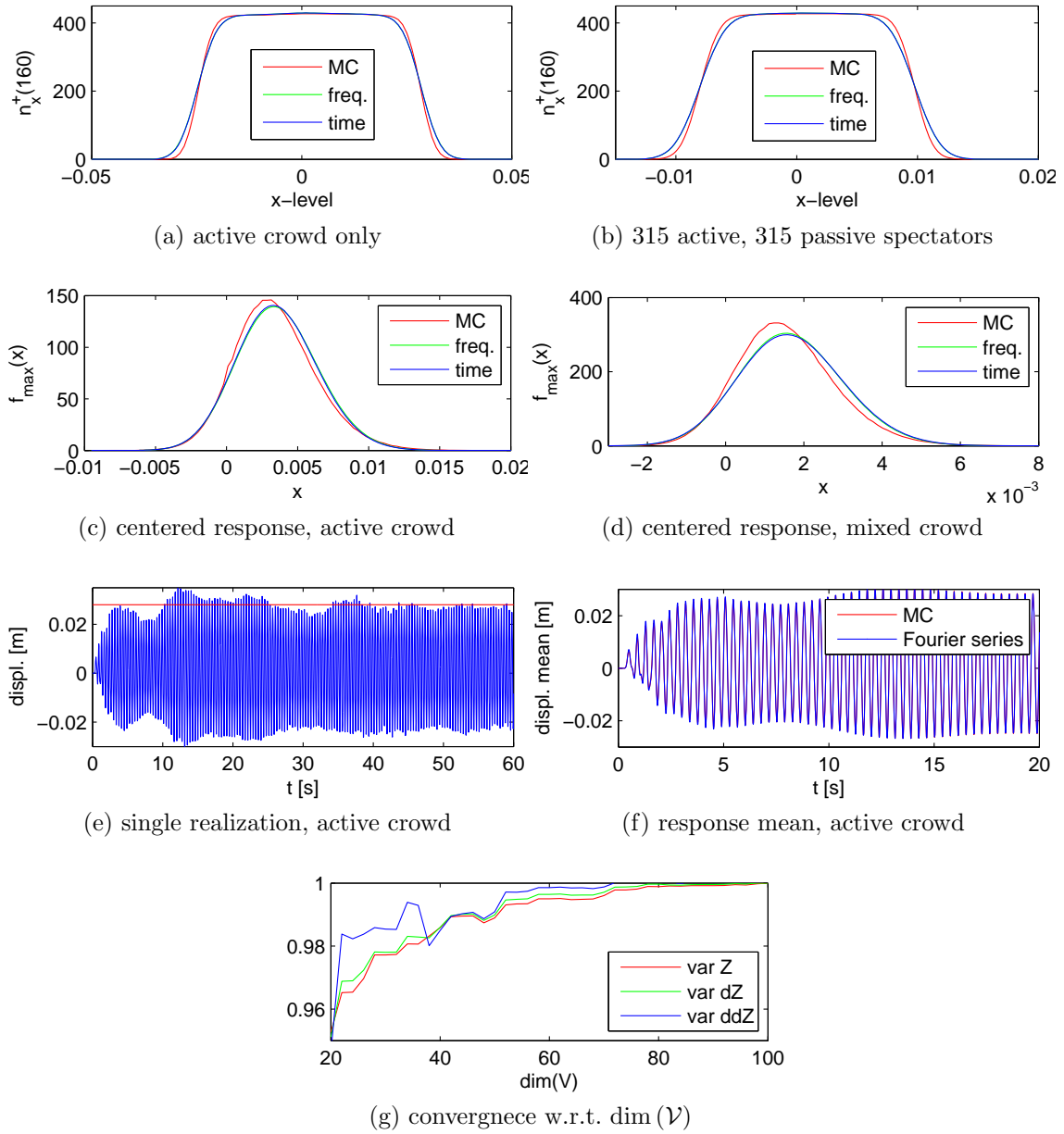


Figure 4.11: Total mean upcrossings of a real grandstand in Appendix C.3, distribution of maxima, single realization and mean responses for an active crowd and for a mixed crowd; convergence of normalized variances with respect to $\dim(\mathcal{V})$

separated. Hence, the corresponding covariance differential equation, *cf* Eq. (4.11), is adjusted as follows: the diffusion term is now $\mathbf{bE}[\boldsymbol{\chi}_n\boldsymbol{\chi}_n^T]\mathbf{b}^T = p\mathbf{b}\mathbf{b}^T$, since $\mathbf{E}[\boldsymbol{\chi}_n\boldsymbol{\chi}_n^T] = \text{diag}(\mathbf{E}\chi_{1,1}^2, \dots, \mathbf{E}\chi_{n_a,n}^2) = p\mathbf{I}_{n_a n \times n_a n}$. Further, an additional term $\mathbf{q}(t, t) + \mathbf{q}^T(t, t)$ appears. The Itô's formula gives

$$\begin{aligned}
 \frac{\partial}{\partial s} q_{ij}(t, s) &= \frac{\partial}{\partial s} \mathbf{E} h_{ir} \tilde{\chi}_{rq} \mu_{Y,q}(t) X_j(s) \\
 &= \mathbf{E} h_{ir} \tilde{\chi}_{rq} \mu_{Y,q}(t) a_{jm} X_m(s) + \mathbf{E} h_{ir} \tilde{\chi}_{rq} \mu_{Y,q}(t) h_{ju} \tilde{\chi}_{uv} \mu_{Y,v}(s) + \\
 &\quad \underbrace{\mathbf{E} h_{ir} \tilde{\chi}_{rq} \mu_{Y,q}(t) b_{ju} \chi_{n,uv} dB_v(s)}_{=0},
 \end{aligned} \tag{4.41}$$

Full system				
Method/Struct.	Harm. osc.	Beam	Cant. grand.	Real. grand.
$n_{\text{DOF},S}$	1	29	504	4,068
MC 100	1.202 s	40.156 s	760.902 s	10,968 s
Freq. domain	0.106 s	2.672 s	74.639 s	4,178 s
Time domain	0.112 s	2.392 s	38.915 s	6,507 s
MS ROM, <i>cf</i> Chap. 3.4.2 and Eqns. (4.22) – (4.25)				
dim (\mathcal{V})	—	10	15	60
MC 100	—	7.083 s	26.201 s	208 s
Freq. domain	—	0.014 s	0.635 s	56 s
Time domain	—	0.036 s	0.072 s	22 s

Table 4.3: Comparison of computational demands

or in compact form

$$\frac{\partial}{\partial s} \mathbf{q}^\top(t, s) = \mathbf{a} \mathbf{q}^\top(t, s) + \mathbf{Q}^\top(t, s), \quad (4.42)$$

which, assuming homogeneous initial conditions, has the solution

$$\mathbf{q}^\top(t, s) = \int_0^s e^{\mathbf{a}(s-\tau)} \mathbf{Q}(\tau, t) d\tau, \quad (4.43)$$

where

$$\mathbf{Q}^\top(t, \tau) = \mathbf{Q}(\tau, t) = \mathbb{E}[\mathbf{h} \tilde{\chi} \boldsymbol{\mu}_Y(\tau)] [\mathbf{h} \tilde{\chi} \boldsymbol{\mu}_Y(t)]^\top = \mathbf{h} \mathbb{E}[\tilde{\chi} \boldsymbol{\mu}_Y(\tau) \boldsymbol{\mu}_Y(t)^\top \tilde{\chi}^\top] \mathbf{h}^\top. \quad (4.44)$$

Separating \mathbf{a} as in Eq. (4.22) yields

$$e^{\mathbf{a}t} = \sum_{k=0}^{\infty} \frac{t^k}{k!} \mathbf{a}^k = \begin{bmatrix} e^{\mathbf{a}_{11}t} & (\square)_{2k \times l} \\ \mathbf{0}_{l \times 2k} & e^{\mathbf{a}_{22}t} \end{bmatrix}, \quad (4.45)$$

where $(\square) \neq \mathbf{0}$. Hence

$$e^{\mathbf{a}(s-\tau)} \mathbf{Q}(\tau, t) = \begin{bmatrix} e^{\mathbf{a}_{11}(s-\tau)} \mathbf{Q}_{11}(\tau, t) & \mathbf{0}_{2k \times l} \\ \mathbf{0}_{l \times 2k} & \mathbf{0}_{l \times l} \end{bmatrix}, \quad (4.46)$$

where

$$\mathbf{Q}_{11}(\tau, t) = \begin{bmatrix} \mathbf{0}_{k \times k} & \mathbf{0}_{k \times k} \\ \mathbf{0}_{k \times k} & M^{-1} \mathbf{G} \mathbb{E} \left[\underbrace{\tilde{\chi} \boldsymbol{\mu}_Y(\tau) \boldsymbol{\mu}_Y(t)^\top \tilde{\chi}^\top}_{(\bullet)} \right] \mathbf{G}^\top M^{-\top} \end{bmatrix}. \quad (4.47)$$

Here, expectation of the terms in square brackets can be rewritten as $(\bullet)_{ij}(\tau, t) = \mathbb{E} \tilde{\chi}_{im} \tilde{\chi}_{jn} \boldsymbol{\mu}_{Y,m}(\tau) \boldsymbol{\mu}_{Y,n}(t) = \mathbb{E} \tilde{\chi}_i \tilde{\chi}_j \boldsymbol{\mu}_{Y,i}(\tau) \boldsymbol{\mu}_{Y,j}(t)$ where the summation over i, k indices is not implied in the last equality. In compact form using the Hadamard product we obtain $(\bullet)(\tau, t) = \text{cov}(\chi_i, \chi_j) \circ [\boldsymbol{\mu}_Y(\tau) \boldsymbol{\mu}_Y^\top(t)]$, *cf* Eq. (3.19), $\text{cov}(\chi_i, \chi_j) \in \mathbb{R}^{n_a \times n_a}$, and

can be expressed for $\boldsymbol{\mu}_Y(t) = [1, \dots, 1]^\top \mu_Y(t)$, which is our case, also as

$$\text{cov}(\chi_i, \chi_j) \circ [\boldsymbol{\mu}_Y(\tau) \boldsymbol{\mu}_Y^\top(t)] = \underbrace{\mu_Y(\tau) \mathbf{I}_{n_a \times n_a}}_{\text{to be integrated}} \underbrace{\text{cov}(\chi_i, \chi_j)}_{\text{to be separated}} \mu_Y(t) \quad (4.48)$$

yielding n_a mean value problems efficiently solved in the frequency domain. ROM is employed in straightforward manner, replacing all matrices with their reduced order counterparts, *cf* Sec. 3.4.2 and 4.2.1.3. Equation (4.25) is then extended with a time average $\mathbf{q}_{11} + \mathbf{q}_{11}^\top$, *cf* also the following text.

Interactions of active spectators can be introduced through χ_i variables to better capture the behaviour of an active crowd. Reasonable assumptions are

- spatially independent spectators,
- spatially correlated spectators, *e.g.* homogeneous isotropic covariance field,

cf Eq. (4.49) where corresponding relations are given in explicit form. In the first case, interactions between active spectators are omitted. In the second case, interactions depend on mutual distance, leading to a covariance field in the exponential form. Some spatial or directional dependencies could be adopted in principle, however, are omitted in further considerations since, to our best knowledge, no relevant information is available in the literature.

$$\mathbb{E} \tilde{\chi}_i \tilde{\chi}_j = \begin{cases} p(1-p) \delta_{ij} & \chi_i \text{s are } iid, \text{ no interaction} \\ p(1-p) e^{-\alpha \rho_{ij}} & \text{homogeneous isotropic interaction,} \end{cases} \quad (4.49)$$

where $\alpha > 0$ and $\rho_{ij} = |\mathbf{r}_i - \mathbf{r}_j|$ denotes the horizontal distance between i -th and j -th spectator, \mathbf{r}_i being the projections of the position vector to the horizontal plane.

Having set some assumptions on χ_i , discussion of solution estimates can be carried out. Non-stationary term $\mathbf{q}(t, t) + \mathbf{q}^\top(t, t)$, *cf* Eq. (4.43), can be managed in several ways: exact time integration of Eq. (4.42) and modified Eq. (4.11); neglecting $\mathbf{q}(t, t)$; approximation with time averages, *e.g.* time-mean $\mathbf{q} = \frac{1}{T} \int_0^T \mathbf{q}(t, t) dt$. It is worth saying also that the spatial correlations of active spectators in Eq. (4.49) influence results only through $\mathbf{q}(t, t)$ term. Therefore, approaches neglecting this term also neglect the differences between δ -correlated and spatially correlated active spectators. The procedure will be demonstrated on the following two examples.

Example 4.6. Let us have a harmonic oscillator with following equation of motion and homogeneous initial conditions

$$\ddot{Z}(t) + 2\zeta\nu\dot{Z}(t) + \nu^2 Z(t) = \chi[W(t) + a \sin(\eta t)], \quad t \geq 0. \quad (4.50)$$

In the state-space form we have Eq. (4.39) together with

$$\mathbf{X}(t) = \begin{bmatrix} Z(t) \\ \dot{Z}(t) \end{bmatrix}, \quad \mathbf{a} = \begin{bmatrix} 0 & 1 \\ -\nu^2 & -2\zeta\nu \end{bmatrix}, \quad \mathbf{G} = \mathbf{M} = 1, \quad \mathbf{b} = \begin{bmatrix} 0 \\ \sqrt{\sigma} \end{bmatrix} \quad (4.51)$$

where $W(t) = dB(t)/dt$ is the Gaussian white noise with intensity $\sqrt{\sigma}$; $a, \zeta, \nu > 0$ denote amplitude, damping ratio and undamped natural frequency. The steady-state mean value

response is obtained in the form

$$\mathbf{E}\mathbf{X}(t) = \mathbf{E}\chi a\vartheta \begin{bmatrix} \sin(\eta t + \varphi) \\ \eta \cos(\eta t + \varphi) \end{bmatrix}, \quad t \geq 0, \quad (4.52)$$

where $\vartheta = \frac{1}{\sqrt{(2\nu\zeta)^2 + (\nu^2 - \eta^2)^2/\eta^2}}$ and $\varphi = \arctan\left(\frac{2\eta\nu\zeta}{\eta^2 - \nu^2}\right)$. Covariance function $\dot{\mathbf{c}}_X(t, t)$ fulfils

$$\dot{\mathbf{c}}_X(t, t) = \mathbf{a}\mathbf{c}_X(t, t) + \mathbf{c}_X(t, t)\mathbf{a}^\top + \mathbf{E}\chi^2\mathbf{b}\mathbf{b}^\top + \mathbf{q}(t, t) + \mathbf{q}^\top(t, t). \quad (4.53)$$

Here

$$\mathbf{Q}(\tau, t) = a^2 \mathbf{var}(\chi) \begin{bmatrix} 0 \\ \sin(\eta\tau) \end{bmatrix} \begin{bmatrix} 0 & \sin(\eta t) \end{bmatrix}, \quad (4.54)$$

$$\mathbf{q}^\top(t, s) = \int_0^s e^{\mathbf{a}(t-s)} \mathbf{Q}(\tau, t) d\tau = \mathbf{var}(\chi) \int_0^s e^{\mathbf{a}(t-s)} \begin{bmatrix} 0 \\ a \sin(\eta\tau) \end{bmatrix} d\tau \begin{bmatrix} 0 & a \sin(\eta t) \end{bmatrix}. \quad (4.55)$$

The integration yields $\mathbf{E}\mathbf{X}(s)/\mathbf{E}\chi$, hence

$$\mathbf{q}^\top(t, t) = \frac{\mathbf{var}(\chi)}{\mathbf{E}\chi} \mathbf{E}\mathbf{X}(t) \begin{bmatrix} 0 & a \sin(\eta t) \end{bmatrix} = a^2 \vartheta \mathbf{var}(\chi) \begin{bmatrix} 0 & \sin(\eta t + \varphi) \sin(\eta t) \\ 0 & \eta \cos(\eta t + \varphi) \sin(\eta t) \end{bmatrix}. \quad (4.56)$$

Results for exact and steady state solutions are depicted in Fig. 4.12 together with a time average for comparison. Since Eq. (4.53) is linear, the two parts of its right hand side can be treated separately. Stationary response due to $\mathbf{E}\chi^2\mathbf{b}\mathbf{b}^\top$ term is $\mathbf{c}_X^b = \frac{\sigma\mathbf{E}\chi^2}{4\zeta\nu} \begin{bmatrix} \frac{1}{\nu^2} & 0 \\ 0 & 1 \end{bmatrix}$. Equation $\dot{\mathbf{c}}_X^q(t, t) = \mathbf{a}\mathbf{c}_X^q(t, t) + \mathbf{c}_X^q(t, t)\mathbf{a}^\top + \mathbf{q}(t, t) + \mathbf{q}^\top(t, t)$ is resolved numerically with respect to $\mathbf{c}_X^q(t, t)$, and for stationary estimate the Lyapunov equation is solved. Results can be found in Fig. 4.13 below. The graphs indicate that the stationary solution

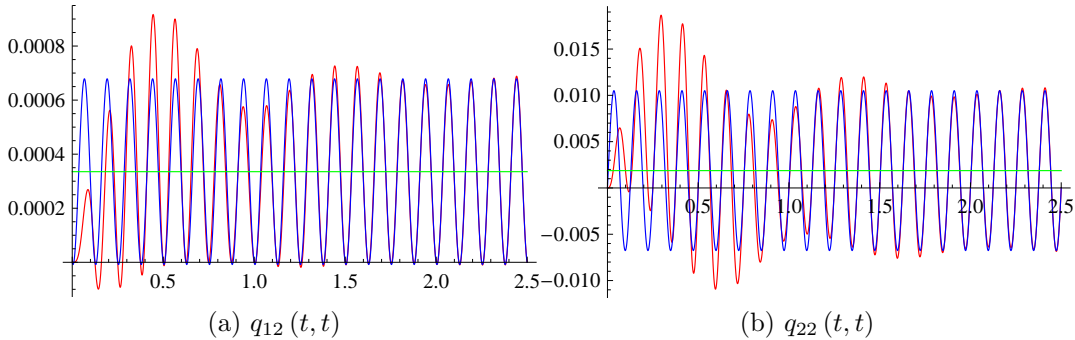


Figure 4.12: $q_{ij}(t, t)$ for $a = 1$, $\nu = 2\pi 5$, $\zeta = 0.05$, $\eta = 2\pi 4$, $\mathbf{var}\chi = 0.25$ and $\sigma = 1$; red – exact, blue – stationary solution, green – time average

using simply the time average of $\mathbf{q}(t, t)$ performs well. Since all quantities are known, *i.e.* $\mathbf{E}\mathbf{F}(t)$ and $\mathbf{E}\mathbf{X}(t)$, resulting stationary approximation of additional term restricts only to evaluation of their tensor product time average in this simple example. Based on comparison with $\mathbf{E}\chi^2\mathbf{b}\mathbf{b}^\top$, the additional term \mathbf{q} can be occasionally neglected.

Example 4.7. Let us further review the results in P_1 point of the cantilever grandstand in Appendix C.2 obtained by MC and by the above analytical solution, load level set

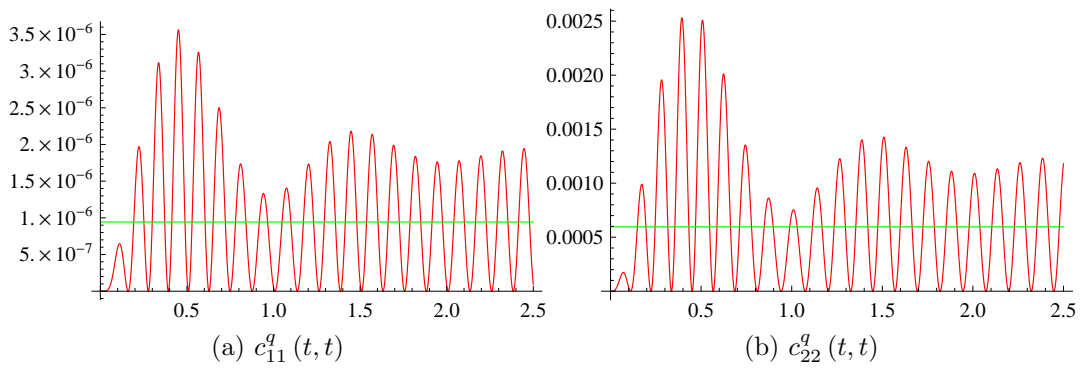


Figure 4.13: $c_{ii}^a(t, t)$ for the same data as in Fig. 4.12, $c_{11}^b = 8.063e-5$, $c_{22}^b = 7.958e-2$;
red – exact, green – time average

to $p = 0.5$. For results *cf* Fig. 4.14 and Tab. 4.4, where the following abbreviations are used: Anl δ – analytical solution with spatially δ -correlated active crowd without additional term \mathbf{q} ; Anl δ add – analytical solution with δ -correlated active crowd and time averaged additional term; MC 1,000 – MC simulation based on 1,000 realizations for δ -correlated active crowd; Anl ρ – analytical solution with spatially correlated crowd according to Eq. (4.49₂) for $\alpha = -2 \ln(0.5)$ and time averaged additional term. Such a covariance means that the correlation coefficient of two 0.5 m distant spectators is 0.5. Clearly, in this particular case, the additional term \mathbf{q} can be neglected when only RMS values are of our interest, since the error is less than 5 %, *cf* the results in Tab. 4.4. Note that all computations were performed in time domain employing MS ROM.

Fig. 4.15a and 4.15b capture the behaviour of $\text{var}\ddot{Z}_{P_1}(p)$ resp. RMS $\ddot{Z}_{P_1}(p)$ for $p \in [0, 1]$ and several values of α . Note that $\text{var}\ddot{Z}_{P_1}(p)$ is linear in p neglecting \mathbf{q} , hence the departure from the straight line reflects the influence of the \mathbf{q} term which is quadratic in p , *cf* Eq. (4.49). Figs. 4.15c, 4.15d capture $\text{var}\ddot{Z}_{P_1}(\alpha)$ resp. RMS $\ddot{Z}_{P_1}(\alpha)$ for $\alpha \in [1e-4, 100]$ with fixed probability p . Note that $\alpha \rightarrow \infty$ is a limit for δ -correlation, *i.e.* a diagonal matrix $\text{cov}(\chi_i, \chi_j)$, and $\alpha \rightarrow 0$ is a limit for a unit spatial correlation, *i.e.* a degenerate case with rank one matrix $\text{cov}(\chi_i, \chi_j)$ of no particular interest. Steepest descend is attained for $\alpha = 0.302$, *i.e.* $\alpha = -2 \ln(0.860)$, meaning that the correlation coefficient of two 0.5 m distant spectators is 0.860, rather strong correlation. Fig. 4.15e captures a single acceleration trajectory $\ddot{Z}_{P_1}(t)$ together with RMS value in comparison with estimate in Eq. (4.29) and floating RMS in Eq. (1.2) for $\tau = 1$ and 10 s.

Model	$\text{var}Z_{P_1}$ [m ²]	$\text{var}\ddot{Z}_{P_1}$ [m ² /s ⁴]	RMS Z_{P_1} [m]	RMS \ddot{Z}_{P_1} [m/s ²]	Time [s]
Anl δ	$1.468e-6$	1.843	$3.187e-3$	2.991	0.202
Anl δ add	$1.702e-6$	2.016	$3.223e-3$	3.020	7.187
MC 1,000	$1.793e-6$	2.181	$3.150e-3$	2.928	30.202 ¹⁾
Anl ρ	$2.499e-6$	2.657	$3.345e-3$	3.124	7.270

Table 4.4: Comparison of variances, RMS values and time consumptions for $p = 0.5$;

¹⁾ time for 100 realizations

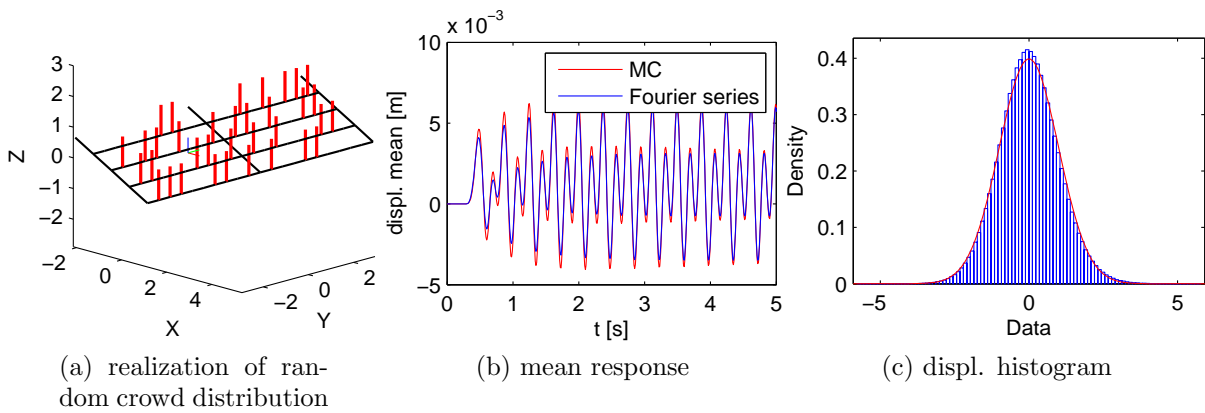


Figure 4.14: Realization of uniform δ -correlated random crowd distribution, mean response and histogram assuming ergodicity for cantilever grandstand in Appendix C.2

4.3 Non-Gaussian input

It was observed in Sec. 4.2.1.5 that the centered forcing term resembles a non-Gaussian coloured noise. Nevertheless, it was assumed that the outputs and hence inputs are Gaussian processes as an approximation. This section attempts to model the forcing of the deterministic system in Eq. (2.1) as non-Gaussian processes, and to solve higher-order moment equations in order to achieve a better agreement in upcrossing rates. Translation and Poisson white noise processes will be considered for this purpose assuming only the deterministic distribution of a crowd. Finally, several other possibilities will be mentioned and discussed.

4.3.1 Translation processes

Firstly, the input forces are approximated with the memoryless translation processes to approach a better agreement in the marginal distribution. This cannot be achieved, however, without affecting the covariance function or the spectral density. Hence, this effect will be discussed in more detail.

4.3.1.1 Approximation of the input

A scalar translation process, *cf* [18], is a process of the form

$$\tilde{F}(t) = g_1(\tilde{Y}(t)) = \mathbb{F}_1^{-1} \left[\Phi(\tilde{Y}(t)) \right], \quad (4.57)$$

where g_1 is a monotonic function, $\tilde{Y}(t)$ a stationary Gaussian process with zero mean, unit variance, covariance function $\rho(\tau) = \mathbb{E}\tilde{Y}(t+\tau)\tilde{Y}(t)$, and marginal distribution $\Phi(y) = \mathbb{P}[\tilde{Y}(t) \leq y]$, previously introduced as AR(p_i) or as a linear combination of AR(2) processes. Assuming that the marginal distribution function \mathbb{F}_1 has no atoms, the translation

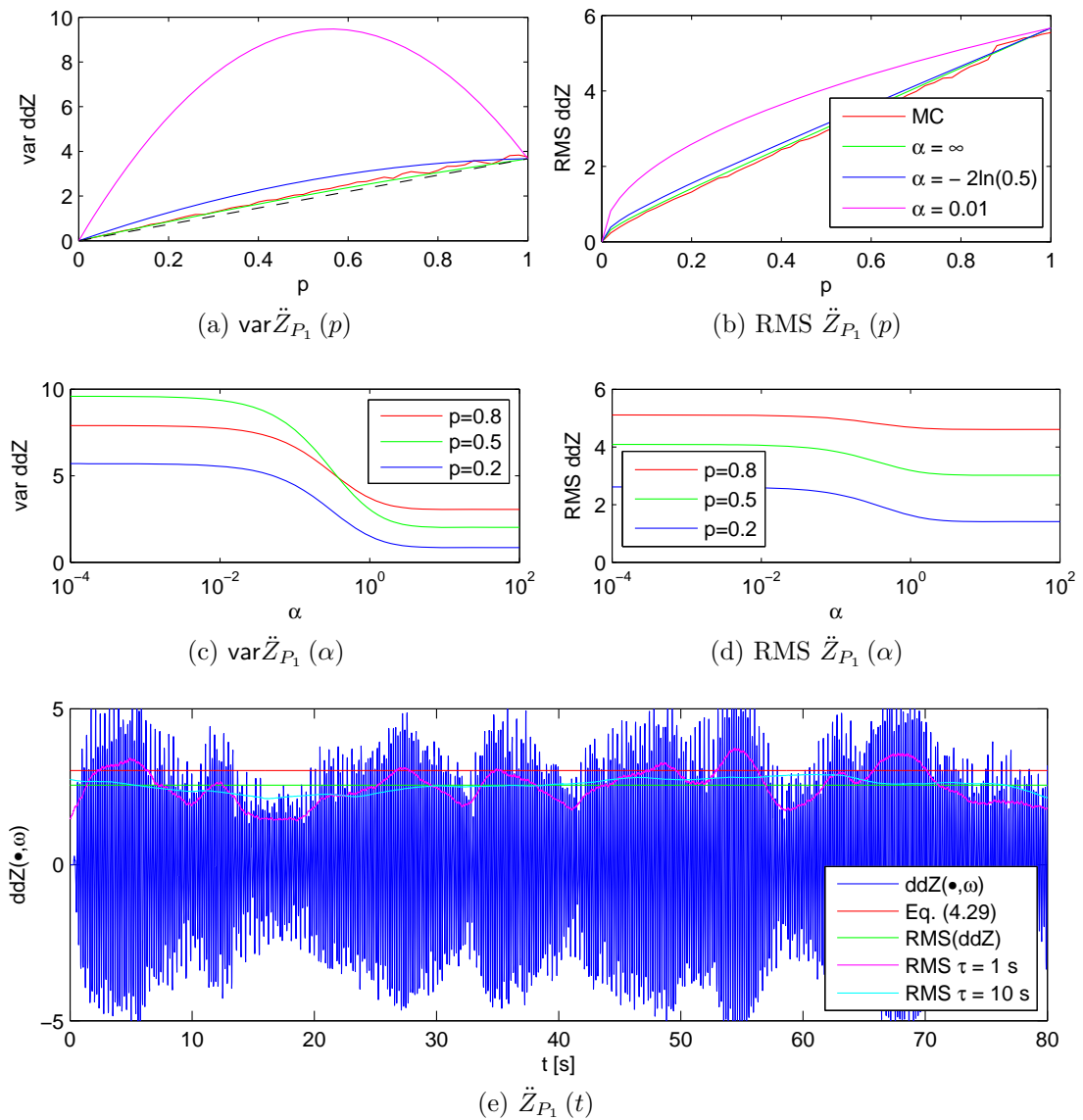


Figure 4.15: Variance and RMS value as functions of p (a) and (b); variance and RMS value as functions of α (c) and (d); single trajectory of $\ddot{Z}_{P_1}(t)$, RMS, floating RMS for $\tau = 1$ resp. 10 s and the stationary estimate in Eq. (4.29) in (e)

process $\tilde{F}(t)$ follows the marginal distribution

$$\begin{aligned} \mathbb{P} \left[\tilde{F}(t) \leq x \right] &= \mathbb{P} \left[\mathbb{F}_1^{-1} \left(\Phi \left(\tilde{Y}(t) \right) \right) \leq x \right] \\ &= \mathbb{P} \left[\tilde{Y}(t) \leq \Phi^{-1} \left(\mathbb{F}_1(x) \right) \right] = \mathbb{F}_1(x) \end{aligned} \quad (4.58)$$

for all x , since g_1 is a monotonic function, with moments

$$\mathbb{E} \left[\tilde{F}(t) \right]^k = \mathbb{E} \left[g_1 \left(\tilde{Y}(t) \right) \right]^k = \int_{-\infty}^{\infty} [g_1(y)]^k \phi(y) dy \quad (4.59)$$

and the correlation function

$$\begin{aligned} r_{\tilde{F}}(\tau) &= \mathbb{E}\tilde{F}(t+\tau)\tilde{F}(t) = \mathbb{E}g_1\left(\tilde{Y}(t+\tau)\right)g_1\left(\tilde{Y}(t)\right) \\ &= \int_{-\infty}^{\infty}\int_{-\infty}^{\infty}g_1(y_1)g_1(y_2)\phi(y_1,y_2;\rho(\tau))dy_1dy_2, \end{aligned} \quad (4.60)$$

where $\phi(y_1, y_2; \rho(\tau))$ is the standard bivariate Gaussian density. Covariance $c_{\tilde{F}}(\tau)$ can be obtained from the Price theorem, *cf* [18], or from Eqns. (4.59) and (4.60). Since $|c_{\tilde{F}}(\tau)/c_{\tilde{F}}(0)| \leq |\rho(\tau)|$, it is not always possible to find such a $\rho(\tau)$ to yield the target covariance $c_{\tilde{F}}(\tau)$ under the transformation in Eq. (4.57). Anyway, new optimization should be performed in order to achieve the best agreement, or to obtain unit variance of $\tilde{Y}(t)$, *cf* Sec. 4.2.1.5.

One of the many possibilities for the memoryless approximation $\tilde{F}(t)$ is the Hermite polynomial approximation,

$$\tilde{F}^*(t) = g_1^*\left(\tilde{Y}(t)\right) = \sum_{k=0}^n a_k H_k\left(\tilde{Y}(t)\right), \quad (4.61)$$

where $H_k(y)$, $k = 0, \dots, n$ are probabilists' Hermite polynomials. The minimization of $e(a_0, \dots, a_n) = \mathbb{E}\left(\tilde{F}^*(t) - \tilde{F}(t)\right)^2$ yields

$$\mathbb{E}\left[\left(\sum_{l=0}^n a_l H_l\left(\tilde{Y}(t)\right) - \tilde{F}(t)\right)H_k\left(\tilde{Y}(t)\right)\right] = 0, \quad k = 0, \dots, n, \quad (4.62)$$

with the solution

$$a_k = \frac{1}{k!}\mathbb{E}\left[\tilde{F}(t)H_k\left(\tilde{Y}(t)\right)\right], \quad k = 0, \dots, n, \quad (4.63)$$

owing to the orthogonality of $H_k(y)$ with respect to the Gaussian measure. Substituting from Eq. (4.57), we arrive at

$$a_k = \frac{1}{k!}\mathbb{E}\left[g_1\left(\tilde{Y}(t)\right)H_k\left(\tilde{Y}(t)\right)\right] = \frac{1}{k!}\int_{-\infty}^{\infty}\mathbb{F}_1^{-1}[\Phi(y)]H_k(y)\phi(y)dy. \quad (4.64)$$

Integration is performed numerically on bounded interval; \mathbb{F}_1 , its inverse and subsequent composition with Φ is based on CDF obtained from MC simulation, *cf* histograms in Figs. 4.2c and 4.2d, evaluated in discrete points with inhomogeneous partition.

Another possibility assuming only the mild nonlinearity of g_1 is a linear form of Hermite polynomials

$$\tilde{F}^*(t) = \sigma\tilde{Y}(t) + \sigma\sum_{k=2}^n\beta_k H_k\left(\tilde{Y}(t)\right) \quad (4.65)$$

yielding to

$$\tilde{F}^*(t) = \sigma\tilde{Y}(t) + \sigma\frac{\gamma_3}{6}H_2\left(\tilde{Y}(t)\right) + \sigma\frac{\gamma_4 - 3}{24}H_3\left(\tilde{Y}(t)\right) \quad (4.66)$$

for $n = 3$, where σ^2 , γ_3 and γ_4 are variance, coefficient of skewness and kurtosis of $\tilde{F}(t)$. Results for both approaches are summarized in Fig. 4.16, where the particular dependencies and their approximations are depicted for $f_p = 2.7$ Hz, and in Tab. 4.5, where the coefficients a_k are presented for $k = 0, \dots, 6$ and for all frequencies f_p .

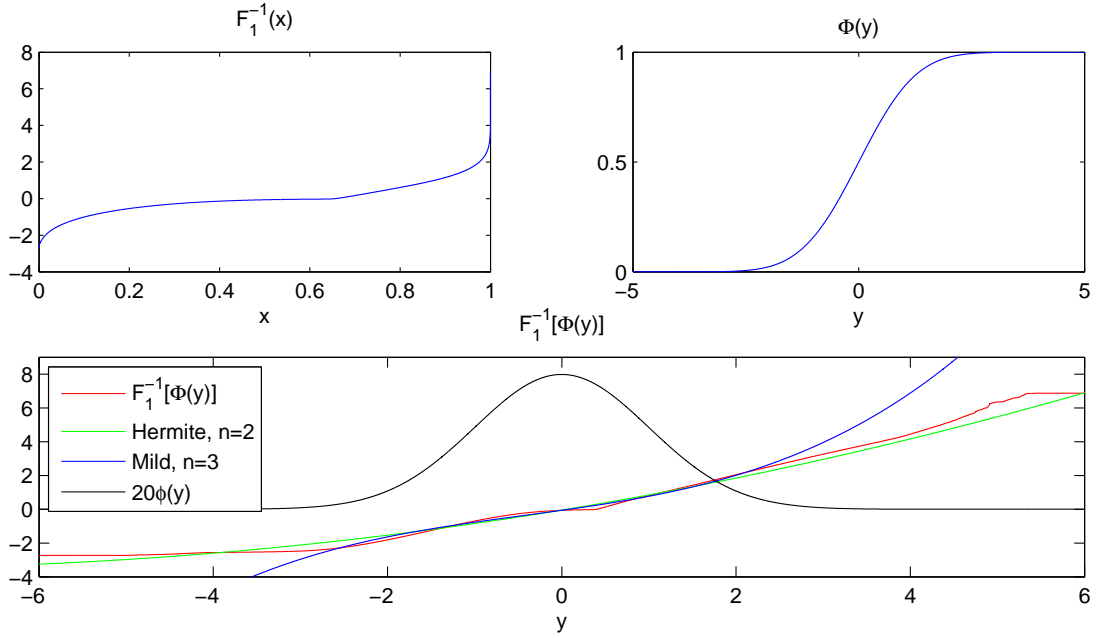


Figure 4.16: Inverse of the marginal distribution \mathbb{F}_1 , Gaussian CDF Φ , translation function $g_1 = \mathbb{F}_1^{-1}\Phi$ and its approximations in Eqns. (4.61) and (4.66)

Coeff.	$f_p = 1.5$ Hz	$f_p = 2.0$ Hz	$f_p = 2.7$ Hz	$f_p = 3.5$ Hz
a_0	0	0	0	0
a_1	0.8690	0.8039	0.8639	0.8151
a_2	0.0853	0.0508	0.0546	0.0465
a_3	0.0351	0.0552	0.0355	0.0131
a_4	0.0013	-0.0011	-0.0032	-0.0048
a_5	-0.0043	-0.0082	-0.0076	-0.0045
a_6	0.0012	0.0009	0.0009	0.0010
σ^2	0.7865	0.6824	0.7486	0.6788
γ_3	0.7000	0.4765	0.4243	0.3504
γ_4	4.8919	5.0459	4.0761	3.4354

Table 4.5: Coefficients a_k in Eq. (4.61) for an arbitrary level n ; variance σ^2 , coefficient of skewness γ_3 and kurtosis γ_4 for centered unit processes of jumping frequencies f_p ; values based on 3,000 MC realizations

Having performed the approximation, we refer back to covariance function and its changes because of nonlinear transformation. Based on explicit expressions for Hermite polynomials and Isserlis' theorem for zero mean unit variance Gaussian variables, it can be shown that

$$c_{\tilde{F}^*}(\tau) = a_1^2 \rho(\tau) + 2a_2^2 \rho(\tau)^2 \quad \text{for } n = 2. \quad (4.67)$$

Relations between the scaled covariances and their Gaussian images are depicted in Fig. 4.17a for approximation in Eq. (4.61) with coefficients from Tab. 4.5, and $\tilde{F}^*(t) =$

$\tilde{Y}^3(t)$ for comparison. To quantify changes in the spectral density, Fig. 4.17b captures the behaviour based on 500 MC simulations. Although the scaled covariance functions are al-

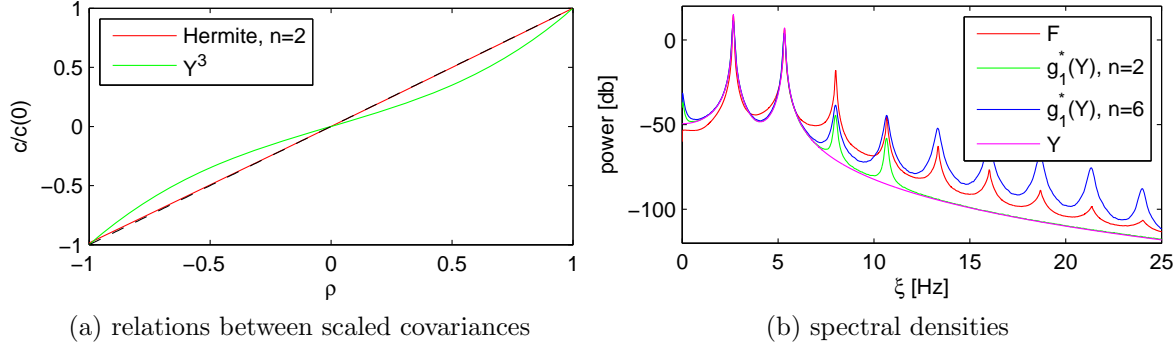


Figure 4.17: Relations between normalized covariance functions, $f_p = 2.7$ Hz; comparison of spectral densities for $\tilde{Y}(t)$ a linear combination of two AR(2) processes

most indistinguishable, we note from Fig. 4.17b that the spectral density is non-negligibly altered, but somewhat in positive manner. This phenomenon can be perhaps explained such that the transformation g_1 is equivalent to some nonlinear dynamical system, yielding super- and sub-harmonics of the input. This could be also utilized in the second order moment approximation to lower the number of AR(2) processes employed in the approximation of $\tilde{Y}(t)$. The price is, however, the solution of Eq. (4.71), which is too high. Note also that $\text{var}\tilde{F}^*(t) \neq \text{var}\tilde{F}(t)$, since $\text{var}\tilde{F}^*(t) = c_{\tilde{F}^*}(0) = a_1^2 + 2a_2^2 = 0.7523$ and is slightly different from the target variance 0.7486 in the case $f_p = 2.7$ Hz and $n = 2$. For completeness, Tab. 4.6 summarizes the coefficients for two AR(2) processes approximating $\tilde{Y}(t)$ in Eq. (4.61) normalized to a unit variance.

$f_p = 1.5$ Hz					$f_p = 2.0$ Hz				
i	$c_{1,i}$	$c_{2,i}$	$c_{3,i}$	f_i	i	$c_{1,i}$	$c_{2,i}$	$c_{3,i}$	f_i
1	12.0710	0.1358	0.0525	1.50	1	17.8514	0.1130	0.0425	2.00
2	40.4630	0.1139	0.0509	3.00	2	44.6022	0.0706	0.0285	4.00
$f_p = 2.7$ Hz					$f_p = 3.5$ Hz				
i	$c_{1,i}$	$c_{2,i}$	$c_{3,i}$	f_i	i	$c_{1,i}$	$c_{2,i}$	$c_{3,i}$	f_i
1	22.4105	0.0796	0.0309	2.67	1	25.8621	0.0535	0.0222	3.50
2	63.6593	0.0565	0.0243	5.34	2	106.0087	0.0548	0.0283	7.00

Table 4.6: Coefficients $c_{k,i}$, $k = 1, 2, 3$ and $i = 1, 2$ of the two independent AR(2) members used for approximation of the centered unit variance forcing term $\tilde{Y}(t)$ in frequency range 0.5 – 10 Hz

4.3.1.2 System response

In this section, the moment equations of the system output up to the third order will be derived assuming $\tilde{F}(t) = a_1 H_1(\tilde{Y}(t)) + a_2 H_2(\tilde{Y}(t))$, *i.e.* at most quadratic, $\tilde{Y}(t)$ being

an AR(p_i) process for simplicity. It is known fact, *cf* [19], that the moment equations of the system driven by polynomials of Gaussian processes are closed. SDE in Eqns. (4.8) resp. (4.9) are assumed in separate form, *cf* also Eq. (4.22),

$$d \begin{bmatrix} \tilde{\mathbf{X}}(t) \\ \mathbf{S}(t) \end{bmatrix} = \begin{bmatrix} \mathbf{a}_{11} & \mathbf{a}_{12} \\ \mathbf{0}_{2k \times 2k} & \mathbf{a}_{22} \end{bmatrix} \begin{bmatrix} \tilde{\mathbf{X}}(t) \\ \mathbf{S}(t) \end{bmatrix} dt + \begin{bmatrix} \mathbf{g}(\mathbf{S}(t)) \\ \mathbf{0}_{l \times n_a} \end{bmatrix} dt + \begin{bmatrix} \mathbf{0}_{2k \times n_a} \\ \mathbf{b} \end{bmatrix} d\mathbf{B}(t), \quad (4.68)$$

where $\tilde{\mathbf{X}}(t) = \left[\tilde{\mathbf{Z}}^\top(t), \dot{\tilde{\mathbf{Z}}}^\top(t) \right]^\top$, $\mathbf{S}(t) = [\mathbf{S}_1^\top(t), \dots, \mathbf{S}_{n_a}^\top(t)]^\top$, $\mathbf{b} = \text{diag}(\mathbf{b}_1, \dots, \mathbf{b}_{n_a})$, and

$$\mathbf{g} = \begin{bmatrix} \mathbf{0}_{k \times n_a} \\ \mathbf{M}^{-1} \mathbf{G} \end{bmatrix} \begin{bmatrix} \hat{g}_1^*(\mathbf{S}_1) \\ \vdots \\ \hat{g}_{n_a}^*(\mathbf{S}_{n_a}) \end{bmatrix}, \quad (4.69)$$

$k = n_{\text{DOF}}$ for brevity, and $l = \sum_{i=1}^{n_a} p_i$; $\hat{g}_i^*(\bullet)$ is a quadratic part of $g_i^*(\bullet)$ in Eq. (4.61), constant part is zero, *cf* Tab. 4.5, and the linear part is included into the diffusion term \mathbf{b} . Then, the Itô's formula yields nine systems of the linear equations to be solved sequentially, written in tensor notation and skipping the function arguments for brevity, Einstein summation implied. The mean value equation reads

$$\frac{d}{dt} \mathbf{E} \tilde{X}_p = a_{pu}^{11} \mathbf{E} \tilde{X}_u + \mathbf{E} g_p \quad (4.70)$$

yielding nonzero mean, since the second order moments of S_i constitute the right hand side. To solve the correlation matrix, following third-order moments are required

$$\begin{aligned} \frac{d}{dt} \mathbf{E} \tilde{X}_p S_q S_r &= a_{pu}^{11} \mathbf{E} \tilde{X}_u S_q S_r + a_{pv}^{12} \underbrace{\mathbf{E} S_v S_q S_r}_{=0} + \mathbf{E} g_p S_q S_r + \\ &\mathbf{E} \tilde{X}_p [a_{qv}^{22} S_v S_r + S_q a_{rv}^{22} S_v] + \mathbf{E} \tilde{X}_p (\mathbf{b} \mathbf{b}^\top)_{qr}, \end{aligned} \quad (4.71)$$

the second term on the right hand side being zero owing to the properties of the zero mean Gaussian variables. Then, separating again into two subsystems as in Eqns. (4.24) and (4.25), the correlation can be computed as

$$\frac{d}{dt} \mathbf{E} \tilde{X}_p S_q = \mathbf{E} \tilde{X}_p a_{qv}^{22} S_v + a_{pu}^{11} \mathbf{E} \tilde{X}_u S_q + a_{pv}^{12} \mathbf{E} S_v S_q + \underbrace{\mathbf{E} g_p S_q}_{=0} \quad (4.72)$$

$$\begin{aligned} \frac{d}{dt} \mathbf{E} \tilde{X}_p \tilde{X}_q &= \mathbf{E} \tilde{X}_p a_{qu}^{11} \tilde{X}_u + a_{pu}^{11} \mathbf{E} \tilde{X}_u \tilde{X}_q + \mathbf{E} \tilde{X}_p g_q + \mathbf{E} g_p \tilde{X}_q + \\ &a_{pv}^{12} \mathbf{E} S_v \tilde{X}_q + \mathbf{E} \tilde{X}_p a_{qv}^{12} S_v. \end{aligned} \quad (4.73)$$

Eventually, in order to obtain the third order moments of \tilde{X}_p , following systems of linear equations have to be solved sequentially

$$\begin{aligned} \frac{d}{dt} \mathbf{E} \tilde{X}_p S_q S_r S_s &= a_{pu}^{11} \mathbf{E} \tilde{X}_u S_q S_r S_s + a_{pv}^{12} \mathbf{E} S_v S_q S_r S_s + \underbrace{\mathbf{E} g_p S_q S_r S_s}_{=0} + \\ &\mathbf{E} \tilde{X}_p \left[a_{qv}^{22} S_v S_r S_s + S_q a_{rv}^{22} S_v S_s + S_q S_r a_{sv}^{22} S_v \right] + \\ &\mathbf{E} \tilde{X}_p \left[(\mathbf{b} \mathbf{b}^\top)_{qr} S_s + S_r (\mathbf{b} \mathbf{b}^\top)_{sq} + S_q (\mathbf{b} \mathbf{b}^\top)_{rs} \right], \end{aligned} \quad (4.74)$$

$$\begin{aligned} \frac{d}{dt} \mathbf{E} \tilde{X}_p \tilde{X}_q S_r &= a_{pu}^{11} \mathbf{E} \tilde{X}_u \tilde{X}_q S_r + a_{pv}^{12} \mathbf{E} S_v \tilde{X}_q S_r + \mathbf{E} g_p \tilde{X}_q S_r + \mathbf{E} \tilde{X}_p a_{qu}^{11} \tilde{X}_u S_r + \\ &\mathbf{E} \tilde{X}_p a_{qv}^{12} S_v S_r + \mathbf{E} \tilde{X}_p g_q S_r + \mathbf{E} \tilde{X}_p \tilde{X}_q a_{rv}^{22} S_v, \end{aligned} \quad (4.75)$$

$$\begin{aligned} \frac{d}{dt} \mathbf{E} \tilde{X}_p S_q S_r S_s S_t &= a_{pu}^{11} \mathbf{E} \tilde{X}_u S_q S_r S_s S_t + \underbrace{a_{pv}^{12} \mathbf{E} S_v S_q S_r S_s S_t}_{=0} + \mathbf{E} g_p S_q S_r S_s S_t + \\ &\mathbf{E} \tilde{X}_p \left[a_{qv}^{22} S_v S_r S_s S_t + S_q a_{rv}^{22} S_v S_s S_t + S_q S_r a_{sv}^{22} S_v S_t + S_q S_r S_s a_{tv}^{22} S_v \right] + \\ &\mathbf{E} \tilde{X}_p \left[(\mathbf{b} \mathbf{b}^\top)_{qr} S_s S_t + (\mathbf{b} \mathbf{b}^\top)_{qs} S_r S_t + S_r S_s (\mathbf{b} \mathbf{b}^\top)_{qt} + S_q (\mathbf{b} \mathbf{b}^\top)_{rs} S_t + \right. \\ &\left. S_q S_s (\mathbf{b} \mathbf{b}^\top)_{rt} + S_q S_r (\mathbf{b} \mathbf{b}^\top)_{st} \right], \end{aligned} \quad (4.76)$$

$$\begin{aligned} \frac{d}{dt} \mathbf{E} \tilde{X}_p \tilde{X}_q S_r S_s &= a_{pu}^{11} \mathbf{E} \tilde{X}_u \tilde{X}_q S_r S_s + a_{pv}^{12} \mathbf{E} S_v \tilde{X}_q S_r S_s + \mathbf{E} g_p \tilde{X}_q S_r S_s + \\ &\mathbf{E} \tilde{X}_p a_{qu}^{11} \tilde{X}_u S_r S_s + \mathbf{E} \tilde{X}_p a_{qv}^{12} S_v S_r S_s + \mathbf{E} \tilde{X}_p g_q S_r S_s + \\ &\mathbf{E} \tilde{X}_p \tilde{X}_q \left[a_{rv}^{22} S_v S_s + S_r a_{sv}^{22} S_v \right] + \mathbf{E} \tilde{X}_p \tilde{X}_q (\mathbf{b} \mathbf{b}^\top)_{rs}, \end{aligned} \quad (4.77)$$

$$\begin{aligned} \frac{d}{dt} \mathbf{E} \tilde{X}_p \tilde{X}_q \tilde{X}_r &= a_{pu}^{11} \mathbf{E} \tilde{X}_u \tilde{X}_q \tilde{X}_r + \mathbf{E} \tilde{X}_p a_{qu}^{11} \tilde{X}_u \tilde{X}_r + \mathbf{E} \tilde{X}_p \tilde{X}_q a_{ru}^{11} \tilde{X}_u + a_{pv}^{12} \mathbf{E} S_v \tilde{X}_q \tilde{X}_r + \\ &\mathbf{E} \tilde{X}_p a_{qv}^{12} S_v \tilde{X}_r + \mathbf{E} \tilde{X}_p \tilde{X}_q a_{rv}^{12} S_v + \mathbf{E} g_p \tilde{X}_q \tilde{X}_r + \mathbf{E} \tilde{X}_p g_q \tilde{X}_r + \mathbf{E} \tilde{X}_p \tilde{X}_q g_r. \end{aligned} \quad (4.78)$$

All coefficient tensors are mapped onto matrices using multiple Kronecker product or direct assembly; multidimensional unknown tensors are vectorized to yield a linear matrix-vector systems of equations. Taking all time derivatives as equal to zero yields a stationary solution. Note that coefficient matrices are mostly non symmetric, increasing overall computational overhead. ROM is performed in standard form; we will not go further into details, since the introduced equations are quite cumbersome and yield many technicalities. Note also that the second order cumulant closure, expressing the third moments in terms of lower order moments, yields high relative errors measured in the Frobenius norm and hence is not even discussed.

4.3.1.3 Upcrossing estimates

For structure safety assessment, the mean upcrossing rates are required. The Rice formula, Eq. (A.1), integrates the joint density $f(x, \dot{x})$ of a random process $X(t)$ which can be approximated having the knowledge of the joint third moments of $X(t)$ and $\dot{X}(t)$. This is, however, the fundamental objective of the so-called problem of moments. For our purposes, following two methods will be employed: Gram-Charlier type A series and translation approximation.

Gram-Charlier series The first approximation is based on the series expansion of the joint density $f(x, \dot{x})$ into the Hermite polynomials, *cf* [18]. Then, in the stationary case, the mean x -upcrossing rate of the level x is approximated by

$$\nu_S(x) = \nu_G(x) \left[1 + \sum_{k=3}^{n_S} \frac{1}{k!} \sum_{\substack{p+q=k \\ p,q \geq 0}} \frac{b_{(p,q)}}{\sigma^p \dot{\sigma}^q} H_p \left(\frac{x - \mu}{\sigma} \right) h_q \right], \quad (4.79)$$

where $H_p(\bullet)$ denotes the Hermite polynomial of order p , coefficients h_q are equal to 1, $\sqrt{\pi/2}$, 1, 0 for $q = 0, \dots, 3$, μ is the mean of $X(t)$ and $\sigma, \dot{\sigma}$ are standard deviations of $X(t), \dot{X}(t)$ and $b_{(p,q)}$ are quasimoments of the vector $[X(t), \dots, X(t), \dot{X}(t), \dots, \dot{X}(t)]^\top$ where $X(t)$ repeats p times and $\dot{X}(t)$ repeats q times. In our case $n_S = 3$ since only the third order moments are available. Denoting $\mu_{(p,q)} = \mathbb{E}X^p(t) \dot{X}^q(t)$, the quasimoments $b_{(p,q)}$ are expressed as

$$\begin{aligned} \sigma^2 &= \mu_{(2,0)} - \mu_{(1,0)}^2, \\ \dot{\sigma}^2 &= \mu_{(0,2)} - \mu_{(0,1)}^2, \\ b_{(3,0)} &= \mu_{(3,0)} - 3\mu_{(1,0)}\mu_{(2,0)} + 2\mu_{(1,0)}^3, \\ b_{(0,3)} &= \mu_{(0,3)} - 3\mu_{(0,1)}\mu_{(0,2)} + 2\mu_{(0,1)}^3, \\ b_{(1,2)} &= \mu_{(1,2)} - 2\mu_{(1,1)}\mu_{(0,1)} - \mu_{(0,2)}\mu_{(1,0)} + 2\mu_{(0,1)}^2\mu_{(1,0)}, \\ b_{(2,1)} &= \mu_{(2,1)} - 2\mu_{(1,1)}\mu_{(1,0)} - \mu_{(2,0)}\mu_{(0,1)} + 2\mu_{(1,0)}^2\mu_{(0,1)}. \end{aligned} \quad (4.80)$$

Translation approximation The second approach, *cf* [18], utilizes again the translation process introduced in Eq. (4.57), where $\tilde{F}(t) \equiv X(t)$ and $\tilde{Y}(t) \equiv Y(t)$ for simplicity, and a Gaussian hypothesis stating that $X(t)$ and $\dot{X}(t)$ are independent random variables, $\dot{X}(t)$ being Gaussian and $X(t)$ with marginal distribution \mathbb{F}_1 . According to these assumptions, mean x -upcrossing rate of $X(t)$ is estimated as

$$\nu_T(x) = \frac{\sigma_{\dot{Y}}}{2\pi} \exp \left[-\frac{1}{2} (g_1^{-1}(x))^2 \right], \quad (4.81)$$

where $\sigma_{\dot{Y}}$ is the standard deviation of $\dot{Y}(t)$ computed from $\mathbb{E}\dot{X}(t)^2 = \sigma_{\dot{Y}}^2 \mathbb{E}g_1'(Y(t))$, obtained easily since $Y(t)$ is a stationary Gaussian unit variance random process, $\mathbb{E}\dot{X}(t)^2$ being known from moment equations. Approximation of g_1 with g_1^* can be again based on Hermite polynomials, *cf* Eq. (4.61). Here, the coefficients a_k are determined from the condition that the differences between the marginal moments

$$e(a_1, \dots, a_n) = \sum_{k=1}^3 (\mathbb{E}[X^k(t)] - \mathbb{E}[X^{*k}(t)])^2 \quad (4.82)$$

are minimized, yielding a nonlinear minimization problem resolved numerically. The covariance function is assumed unchanged for simplicity. Mildly nonlinear transformation in Eq. (4.66) can be also employed with advantage.

Example 4.8. To verify correctness of the implementation, Eqns. (4.70) – (4.78), an SDOF system forced by $\tilde{F}(t) = \tilde{Y}(t) + \tilde{Y}(t)^2$, where $\tilde{Y}(t) = \tilde{Y}_1(t) + \tilde{Y}_2(t)$ with unit variance, $\tilde{Y}_i(t) \sim \text{AR}(2)$ processes from Tab. 4.6 for $f_p = 2.7$ Hz, *cf* Eqns. (4.57) and (4.50), will be compared on the basis of MC simulation. Results for the first three moments are summarized in Tab. 4.7, $\nu = 2\pi 5$ and $\zeta = 0.07$. Since all relative errors are within 3.7 % bounds, the implementation is assumed without substantial errors.

Quantity	MC	mom. Eqns.	Quantity	MC	mom. Eqns.
$EZ(t)$	$1.049e-3$	$1.059e-3$	$E\dot{Z}(t)$	$-4.871e-7$	0.0
$\text{var}Z(t)$	$2.359e-5$	$2.444e-5$	$\text{var}\dot{Z}(t)$	$2.369e-2$	$2.455e-2$
$\gamma_3(Z(t))$	$5.610e-1$	$5.512e-1$	$\gamma_3(\dot{Z}(t))$	$-9.323e-2$	$-9.321e-2$

Table 4.7: Comparison of the first three moments of SDOF system based on moment equations and MC simulation

Example 4.9. Next example compares the stationary mean x -upcrossing $\nu_x^+(t)$ and the third moments of the response in P_1 point of the simply supported beam in Appendix C.1, occupied by two active and two passive spectators, *cf* also Ex. 4.3, active spectators jumping with frequency $f_p = 3.5$ Hz. Centered forces are approximated with translation processes in Eq. (4.61) with coefficients in Tab. 4.5 and Tab. 4.6. Fig. 4.18 captures stationary mean x -upcrossing of centered response based on 1,000 MC realizations 160 s in length, moment equations with Gram-Charlier series in Eq. (4.79) and moment equations with translation approximation in Eq. (4.82). The first three moments are compared in Tab. 4.8. Results are quite in agreement with the simulation.

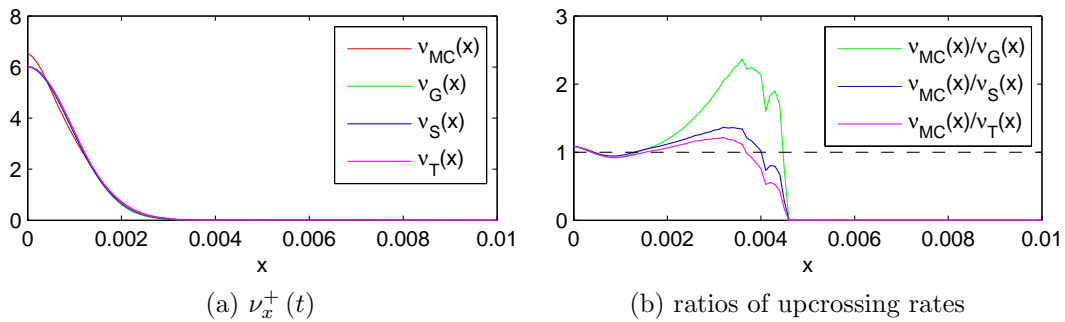


Figure 4.18: Mean stationary x -upcrossing rates of centered response in P_1 point of example in Appendix C.1; ratios of exact to approximate upcrossing rates

4.3.2 Poisson white noise process

Based on heuristic arguments, loading process can be idealized by series of impulses and thus modeled with Poisson white noise, which is viewed as a formal derivative of the compound Poisson process $C(t) = \sum_{k=1}^{N(t)} Y_k = \sum_{k=1}^{\infty} Y_k \mathbb{1}_{[t \geq T_k]}$, where $N(t)$ is a Poisson counting process with intensity λ and jump times T_k , Y_k are real-valued *iid* random variables independent of $N(t)$, $\mathbb{1}_{[t \geq T_k]}$ denotes the indicator function of the time interval $t \geq T_k$.

Quantity	MC	mom. Eqns.	frekv. sol.
$\text{var}Z_{P_1}(t)$	$8.898e-7$	$8.437e-7$	$8.780e-7$
$\gamma_3(Z_{P_1}(t))$	$1.034e-1$	$0.956e-1$	$0.769e-1$
$\text{var}\dot{Z}_{P_1}(t)$	$1.312e-3$	$1.200e-3$	$1.275e-3$
$\gamma_3(\dot{Z}_{P_1}(t))$	$-5.731e-2$	$-7.260e-2$	—

Table 4.8: Comparison of the first three moments of simply supported beam in Appendix C.1 and in the point P_1 based on moment equations, MC simulation and higher order spectra

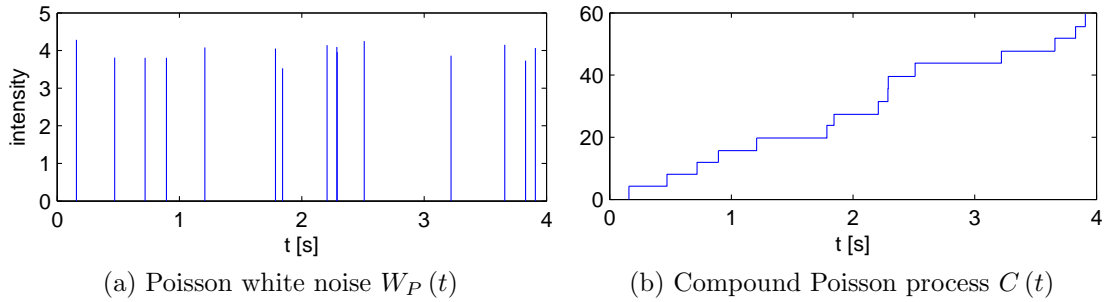


Figure 4.19: Sample of the compound Poisson process $C(t)$ and its formal time derivative $W_P(t) = dC(t)/dt$

Realization and its formal derivative are depicted in Fig. 4.19. The intensity is interpreted as a jumping frequency $\lambda = f_p$ and Y_k are understood as impulse sizes. Since T_k and Y_k in Poisson process are independent, poor quality of the model is expected, because dependencies between T_{k-1} and T_k , Y_{k-1} and Y_k , T_{k-1} and Y_k were observed, *cf* [51] and Sec. 3.2. Adopting independence, the distribution of Y_k corresponds to Erlang with the density $f_Y(y; 2, 2f_p) = (2f_p)^2 ye^{-2f_p y}$ since, *cf* Eq. (3.1) and the discussion therein, the impulse size is $I_k = (T_k + T_{k-1})/2$, T_k being exponential with the mean value $1/\lambda$. Let us compare the performance of this approximation on following simple example.

Example 4.10. In the case of Poisson white noise and a harmonic oscillator, Eq. (4.4) is of the form

$$d \begin{bmatrix} X(t) \\ \dot{X}(t) \end{bmatrix} = \begin{bmatrix} 0 & 1 \\ -\nu^2 & -2\zeta\nu \end{bmatrix} \begin{bmatrix} X(t) \\ \dot{X}(t) \end{bmatrix} dt + \int_{\mathbb{R}} \begin{bmatrix} 0 \\ y \end{bmatrix} \mathcal{M}(dt, dy), \quad t \geq 0, \quad (4.83)$$

where $\mathcal{M}(dt, dy)$ is Poisson random measure, *cf* [19] and Appendix A, with $\mathbf{E}\mathcal{M} = \lambda dt d\mathbb{F}_Y(y)$ used for convenience. Here, \mathbb{F}_Y denotes the distribution function of a y -valued random variable, λ denotes the intensity of homogeneous Poisson counting process $N(t)$ in $C(t)$. Substituting $g(\mathbf{X}(t)) = X(t)^p \dot{X}(t)^q$ into the Itô's formula gives

$$dg(\mathbf{X}) = \left[pX^{p-1}\dot{X}^q\dot{X} + qX^p\dot{X}^{q-1}(-\nu^2 X - 2\zeta\nu\dot{X}) \right] dt + \int_{\mathbb{R}} \left[X^p(\dot{X} + y)^q - X^p\dot{X}^q \right] \mathcal{M}(dt, dy) \quad (4.84)$$

yielding the moment equations in the form

$$\dot{\mu}(t; p, q) = p\mu(t; p-1, q+1) - \nu^2 q\mu(t; p+1, q-1) - 2\zeta\nu q\mu(t; p, q) + \lambda \sum_{k=1}^q \frac{q!}{k!(q-k)!} \mu(t; p, q-k) \mathbf{E}Y_1^k, \quad t \geq 0, \quad (4.85)$$

where $\mu(t; p, q) = \mathbf{E}X(t)^p \dot{X}(t)^q$ with the convention $\mu(t; p, q) = 0$ if at least one of the p or q is strictly negative. $\mathbf{E}Y_1^k$ denotes the moments of order k of the variable Y_1 . Since Eq. (4.83) is linear, corresponding system of moment equations is closed and can be solved without any closure techniques. Stationary solution of Eqns. (4.85) up to fourth order as a function of oscillator eigenfrequency $f_1 = \nu/2\pi$ and for two values of relative damping ζ leads to results depicted in Fig. 4.20, where we notice rather poor quality of approximation of the simulated process except for stationary mean value.

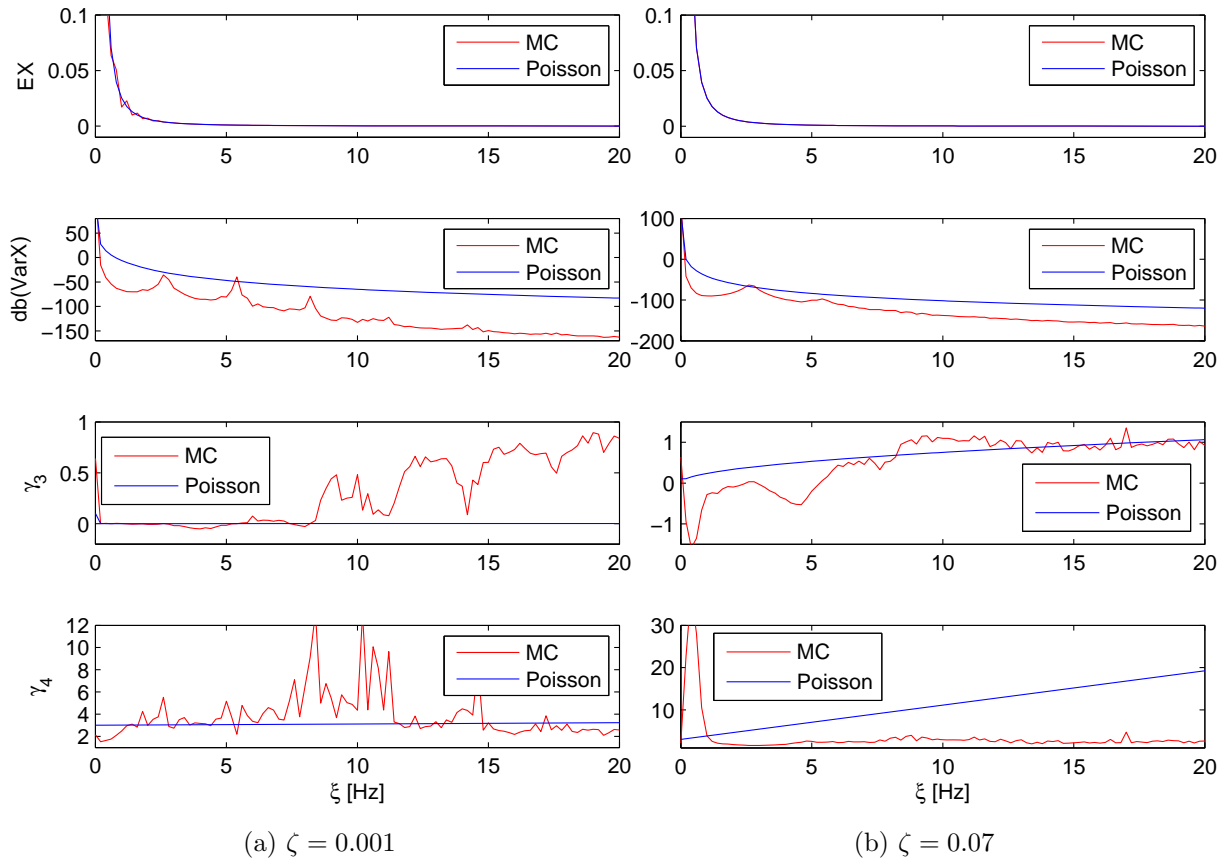


Figure 4.20: Resulting moments as functions of SDOF eigenfrequency f_1 for two relative dampings $\zeta = 0.001$ and $\zeta = 0.07$ and the case of Poisson white noise excitation

4.3.3 Frequency domain solution

It is possible to obtain higher-order moments also in the frequency domain employing FRF and so-called polyspectra. Since we have computed only the third moments in time domain, we will restrict our attention to bi-spectra [42], generalization to higher-order

statistics causing no complication, *cf* [31]. Bi-spectra for a stationary process is defined as an \mathbb{R}^2 Fourier transform of the third order cumulant $\kappa_{3,\tilde{F}}(\boldsymbol{\tau}) = \mathbb{E} \left[\tilde{F}(t) \tilde{F}(t + \tau_1) \tilde{F}(t + \tau_2) \right]$

$$s_{3,\tilde{F}}(\boldsymbol{\xi}) = \mathcal{F}(\kappa_{3,\tilde{F}}(\boldsymbol{\tau}))(\boldsymbol{\xi}) = \int_{\mathbb{R}^2} \kappa_{3,\tilde{F}}(\boldsymbol{\tau}) e^{-i2\pi\boldsymbol{\tau}\cdot\boldsymbol{\xi}} d\boldsymbol{\tau}, \quad (4.86)$$

where $\boldsymbol{\xi} = [\xi_1, \xi_2]$ and $\boldsymbol{\tau} = [\tau_1, \tau_2]$. $s_{3,\tilde{F}}(\boldsymbol{\xi})$ can be estimated in analogy to the spectral density employing bi-periodograms and various window functions not discussed here. The bi-spectra of the output vector process $\tilde{\mathbf{Z}}(t)$ is obtained according to

$$S_{\tilde{\mathbf{Z}}\tilde{\mathbf{Z}}\tilde{\mathbf{Z}},ijk}(\boldsymbol{\xi}) = H_{il}^\dagger(\xi_1 + \xi_2) G_{lr} H_{ju}(\xi_1) G_{us} H_{kv}(\xi_2) G_{vt} S_{\tilde{F}\tilde{F}\tilde{F},rst}(\boldsymbol{\xi}), \quad (4.87)$$

where $S_{\tilde{F}\tilde{F}\tilde{F}}(\boldsymbol{\xi}) \in \mathbb{R}^{n_a \times n_a \times n_a}$ is an input bi-spectra tensor, *cf* also Sec. 4.2.1.2 and [20]. Note that $\mathbf{H}(\boldsymbol{\xi})$ is symmetric in our case and hence $\mathbf{H}^\dagger(\boldsymbol{\xi}) = \overline{\mathbf{H}(\boldsymbol{\xi})}$. The third cumulant of the centered process $\tilde{Z}_i(t)$ is then evaluated as

$$\mathbb{E}\tilde{Z}_i(t)^3 = \kappa_{3,\tilde{Z}_i}(\mathbf{0}) = \int_{\mathbb{R}^2} S_{\tilde{F}\tilde{F}\tilde{F},iii}(\boldsymbol{\xi}) d\boldsymbol{\xi}. \quad (4.88)$$

ROM techniques are employed in standard fashion using also various kinds of symmetries of $s_{3,\tilde{F}}(\boldsymbol{\xi})$ with advantage. Compare the displacement results of the simply supported beam in Appendix C.1 obtained in the frequency domain summarized in Tab. 4.8 of Ex. 4.9 and Fig. 4.21 below.

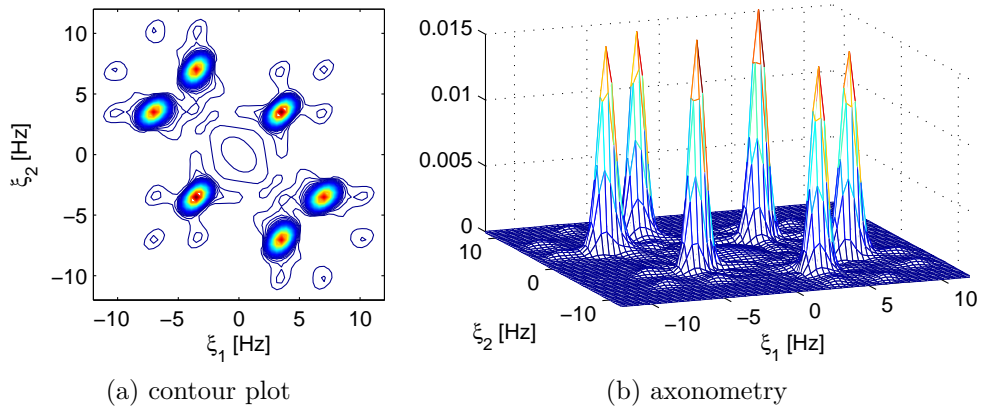


Figure 4.21: Bi-spectra of centered forcing process with jumping frequency $f_p = 3.5$ Hz based on MC according to [51], HOSA package used [54]

4.3.4 Other non-Gaussian inputs

Many other approaches can be employed in order to face the problem stated in Eq. (2.1) in terms of non-Gaussian processes, *e.g.* time series and filtered Poisson processes with nonstationary intensity $\lambda(t)$ and nonstationary diffusions $\mathbf{b}(t)$ of the Gaussian processes. Attractive seems to be also processes with random parameters and parametric representations such as Fourier series and Karhunen-Loève decomposition. These methods can be perhaps the objective of further study.

4.4 Conclusion

This chapter has presented in its first part a study of the vibration of grandstands loaded by an active crowd using Gaussian approximation of the forcing terms and of the response. The main results of the first part can be summarized as follows:

1. A mathematical description of the response of a mechanical system employing spectral and time domain solutions for weakly stationary Gaussian excitations has been recalled. Transformations of ROM techniques have been discussed briefly.
2. A motivating example of a harmonic oscillator has shown that the normalized displacement and velocity have approximately normal distribution under the conditions on eigenfrequencies and damping.
3. Taking this fact into account, the forcing process was approximated by mean value with superposed Gaussian coloured stationary noise. The mean value was further expressed as a truncated Fourier series and the spectral density of the fluctuating part was found by means of the periodogram and Parzen window. For the time domain solution, a linear combination of independent autoregression processes of the second order with L^2 -optimal coefficients has been employed.
4. Three different examples of varying complexity have shown the quality of the response approximation in terms of total displacement up-crossings, distribution of maxima and acceleration RMS in comparison with Monte Carlo simulation. Limitations following from a simple oscillator have been confirmed on multi-degree-of-freedom systems.
5. The computational demands have been measured and summarized in terms of the time consumptions, and the applicability of techniques has been proved.
6. On the basis of developed force approximation, a random spatial distribution of an active crowd has been described through random indicator variables. Two basic forms of a crowd interaction have been proposed by means of the indicator covariance function.

Since the forcing and hence also the response processes are non-Gaussian, a short excursion into translation and Poisson white noise processes has been performed in the second part of this chapter in order to improve the description of the output statistics. The main results of the second part include:

7. Solution in the time domain in terms of translation processes has been performed. Hermite polynomials employed for an approximation of the nonlinear transformation proved to be sufficient for the third order moments. Random functions entering the transformation were assumed as a linear combination of two AR(2) processes of the overall unit variance; transformation affected the correlation and spectral density functions in rather positive manner. Eventually, moment equations have been derived for two Hermite polynomials, *i.e.* for quadratic memoryless transformation.
8. Knowing the third order moments of the outputs, two methods for upcrossing estimates have been mentioned: the Gram-Charlier type A series and the translation approximation, again in polynomial form. These methods significantly contributed to the improvement of the upcrossing approximation.

9. A short discussion of the possibilities offered by Poisson white noise were discussed and demonstrated on simple example. Poor results have been, however, achieved.
10. Eventually, solution of the third-order moments by means of polyspectra and transfer function was briefly mentioned. All approaches were demonstrated on two examples compared with Monte Carlo simulation.

The quality of the output distributions is undoubtedly increased employing higher-order moments, but it has to be stressed that in spite of the significant model order reduction, all the non-Gaussian approaches are computationally intensive and hence their utilization in context of real structures is questionable.

Chapter 5

Random parameters of a passive crowd

5.1 Introduction

Complementary conditions in the sense of spectators to that introduced in Chap. 4 will be now assumed. Namely, a passive crowd will be described by means of stochastic biodynamic models, *cf* Tab. 3.2 and 3.3, possibly with a random spatial distribution over the structure. This leads to random and time-invariant coefficient matrices $\mathbf{K}(\omega)$, $\mathbf{M}(\omega)$ and $\mathbf{C}(\omega)$ in Eq. (2.1) which defines the grandstand problem. The active spectators will be, contrary to passive ones, assumed to have spatially fixed positions, and will be described through independent AR(p) processes.

Such level of complexity leads to a random operator equation arising from Eq. (2.1) which can be rewritten as

$$\mathcal{L}(\omega) \mathbf{Z}(t, \omega) = \mathbf{G}\mathbf{F}(t, \omega), \quad t \geq 0. \quad (5.1)$$

Here, $\mathbf{F}(t, \omega)$ is a random forcing term induced by an active crowd, $\mathbf{Z}(t, \omega)$ is a displacement variable and $\mathcal{L}(\omega)$ is a random differential operator. At this level, no dependencies between the right hand side and the system operator exist. Thanks to the growing complexity, we will restrict our attention only to the second order moment approximations despite clear non-Gaussianity of the outputs. Equation (5.1) is manageable in terms of Adomian, Perturbation, Taylor series and other approximate methods.

5.2 Sensitivity analysis

In this short section, the sensitivity factors of the structure response reflecting the randomness of the biodynamic model parameters, *cf* Sec. 3.3 and Tab. 3.3, will be derived. The analysis is given by means of Taylor series method under the deterministic load, *cf* [19, 29]; let the state of the mechanical system be described as

$$\mathcal{L}(\Theta(\omega)) \mathbf{Z}(t, \Theta(\omega)) = \mathbf{G}\mathbf{f}(t), \quad t \geq 0, \quad (5.2)$$

where the differential operator is of the second order

$$\mathcal{L}(\Theta) = \mathbf{M}(\Theta) \frac{d^2}{dt^2} + \mathbf{C}(\Theta) \frac{d}{dt} + \mathbf{K}(\Theta), \quad (5.3)$$

$\Theta(\omega) = [\Theta_1, \dots, \Theta_{n_p k_p}]$ is an $\mathbb{R}^{n_p k_p}$ -valued random variable, n_p being the number of passive spectators and k_p the number of random variables describing the single biodynamic model, \mathbf{G} is the load distribution matrix, $\mathbf{f}(t)$ a deterministic load, \mathbf{K} , \mathbf{M} and \mathbf{C} matrices have the usual meaning of system stiffness, mass and viscous damping. As indicated, \mathbf{Z} is now viewed also as a function of Θ . Then, the functions $\mathbb{V}_i(t, \mathbf{E}\Theta) = \partial \mathbf{Z}(t, \mathbf{E}\Theta) / \partial \Theta_i$ provide a measure of the sensitivity of \mathbf{Z} to perturbations about $\mathbf{E}\Theta$ and are called sensitivity factors; they satisfy

$$\mathcal{L}(\mathbf{E}\Theta) \mathbb{V}_i(t, \mathbf{E}\Theta) = - \left. \frac{\partial \mathcal{L}(\Theta)}{\partial \Theta_i} \right|_{\Theta=\mathbf{E}\Theta} \mathbf{Z}(t, \mathbf{E}\Theta), \quad t \geq 0. \quad (5.4)$$

The process $\mathbf{Z}(t, \mathbf{E}\Theta)$ satisfies the equation

$$\mathcal{L}(\mathbf{E}\Theta) \mathbf{Z}(t, \mathbf{E}\Theta) = \mathbf{G} \mathbf{f}(t), \quad t \geq 0. \quad (5.5)$$

Eventually, the resulting process $\mathbf{Z}(t, \Theta)$ is approximated according to

$$\mathbf{Z}(t, \Theta) \approx \mathbf{Z}(t, \mathbf{E}\Theta) + \sum_{i=1}^{n_p k_p} \mathbb{V}_i(t, \mathbf{E}\Theta) (\Theta_i - \mathbf{E}\Theta_i) \quad (5.6)$$

with the mean value $\mathbf{E}\mathbf{Z}(t, \Theta) = \mathbf{Z}(t, \mathbf{E}\Theta)$ and the second moment properties

$$\mathbf{c}_Z(s, t) \approx \sum_{i,j=1}^{n_p k_p} \mathbb{V}_i(s, \mathbf{E}\Theta) \mathbb{V}_j^T(t, \mathbf{E}\Theta) \text{cov}(\Theta_i, \Theta_j). \quad (5.7)$$

Example 5.1. Let us perform the sensitivity analysis of the simplest possible example with two DOFs, one representing a structure and one a passive crowd. Particular data for $\mathbf{Z} = [Z_S, Z_H]^T$ are

$$\mathbf{K} = \begin{bmatrix} k_S + K_{H_1} & -K_{H_1} \\ -K_{H_1} & K_{H_1} \end{bmatrix}, \quad \mathbf{M} = \begin{bmatrix} m_S + M_{H_0} & 0 \\ 0 & M_{H_1} \end{bmatrix}, \quad \mathbf{C} = \begin{bmatrix} c_S + C_{H_1} & -C_{H_1} \\ -C_{H_1} & C_{H_1} \end{bmatrix} \quad (5.8)$$

with $\Theta = [K_{H_1}, M_{H_1}, C_{H_1}, M_{H_0}]$ being the parameters of the biodynamic model introduced in Tab. 3.3; k_S , m_S and c_S describe the grandstand. Partial derivatives of the operator with respect to Θ_i read

$$\begin{aligned} \frac{\partial \mathcal{L}(\Theta)}{\partial \Theta_1} &= \begin{bmatrix} 1 & -1 \\ -1 & 1 \end{bmatrix}, & \frac{\partial \mathcal{L}(\Theta)}{\partial \Theta_2} &= \begin{bmatrix} 0 & 0 \\ 0 & 1 \end{bmatrix} \frac{d^2}{dt^2}, \\ \frac{\partial \mathcal{L}(\Theta)}{\partial \Theta_3} &= \begin{bmatrix} 1 & -1 \\ -1 & 1 \end{bmatrix} \frac{d}{dt}, & \frac{\partial \mathcal{L}(\Theta)}{\partial \Theta_4} &= \begin{bmatrix} 1 & 0 \\ 0 & 0 \end{bmatrix} \frac{d^2}{dt^2}, \end{aligned} \quad (5.9)$$

$\mathcal{L}(\mathbf{E}\Theta) = \mathbf{E}\mathcal{L}(\Theta)$. Force distribution matrix is $\mathbf{G} = [1, 0]^T$ since only the grandstand is loaded, $f(t)$ being the mean value of the jumping process for $f_p = 2.7$ Hz, cf Eq. (4.30) and

Tab. 4.1. Results for particular data are depicted in Fig. 5.1; dependencies of $L^2(T_1, T_2)$ norms for all constituents $c_{Z}^{ij}(t, t)$, as functions of the mass ratio γ and of the eigenfrequency f_1 of an empty grandstand are given in Fig. 5.2. $c_{Z,kl}^{ij}(t, t)$ denotes the k -th row, l -th column of an ij -th constituent in Eq. (5.7) and time $s = t$.

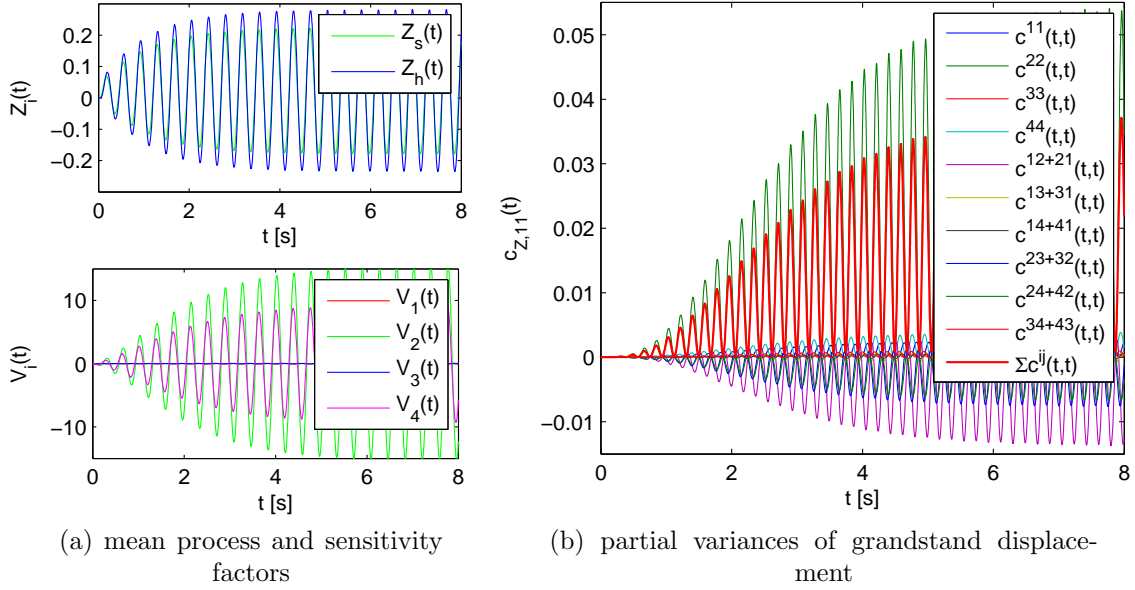


Figure 5.1: Behaviour of $\mathbf{Z}(t, \mathbf{E}\Theta)$ and $\mathbb{V}_i(t, \mathbf{E}\Theta)$ for the displacement of the structure (a); decomposed variance of the structure displacement $\text{var}Z_S(t)$ (b); $\gamma = 0.5$, $\zeta_S = 0.05$, $f_1 = 3.5$ Hz

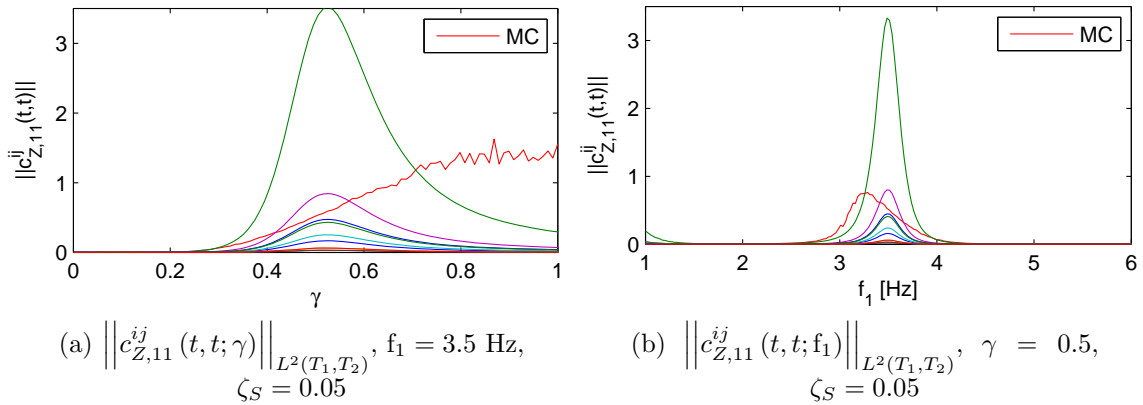


Figure 5.2: $L^2(T_1, T_2)$ norms of members $c_{Z,11}^{ij}(t, t)$ constituting the variance of the structure displacement $c_{Z,11}(t, t) = \text{var}Z_S(t)$ as functions of the mass ratio γ and eigenfrequency f_1 of an empty structure, $T_1 = 10$ and $T_2 = 20$ s; for the legend cf Fig. 5.1b

It can be concluded from given results that the most significant contribution to the structure response variance is due to $c_{11}^{22}(t, t)$, *i.e.* due to the randomness in the vibrating mass M_{H_1} . The second most significant constituent is $c_{11}^{12}(t, t) + c_{11}^{21}(t, t)$ reflecting the stochastic dependency between K_{H_1} and M_{H_1} . Peak values in Fig. 5.2 are achieved for $\gamma = 0.54$ and $f_1 = 3.49$ Hz. The former one is caused by growing influence of the human mass

being most significant for the case of approximate equality attaining also the state of resonance; the second peak is due to the fact that the first eigenfrequency of the coupled two DOF system is equal to f_p , hence it is the state of resonance.

It should be also noted that the Taylor series method is only an approximate one, reflecting the behaviour of a stochastic system in certain bounds of a small randomness. To quantify the difference, Fig. 5.2 captures an $L^2(T_1, T_2)$ norm of the response variance caused by the randomness in M_{H_1} estimated by MC simulation which is based on 500 realizations. The mass is represented as $M_{H_1} \sim \mathcal{U}(a, b)$, where $a, b > 0$ are chosen such that to yield the same first two moments; remind that the coefficient of variation for M_{H_1} is $c_v = \sigma/\mu = 0.302$. Then, M_{H_1} has support in \mathbb{R}^+ and hence the mass matrix \mathbf{M} is positive definite almost surely. We notice that the Taylor series method performs acceptably for $\gamma < 0.35$ and for non resonant case. High structure damping ζ_S also contributes positively to the accuracy of the approximation.

5.3 Deterministic distribution of a passive crowd

On the basis of the sensitivity analysis results, we will assume in this section only the randomness inherent to vibrating mass of the SDOF biodynamic models. Taylor series method can be employed to estimate the variance of the response in the case of real structures, nevertheless, n_p problems analogous to Eq. (4.11) have to be solved under the assumption of stochastic forcing. Having on mind the dimensions and the overall scope of the real structures, other methods such as Perturbation with only the first two terms can be efficiently employed. Except for light weight temporary grandstands, the requirement for the mass ratio $\gamma < 0.35$ is usually fulfilled, cf Appendix A where the maximal value is $\gamma = 0.37$, nevertheless remind that these structures are not representative for real grandstands.

5.3.1 Taylor series method

For further considerations, we will again reduce the grandstand problem in Eq. (2.1) to the Cauchy form in analogy to Eq. (4.3) and approximate the forcing terms $\mathbf{F}(t, \omega) = \boldsymbol{\mu}_F(t) + \dot{\mathbf{Y}}(t, \omega)$ where $\dot{\mathbf{Y}}(t, \omega)$ is a linear combination of independent AR(2) processes with state variable $\mathbf{S}(t)$ as usual. In rewritten form, we have

$$\mathcal{L}(\boldsymbol{\Theta}) \mathbf{X}(t, \boldsymbol{\Theta}, \omega) = \mathbf{h}\boldsymbol{\mu}_Y(t) + \mathbf{b}\mathbf{W}(t, \omega), \quad t \geq 0, \quad (5.10)$$

where $\mathbf{X} = [\mathbf{Z}^\top, \dot{\mathbf{Z}}^\top, \mathbf{S}^\top]^\top$. Unlike the previously used notation, now $\mathcal{L}(\boldsymbol{\Theta}) = \mathbf{m}(\boldsymbol{\Theta})d/dt - \mathbf{a}$ with explicitly introduced mass matrix \mathbf{m} , where

$$\mathbf{m} = \begin{bmatrix} \mathbf{I}_{k \times k} & \mathbf{0}_{k \times k} & \mathbf{0}_{k \times l} \\ \mathbf{0}_{k \times k} & \mathbf{M} & \mathbf{0}_{k \times l} \\ \mathbf{0}_{l \times k} & \mathbf{0}_{l \times k} & \mathbf{I}_{l \times l} \end{bmatrix}, \mathbf{a} = \begin{bmatrix} \mathbf{0}_{k \times k} & \mathbf{I}_{k \times k} & \mathbf{0}_{k \times l} \\ -\mathbf{K} & -\mathbf{C} & \mathbf{G}\mathbf{d} \\ \mathbf{0}_{l \times k} & \mathbf{0}_{l \times k} & \mathbf{A} \end{bmatrix}, \mathbf{h} = \begin{bmatrix} \mathbf{0}_{k \times n_a} \\ \mathbf{G} \\ \mathbf{0}_{l \times n_a} \end{bmatrix}, \mathbf{b} = \begin{bmatrix} \mathbf{0}_{k \times r} \\ \mathbf{0}_{k \times r} \\ \mathbf{b}_A \end{bmatrix}, \quad (5.11)$$

$k = n_{\text{DOF}}$, $l = \dim(\mathbf{S})$, $r = n_a n$, n being a number of AR(2) processes used for an approximation of the jumping process, $\mathbf{W}(t) \in \mathbb{R}^r$. Compare also Eq. (4.8) for the particular meaning of \mathbf{A} , \mathbf{d} and \mathbf{b}_A . Moreover, only a diagonal submatrix $\mathbf{M}_{HH}(\boldsymbol{\Theta})$ is

random, $\Theta(\omega) = [M_{H_1,1}, \dots, M_{H_1,n_p}]$, $M_{H_1,i}$ being *iid*. Since $\mathcal{L}(\mathbf{E}\Theta) = \mathbf{E}\mathbf{m}(\Theta) d/dt - \mathbf{a} = \bar{\mathbf{m}} d/dt - \mathbf{a}$, the mean process $\mathbf{X}(t, \mathbf{E}\Theta, \omega) = \mathbf{X}_0(t)$ satisfies the Itô's SDE

$$d\mathbf{X}_0(t) = \bar{\mathbf{m}}^{-1} \mathbf{a} \mathbf{X}_0(t) dt + \bar{\mathbf{m}}^{-1} \mathbf{h} \boldsymbol{\mu}_Y(t) dt + \bar{\mathbf{m}}^{-1} \mathbf{b} d\mathbf{B}(t), \quad t \geq 0, \quad (5.12)$$

which can be solved for $\boldsymbol{\mu}_{X_0}(t)$ and \mathbf{c}_{X_0} employing methods reviewed in Sec. 4.2. Assuming $\mathbf{X}_0(t) = \boldsymbol{\mu}_{X_0}(t) + \tilde{\mathbf{X}}_0$, the sensitivity factors $\mathbf{X}_i(t) = [\mathbb{V}_i^\top, \dot{\mathbb{V}}_i^\top]^\top$, *cf* Sec.(5.2), satisfy

$$\begin{aligned} d\mathbf{X}_i(t) &= \bar{\mathbf{m}}_{11}^{-1} \mathbf{a}_{11} \mathbf{X}_i(t) dt - \bar{\mathbf{m}}_{11}^{-1} \mathbf{v}_i d\mathbf{X}_0(t) \\ &= \bar{\mathbf{m}}_{11}^{-1} \mathbf{a}_{11} \mathbf{X}_i(t) dt - \bar{\mathbf{m}}_{11}^{-1} \mathbf{v}_i \dot{\boldsymbol{\mu}}_{X_0}(t) dt - \underbrace{\bar{\mathbf{m}}_{11}^{-1} \mathbf{v}_i \bar{\mathbf{m}}^{-1} \mathbf{a} \tilde{\mathbf{X}}_0(t)}_{=0} dt - \bar{\mathbf{m}}_{11}^{-1} \mathbf{v}_i \bar{\mathbf{m}}^{-1} \mathbf{b} d\mathbf{B}(t), \quad t \geq 0, \end{aligned} \quad (5.13)$$

with matrices

$$\begin{aligned} \mathbf{m}_{11} &= \begin{bmatrix} \mathbf{I}_{k \times k} & \mathbf{0}_{k \times k} \\ \mathbf{0}_{k \times k} & \mathbf{M} \end{bmatrix}, \quad \mathbf{a}_{11} = \begin{bmatrix} \mathbf{0}_{k \times k} & \mathbf{I}_{k \times k} \\ -\mathbf{K} & -\mathbf{C} \end{bmatrix}, \\ \left. \frac{\partial \mathcal{L}(\Theta)}{\partial \Theta_i} \right|_{2k \times (2k+l)} &= \mathbf{v}_i \frac{d}{dt} = \begin{bmatrix} \mathbf{0}_{v \times v} & \mathbf{0}_{v \times n_p} & \mathbf{0}_{v \times l} \\ \mathbf{0}_{n_p \times v} & \tilde{\mathbf{e}}_i \otimes \tilde{\mathbf{e}}_i & \mathbf{0}_{n_p \times l} \end{bmatrix} \frac{d}{dt}, \end{aligned} \quad (5.14)$$

in analogy to Eq. (4.23) since $\mathbf{S}(t)$ is separated out and moreover is of no interest. $v = 2n_{\text{DOF}} - n_p$ for simplicity; $\tilde{\mathbf{e}}_i \in \mathbb{R}^{n_p}$ is an i -th canonical basis vector. Employing Itô's formula, the stationary covariance matrices of $\tilde{\mathbf{X}}_i$ satisfy

$$\mathbf{0} = \mathbf{c}_{X_i} \mathbf{a}_{11}^\top \bar{\mathbf{m}}_{11}^{-\top} + \bar{\mathbf{m}}_{11}^{-1} \mathbf{a}_{11} \mathbf{c}_{X_i} + \mathbf{E} \tilde{\mathbf{X}}_i \tilde{\mathbf{X}}_0^\top \mathbf{a}^\top \bar{\mathbf{m}}^{-\top} \mathbf{v}_i^\top \bar{\mathbf{m}}_{11}^{-\top} + \bar{\mathbf{m}}_{11}^{-1} \mathbf{v}_i \bar{\mathbf{m}}^{-1} \mathbf{a} \mathbf{E} \tilde{\mathbf{X}}_0 \tilde{\mathbf{X}}_i^\top \quad (5.15)$$

with auxiliary Sylvester equation

$$\mathbf{0} = \mathbf{E} \tilde{\mathbf{X}}_0 \tilde{\mathbf{X}}_i^\top \mathbf{a}_{11}^\top \bar{\mathbf{m}}_{11}^{-\top} + \bar{\mathbf{m}}^{-1} \mathbf{a} \mathbf{E} \tilde{\mathbf{X}}_0 \tilde{\mathbf{X}}_i^\top + \mathbf{c}_{X_0} \mathbf{a}^\top \bar{\mathbf{m}}^{-\top} \mathbf{v}_i^\top \bar{\mathbf{m}}_{11}^{-\top}. \quad (5.16)$$

Mean value is again solved separately in the frequency domain with advantage. Again employing a time average and denoting $\hat{\mathbf{c}}_{X_i} = \mathbf{c}_{X_i} + \frac{1}{T} \int_0^T \boldsymbol{\mu}_{X_i}(t) \boldsymbol{\mu}_{X_i}^\top(t) dt$, the resulting variance in analogy to Eq. (5.6) reads

$$\mathbf{c}_X = \bar{\mathbf{c}}_{X_0} + \sum_{i=1}^{n_p} \hat{\mathbf{c}}_{X_i} \text{var}(M_{H_1}), \quad (5.17)$$

where $\bar{\mathbf{c}}_{X_0}$ is an appropriate submatrix of \mathbf{c}_{X_0} without state variables of the forcing terms $\mathbf{S}(t)$; mean value solution is $\boldsymbol{\mu}_{X_0}(t)$. The solution can be, with advantage, performed also in the frequency domain, or employing the ROM methods. Note, however, that instead of computing sensitivity factors for a diagonal matrix \mathbf{M}_{HH} with independent entries, it is possible upon employing MS ROM to compute sensitivity factors for a symmetric matrix $\mathbf{V}_{HH}^\top \mathbf{M}_{HH} \mathbf{V}_{HH}$ much smaller in dimension, *cf* Eq.(3.12), but with dependent entries. This is, however, out of scope of this thesis, and is viewed rather as a matter of efficient implementation.

Example 5.2. Let us compare the influence of the random vibrating mass of the SDOF biodynamic model M_{H_1} , in the scope of the approximation of the jumping spectators introduced in Sec. 4.2. Jumping processes are scaled with human *iid* weights $G_i \sim \mathcal{U}(0.414, 1.310)$ yielding $\mathbb{E}G_i = 0.862$ kN and $\mathbb{E}G_i^2 = (1 + 0.3^2) \cdot 0.862^2 = 0.810$ kN², $i \in \mathbf{n}_a$. Structure in Appendix C.2 with randomly generated, but fixed distribution of a crowd, is used. Then, SDOF biodynamic models according to Coermann are employed; mass is assumed random with coefficient of variation $c_v = 0.3$, response is measured in P_1 point. Results for the case of 36 active and 36 passive spectators with randomly generated but fixed spatial distribution are summarized in Tab. 5.1, MC simulation is based on 1,000 realizations 160 s in length. Clearly, in this particular case and the scope of

	Time sol.		MC	
	rand. mass	det. mass	rand. mass	det. mass
$\text{var}Z_{P_1}$	$3.981e-7$	$3.920e-7$	$4.370e-7$	$4.248e-7$
$\text{var}\dot{Z}_{P_1}$	$3.713e-4$	$3.644e-4$	$4.038e-4$	$3.903e-4$
$\text{var}\ddot{Z}_{P_1}$	$4.444e-1$	$4.365e-1$	$4.946e-1$	$4.796e-1$
Time	7.825	0.765	34.479 ¹⁾	30.825 ¹⁾

Table 5.1: Stationary variances of structure response measured in P_1 point for random and deterministic mass of the SDOF biodynamic models, 36 active and 36 passive spectators, example in Appendix C.2; ¹⁾ time for 100 realizations

the randomness induced by the forcing, the influence of the uncertainty of the biodynamic models can be neglected since the relative increase in variance is lower than 3.5 % in all cases. Mean value response also shows a good agreement with the MC and is not presented. Note that $\|\bar{\mathbf{c}}_{X_0}\|_F = 2.487e-2$, $\|\text{var}(M_{H_1}) \sum_{i=1}^{n_p} \mathbf{c}_{X_i}\|_F = 3.595e-4$ and $\|\text{var}(M_{H_1}) \sum_{i=1}^{n_p} \frac{1}{T} \int_0^T \boldsymbol{\mu}_{X_i}(t) \boldsymbol{\mu}_{X_i}^\top(t) dt\|_F = 10.788e-4$, where $\|\bullet\|_F$ stands for the Frobenius norm of a matrix \bullet .

5.4 Random distribution of a passive crowd

In this section, a generalization of the grandstand problem to the case of a random spatial distribution of a passive crowd will be given. For simplicity, deterministic SDOF biodynamic models will be assumed, randomness being rather matter of a spatial distribution. Then, employing indicator variables already introduced in Eq. (4.38), *cf* also notation and the discussion therein together with Sec. 3.4.1, we can write the system matrices as

$$\mathbf{A}(\boldsymbol{\chi}) = \begin{bmatrix} \mathbf{A}_S + \mathbf{A}_H(\boldsymbol{\chi}) & \mathbf{A}_{HS}^\top (\mathbf{I}_{n_p \times n_p} - \boldsymbol{\chi})^\top \\ (\mathbf{I}_{n_p \times n_p} - \boldsymbol{\chi}) \mathbf{A}_{HS} & (\mathbf{I}_{n_p \times n_p} - \boldsymbol{\chi}) \mathbf{A}_{HH} \end{bmatrix}, \quad (5.18)$$

where \mathbf{A} represents stiffness, mass or the damping matrix, $\mathbf{A}_H(\boldsymbol{\chi}) = \sum_{i=1}^{n_p} \mathbf{e}_{n_p(i)} \otimes \mathbf{e}_{n_p(i)} a_H (1 - \chi_i)$, $\mathbf{e}_i \in \mathbb{R}^{n_{\text{DOF},S}}$, a_H denoting k_{H_1} , m_{H_0} or c_{H_1} . Complementary indicator variables $1 - \chi_i$ are used because an arbitrary position from the set \mathbf{n}_s can be occupied either with a passive or an active spectator, χ_i represent the switch. This question will be further discussed in Chap. 6. Reducing the system to the Cauchy form and approximating the forcing terms, we arrive at Eq. (5.10) with $\mathcal{L}(\boldsymbol{\chi}) = \mathbf{m}(\boldsymbol{\chi}) d/dt - \mathbf{a}(\boldsymbol{\chi})$.

Then, $\mathcal{L}(\mathbf{E}\boldsymbol{\chi}) = \mathbf{E}\mathcal{L}(\boldsymbol{\chi}) = \mathbf{E}\mathbf{m}(\boldsymbol{\chi})d/dt - \mathbf{E}\mathbf{a}(\boldsymbol{\chi}) = \bar{\mathbf{m}}d/dt - \bar{\mathbf{a}}$. Since $\mathbf{E}(\mathbf{I}_{n_p \times n_p} - \boldsymbol{\chi}) = (1-p)\mathbf{I}_{n_p \times n_p}$, the mean drift matrix $\bar{\mathbf{m}}^{-1}\bar{\mathbf{a}}$ has a simple form, but is not given here because of the space requirements. Then,

$$-\left. \frac{\partial \mathcal{L}(\boldsymbol{\chi})}{\partial \chi_i} \right|_{2k \times (2k+l)} = \left(-\frac{\partial \mathbf{m}(\boldsymbol{\chi})}{\partial \chi_i} \frac{d}{dt} + \frac{\partial \mathbf{a}(\boldsymbol{\chi})}{\partial \chi_i} \right) \Big|_{2k \times (2k+l)} = -\mathbf{v}_i \frac{d}{dt} + \mathbf{w}_i, \quad (5.19)$$

where

$$\mathbf{v}_i = \begin{bmatrix} \mathbf{0}_{k \times k} & \mathbf{0}_{k \times k} & \mathbf{0}_{k \times l} \\ \mathbf{0}_{k \times k} & \frac{\partial \mathbf{M}(\boldsymbol{\chi})}{\partial \chi_i} & \mathbf{0}_{k \times l} \end{bmatrix}, \quad \mathbf{w}_i = \begin{bmatrix} \mathbf{0}_{k \times k} & \mathbf{0}_{k \times k} & \mathbf{0}_{k \times l} \\ -\frac{\partial \mathbf{K}(\boldsymbol{\chi})}{\partial \chi_i} & -\frac{\partial \mathbf{C}(\boldsymbol{\chi})}{\partial \chi_i} & \mathbf{0}_{k \times l} \end{bmatrix}, \quad (5.20)$$

together with

$$\begin{aligned} \frac{\partial \mathbf{M}(\boldsymbol{\chi})}{\partial \chi_i} &= \begin{bmatrix} -\mathbf{e}_{n_p(i)} \otimes \mathbf{e}_{n_p(i)} m_{H_0} & \mathbf{0}_{n_{\text{DOF},S} \times n_p} \\ \mathbf{0}_{n_p \times n_{\text{DOF},S}} & -\tilde{\mathbf{e}}_i \otimes \tilde{\mathbf{e}}_i m_{H_1} \end{bmatrix}, \\ \frac{\partial \mathbf{A}(\boldsymbol{\chi})}{\partial \chi_i} &= \begin{bmatrix} -\mathbf{e}_{n_p(i)} \otimes \mathbf{e}_{n_p(i)} a_H & -\mathbf{A}_{HS}^\top \tilde{\mathbf{e}}_i \otimes \tilde{\mathbf{e}}_i \\ -\tilde{\mathbf{e}}_i \otimes \tilde{\mathbf{e}}_i \mathbf{A}_{HS} & -\tilde{\mathbf{e}}_i \otimes \tilde{\mathbf{e}}_i a_H \end{bmatrix}, \end{aligned} \quad (5.21)$$

where $\mathbf{e}_i \in \mathbb{R}^{n_{\text{DOF},S}}$ and \mathbf{A} stands now only for stiffness or damping. \mathbf{X}_0 then satisfy Eq. (5.12) with $\bar{\mathbf{a}}$ instead of \mathbf{a} and $\mathbf{X}_i, i = 1, \dots, n_p$ satisfy the following system of SDEs, having an analogous form to Eq. (5.13), namely

$$\begin{aligned} d\mathbf{X}_i(t) &= \bar{\mathbf{m}}_{11}^{-1} \bar{\mathbf{a}}_{11} \mathbf{X}_i(t) dt + \bar{\mathbf{m}}_{11}^{-1} [-\mathbf{v}_i d\mathbf{X}_0(t) dt + \mathbf{w}_i \mathbf{X}_0(t) dt] = \\ &= \bar{\mathbf{m}}_{11}^{-1} \bar{\mathbf{a}}_{11} \mathbf{X}_i(t) dt + \bar{\mathbf{m}}_{11}^{-1} \left[(\mathbf{w}_i - \mathbf{v}_i \bar{\mathbf{m}}^{-1} \bar{\mathbf{a}}) \tilde{\mathbf{X}}_0(t) dt + \right. \\ & \left. \mathbf{w}_i \boldsymbol{\mu}_{X_0}(t) dt - \mathbf{v}_i \dot{\boldsymbol{\mu}}_{X_0}(t) dt - \underbrace{\mathbf{v}_i \bar{\mathbf{m}}^{-1} \mathbf{b} d\mathbf{B}(t)}_{=0} \right], \quad i = 1, \dots, n_p, \quad t \geq 0. \end{aligned} \quad (5.22)$$

The covariance matrices \mathbf{c}_{X_i} , satisfying

$$\mathbf{0} = \mathbf{c}_{X_i} \bar{\mathbf{a}}_{11}^\top \bar{\mathbf{m}}_{11}^{-\top} + \bar{\mathbf{m}}_{11}^{-1} \bar{\mathbf{a}}_{11} \mathbf{c}_{X_i} + \mathbf{E} \tilde{\mathbf{X}}_i \tilde{\mathbf{X}}_0^\top \mathbf{Q}^\top + \mathbf{Q} \mathbf{E} \tilde{\mathbf{X}}_0 \tilde{\mathbf{X}}_i^\top \quad (5.23)$$

with $\mathbf{Q} = \bar{\mathbf{m}}_{11}^{-1} (\mathbf{w}_i - \mathbf{v}_i \bar{\mathbf{m}}^{-1} \bar{\mathbf{a}})$ in analogy to Eq. (5.15), require the solution of auxiliary Sylvester equation

$$\mathbf{0} = \mathbf{E} \tilde{\mathbf{X}}_0 \tilde{\mathbf{X}}_i^\top \bar{\mathbf{a}}_{11}^\top \bar{\mathbf{m}}_{11}^{-\top} + \bar{\mathbf{m}}^{-1} \bar{\mathbf{a}} \mathbf{E} \tilde{\mathbf{X}}_0 \tilde{\mathbf{X}}_i^\top + \mathbf{c}_{X_0} \mathbf{Q}^\top. \quad (5.24)$$

Clearly, Eqns. (5.23) and (5.24) can be included into one global system. Nevertheless, since the solution of the Lyapunov equation requires $O(n^3)$ operations, n being the size of the state space variable, it is expedient to solve sequentially a system of smaller equations. For resulting variance, Eq. (5.17) is employed replacing $\text{var}(M_{H_1})$ with $\text{var}(\chi_i)$. Here, however, comes a drawback: if χ_i were correlated, *cf* Sec. 4.2.2 and Eq. (4.49), crosscorrelations $\mathbf{E}\mathbf{X}_i \mathbf{X}_j$ would be required yielding $n_p(n_p + 1)/2$ problems instead of n_p resulting eventually in one global Lyapunov equation as mentioned earlier. This can be in principle handled, but with significant increase in computational effort.

Example 5.3. This example provides a sense of the introduced issue together with the restrictions implied and the area of validity. A harmonic oscillator, representing a grandstand, is forced by the Gaussian white noise $W(t)$. With probability $1-p$, second harmonic oscillator representing a passive spectator is attached. Corresponding matrices

read

$$\begin{aligned}
 \mathbf{m} &= \begin{bmatrix} 1 & 0 & 0 & 0 \\ 0 & 1 & 0 & 0 \\ 0 & 0 & m_S & 0 \\ 0 & 0 & 0 & (1-\chi)m_H \end{bmatrix}, \quad \mathbf{b} = \begin{bmatrix} 0 \\ 0 \\ 1 \\ 0 \end{bmatrix}, \\
 \mathbf{a} &= \begin{bmatrix} 0 & 0 & 1 & 0 \\ 0 & 0 & 0 & 1 \\ -(k_S + (1-\chi)k_H) & (1-\chi)k_H & -(c_S + (1-\chi)c_H) & (1-\chi)c_H \\ (1-\chi)k_H & -(1-\chi)k_H & (1-\chi)c_H & -(1-\chi)c_H \end{bmatrix}, \\
 \mathbf{v}_1 &= \begin{bmatrix} 0 & 0 & 0 & 0 \\ 0 & 0 & 0 & 0 \\ 0 & 0 & 0 & 0 \\ 0 & 0 & 0 & -m_H \end{bmatrix}, \quad \mathbf{w}_1 = \begin{bmatrix} 0 & 0 & 0 & 0 \\ 0 & 0 & 0 & 0 \\ k_H & -k_H & c_H & -c_H \\ -k_H & k_H & -c_H & c_H \end{bmatrix},
 \end{aligned} \tag{5.25}$$

with k_H , m_H and c_H being physical constants describing the biodynamic model after Coermann as usual, and k_S , m_S and c_S constants describing the grandstand. In this simple case, the analytical solution can be obtained by means of conditional analysis with averaging degenerated to the sum over the atoms/states of χ yielding to a linear interpolation between the response of SDOF and two DOF system forced by $W(t)$. Dependency of $\text{var}Z_S$ on the eigenfrequency of an empty grandstand f_1 , on the probability p and on the mass ratio γ are depicted in Fig. 5.3. The results indicate that for reasonable mass

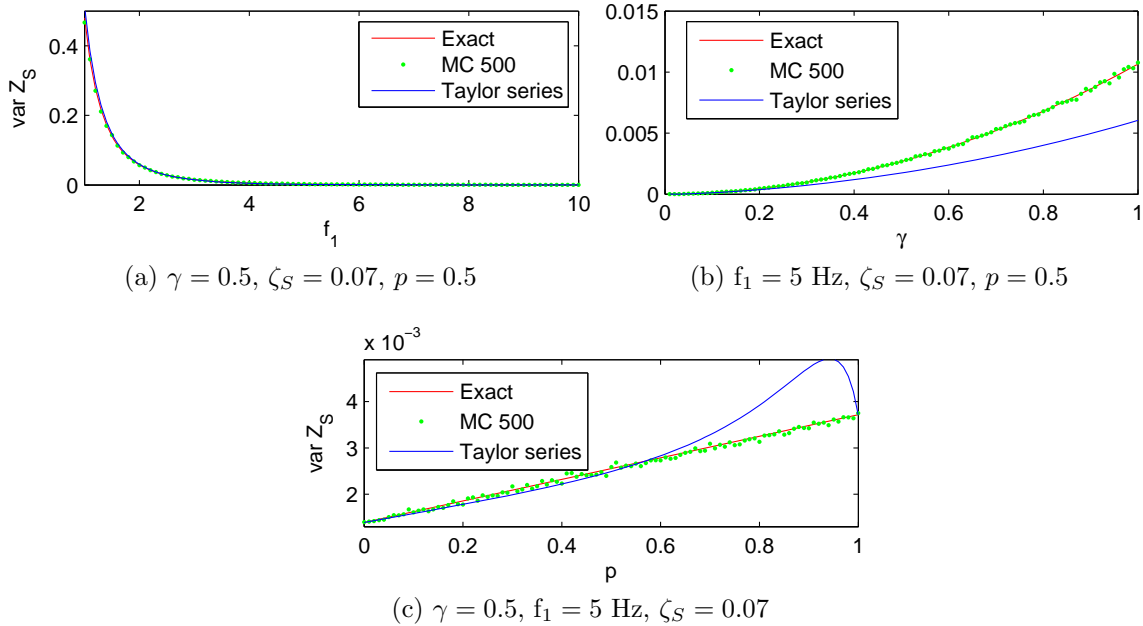


Figure 5.3: Dependencies of the structure displacement variance $\text{var}Z_S$ on the mass ratio γ , on the empty grandstand eigenfrequency f_1 and on the probability p

ratios, the approximation is acceptable. Note, however, that the quality of results highly depends on ζ_S ; for $\zeta_S < 0.01$, the approximation is very poor.

Example 5.4. Let us compare here a performance of the method on the structure described in Appendix C.2. To this end, 36 active spectators with a random but fixed

spatial distribution over the structure are assumed. Jumping processes are approximated similarly as in Ex. 5.2. Then, 36 passive spectators occupy the reminder of the seats, each of them is assumed to appear independently with a probability $1 - p$. Response of the structure is measured in the point P_1 . Variances $\text{var}Z_{P_1}$ and $\text{var}\ddot{Z}_{P_1}$ as functions of p are depicted in Figs. 5.4a and 5.4b in comparison with MC simulation based on 500 realizations, 160 s in length; contribution of \mathbf{c}_{X_0} is also captured. Figures 5.4c and 5.4d display the comparison of the mean value solutions. Results show an acceptable accuracy in comparison with the MC. Noting that computation of \mathbf{c}_{X_0} is order of magnitude faster than that of \mathbf{c}_X , the results based only on the variance of $\mathbf{X}_0(t)$ are also acceptable and can serve as a first estimate of the results.

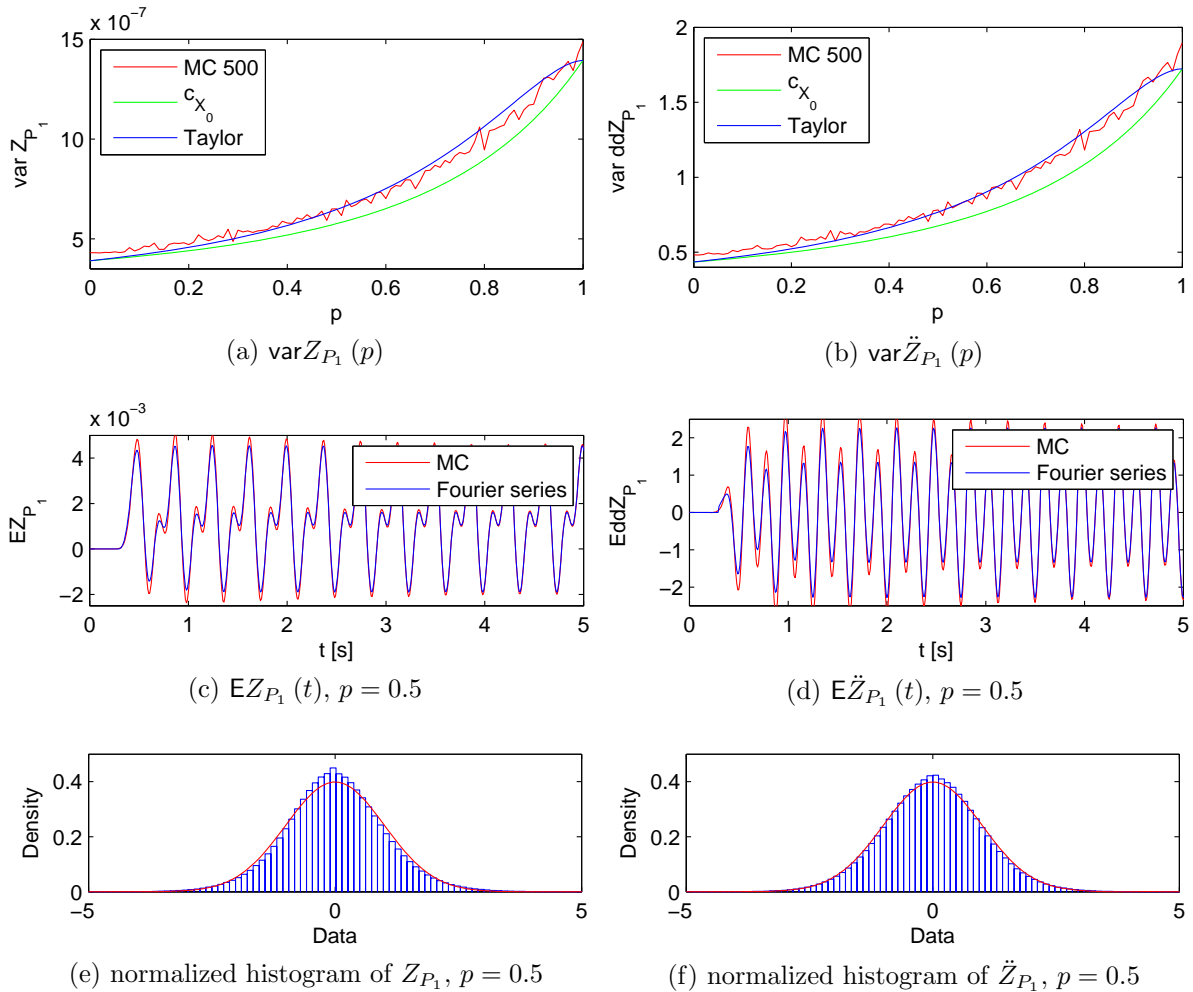


Figure 5.4: Dependencies of the structure displacement and acceleration variances on the probability p ; mean value solutions and normalized histograms with standard normal density for $p = 0.5$, ergodicity in variance assumed

5.5 Conclusion

This chapter focused mainly on the random properties of the operator appearing in the grandstand problem equation under both the deterministic and the stochastic loading.

Stochastic loading was again assumed in the form introduced in Sec. 4.2. The list of the main contributions include:

1. As a first step, the sensitivity analysis of the simple coupled human-grandstand system comprising all possible randomness of the SDOF biodynamic model under deterministic harmonic loading was performed. It turned out that the vibrating mass has the most significant contribution to the response variance.
2. Upon results achieved in the sensitivity analysis, a general approach in the case of MDOF structures and stochastic loadings was reviewed, assuming only the human mass matrix random. As a result, on the basis of example used, it turned out that within the scope of the overall randomness, the contribution of the random mass is only up to 3.5 %. Hence, the randomness in the mass was neglected in further considerations.
3. Random spatial distribution of the passive crowd was introduced by means of complements of the indicator variables. Despite the large randomness and utilization of the Taylor series method, overall results proved to be in an acceptable agreement with the MC and the scope of the employed examples.

Chapter 6

Stochastic system and input

6.1 Introduction

This section tries to approach the grandstand problem in Eq. (2.1) from the most general direction and to reflect all the major sources of randomness under the assumption of the fully occupied structure, *i.e.* no empty seats. This leads to the random forcing, already approximated in Sec. 4.2, to the random spatial distribution of an active crowd, outlined in Sec. 4.2.2 and to the complementary random distribution of a passive crowd discussed in Sec. 5.4. It is also possible to reflect random masses of the biodynamic models representing the passive spectators as reviewed in Sec. 5.3, however, such uncertainty will be neglected. Hence, this concluding chapter can be, to some extent, understood as a synthesis of all the methods introduced so far. Adopting all the assumptions, the operator form of our problem reads, *cf* Eq. (5.1),

$$\mathcal{L}(\boldsymbol{\chi}) \mathbf{Z}(t, \boldsymbol{\chi}, \omega) = \mathbf{GF}(t, \boldsymbol{\chi}, \omega), \quad t \geq 0, \quad (6.1)$$

or, assuming approximation in terms of the linear combination of the AR(2) processes, the corresponding Itô's SDE reads

$$\mathbf{m}(\boldsymbol{\chi}) d\mathbf{X}(t) = \mathbf{a}(\boldsymbol{\chi}) \mathbf{X}(t) dt + \mathbf{h}\boldsymbol{\chi}\boldsymbol{\mu}_Y(t) dt + \mathbf{b}\boldsymbol{\chi}_n d\mathbf{B}(t), \quad t \geq 0. \quad (6.2)$$

Unlike the previous Chap. 5, the operator and the right hand side are mutually dependent, having moreover correlation equal to one. However is our attempt condemned to failure right from the beginning, we will try to derive some moment equations and to compare the results.

6.2 Random distribution of a crowd

At all possible locations included in \mathbf{n}_s , we are alternating between an active and a passive spectator by means of *iid* indicator variables χ_i , $i = 1, \dots, n_s$, *i.e.* between the force on the right hand side of Eq. (6.1) and the biodynamic model appearing in, and enlarging the matrices \mathbf{K} , \mathbf{M} and \mathbf{C} of the operator \mathcal{L} . Resulting Itô's formula is in Eq. (6.2); employing again the Taylor series method, $\mathbf{X}(t, \mathbf{E}\boldsymbol{\chi}, \omega) = \mathbf{X}_0(t)$ satisfies

$$\bar{\mathbf{m}}d\mathbf{X}_0(t) = \bar{\mathbf{a}}\mathbf{X}_0(t) dt + \mathbf{p}\mathbf{h}\boldsymbol{\mu}_Y(t) dt + \mathbf{p}\mathbf{b}d\mathbf{B}(t), \quad t \geq 0, \quad (6.3)$$

since $\mathbf{E}\chi = p\mathbf{I}_{n_s \times n_s}$ and $\mathbf{E}\chi_n = p\mathbf{I}_{n_s n \times n_s n}$; forcing is $d\mathbf{B}(t) \in \mathbb{R}^{n_s n}$. Sensitivity factors $\partial\mathbf{X}(t, \mathbf{E}\chi, \omega) / \partial\chi_i = \mathbf{X}_i(t)$ are of the same dimension as $\mathbf{X}_0(t)$ and fulfil

$$\begin{aligned} \bar{m}d\mathbf{X}_i(t) = & \bar{\mathbf{a}}\mathbf{X}_i(t) dt + \mathbf{h}_i\boldsymbol{\mu}_Y(t) dt + \mathbf{b}_i d\mathbf{B}(t) + (\mathbf{w}_i - \mathbf{v}_i\bar{\mathbf{m}}^{-1}\bar{\mathbf{a}}) \tilde{\mathbf{X}}_0(t) dt + \\ & \mathbf{w}_i\boldsymbol{\mu}_{X_0}(t) dt - \mathbf{v}_i\dot{\boldsymbol{\mu}}_{X_0}(t) dt - \underbrace{p\mathbf{v}_i\bar{\mathbf{m}}^{-1}\mathbf{b}d\mathbf{B}(t)}_{=0}, \quad t \geq 0, \end{aligned} \quad (6.4)$$

with $\bar{\mathbf{m}}$ and $\bar{\mathbf{a}}$ introduced in Sec. 5.4, \mathbf{v}_i and \mathbf{w}_i in Eq. (5.20) but not restricted to $2k \times (2k + l)$, and

$$\mathbf{h}_i = \frac{\partial \mathbf{h}\chi}{\partial \chi_i} = \mathbf{h}\tilde{\mathbf{e}}_i \otimes \tilde{\mathbf{e}}_i, \quad \mathbf{b}_i = \mathbf{b} \sum_{j=n(i-1)+1}^{ni} \mathbf{e}_i \otimes \mathbf{e}_i, \quad i = 1, \dots, n_s, \quad (6.5)$$

with $\tilde{\mathbf{e}}_i \in \mathbb{R}^{n_s}$ and $\mathbf{e}_i \in \mathbb{R}^{n_s n}$, for \mathbf{h} and \mathbf{b} see Eq. (5.11). Then, the stationary covariance function \mathbf{c}_{X_0} satisfies

$$\mathbf{0} = \bar{\mathbf{m}}^{-1}\bar{\mathbf{a}}\mathbf{c}_{X_0} + \mathbf{c}_{X_0}\bar{\mathbf{a}}^T\bar{\mathbf{m}}^{-T} + p\mathbf{b}\mathbf{b}^T, \quad (6.6)$$

with the mean value $\boldsymbol{\mu}_{X_0}(t)$ solved separately; stationary covariances \mathbf{c}_{X_i} fulfil

$$\mathbf{0} = \bar{\mathbf{m}}^{-1}\bar{\mathbf{a}}\mathbf{c}_{X_i} + \mathbf{c}_{X_i}\bar{\mathbf{a}}^T\bar{\mathbf{m}}^{-T} + \mathbf{E}\tilde{\mathbf{X}}_i\tilde{\mathbf{X}}_0^T\mathbf{Q}^T + \mathbf{Q}\mathbf{E}\tilde{\mathbf{X}}_0\tilde{\mathbf{X}}_i^T + \mathbf{b}_i\mathbf{b}_i^T, \quad (6.7)$$

where $\mathbf{Q} = \bar{\mathbf{m}}^{-1}(\mathbf{w}_i - \mathbf{v}_i\bar{\mathbf{m}}^{-1}\bar{\mathbf{a}})$, with auxiliary Lyapunov equation

$$\mathbf{0} = \mathbf{E}\tilde{\mathbf{X}}_0\tilde{\mathbf{X}}_i^T\bar{\mathbf{a}}^T\bar{\mathbf{m}}^{-T} + \bar{\mathbf{m}}^{-1}\bar{\mathbf{a}}\mathbf{E}\tilde{\mathbf{X}}_0\tilde{\mathbf{X}}_i^T + \mathbf{c}_{X_0}\mathbf{Q}^T + p\mathbf{b}\mathbf{b}_i^T. \quad (6.8)$$

Employing the time average, the resulting covariance \mathbf{c}_X is again of the form introduced in Eq. (5.17) with $\text{var}(\chi_i)$ instead of $\text{var}(M_{H_1})$ for independent spectators. The performance and the quality of approximation will be compared on following two examples.

Example 6.1. Let us have a harmonic oscillator representing a grandstand with two positions for spectators, *cf* Fig. 6.1, where only one of them can be occupied by an active spectator with probability p , or a passive spectator with probability $1 - p$, and where the forcing terms are independent Gaussian white noise processes for simplicity. The

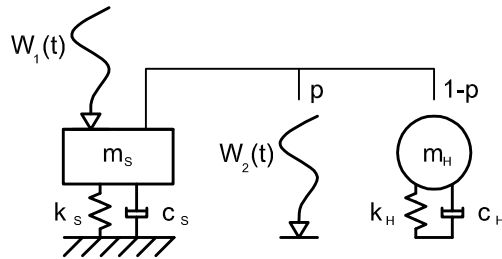


Figure 6.1: Simple example of harmonic oscillator with two positions for spectators, forced with two mutually independent white noise processes $W_i(t)$

governing equation reads

$$\begin{bmatrix} m_S & 0 \\ 0 & (1-\chi)m_H \end{bmatrix} \begin{bmatrix} \ddot{Z}_S \\ \ddot{Z}_H \end{bmatrix} + \begin{bmatrix} c_S + (1-\chi)c_H & -(1-\chi)c_H \\ -(1-\chi)c_H & (1-\chi)c_H \end{bmatrix} \begin{bmatrix} \dot{Z}_S \\ \dot{Z}_H \end{bmatrix} + \begin{bmatrix} k_S + (1-\chi)k_H & -(1-\chi)k_H \\ -(1-\chi)k_H & (1-\chi)k_H \end{bmatrix} \begin{bmatrix} Z_S \\ Z_H \end{bmatrix} = \begin{bmatrix} W_1 + \chi W_2 \\ 0 \end{bmatrix}. \quad (6.9)$$

There are several approximation techniques with different levels of accuracy for the solution of stated SDE: moment equations under some closure techniques, Perturbation method, Taylor series reviewed in Chap. 5, Decomposition method, *etc.* Let us stress again that only the second order moments are of our interest.

1. Moment closure

Equation (6.9) in Cauchy form reads

$$d\mathbf{X}(t) = \mathbf{a}\mathbf{X}(t)dt + \tilde{\chi}\mathbf{w}_1\mathbf{X}(t)dt + \mathbf{b}d\mathbf{B}(t), \quad t \geq 0, \quad (6.10)$$

where $\mathbf{a} = \bar{\mathbf{m}}^{-1}\bar{\mathbf{a}}$, and

$$\mathbf{w}_1 = \frac{1}{m_S} \begin{bmatrix} 0 & 0 & 0 & 0 \\ 0 & 0 & 0 & 0 \\ k_H & -k_H & c_H & -c_H \\ 0 & 0 & 0 & 0 \end{bmatrix}, \quad \mathbf{b} = \frac{1}{m_S} \begin{bmatrix} 0 & 0 \\ 0 & 0 \\ 1 & \chi \\ 0 & 0 \\ 0 & 0 \end{bmatrix}, \quad (6.11)$$

$d\mathbf{B}(t) \in \mathbb{R}^2$ and $\mathbf{X} = [Z_S, Z_H, \dot{Z}_S, \dot{Z}_H]^\top$, for the remaining matrices refer to Eq. (5.25) in Ex. 5.3. Employing the Itô's formula, moment equations are derived. Mean value is clearly zero and the second order moments satisfy Lyapunov equation extended with the term $\mathbf{E}[\mathbf{w}_1\tilde{\chi}\mathbf{X}\mathbf{X}^\top + \tilde{\chi}\mathbf{X}\mathbf{X}^\top\mathbf{w}_1^\top]$ which is cubic. The only nonzero element in the diffusion term is $(\mathbf{b}\mathbf{b}^\top)_{3,3} = (1 + \mathbf{E}\chi^2)/m_S^2 = (1+p)/m_S^2$. Hence, adopting the Gaussian closure (assumes that moments of \mathbf{X} of order $q \geq 3$ have the same properties as the corresponding moments of Gaussian vectors, *i.e.* odd moments are zero and even are expressed through correlations), the additional terms disappear and we are led to the same equation as Eq. (4.11), but with adjusted drift and diffusion matrices.

Assuming higher order moments and denoting $\mathbf{c}^\chi = \mathbf{E}[\tilde{\chi}\mathbf{X}\mathbf{X}^\top]$, auxiliary Lyapunov equation has to be solved

$$\mathbf{0} = \mathbf{a}\mathbf{c}^\chi + \mathbf{c}^\chi\mathbf{a}^\top + [\mathbf{w}_1\mathbf{E}(\tilde{\chi}^2\mathbf{X}\mathbf{X}^\top) + \mathbf{E}(\tilde{\chi}^2\mathbf{X}\mathbf{X}^\top)\mathbf{w}_1^\top] + (\mathbf{b}\mathbf{b}^\top)^\chi, \quad (6.12)$$

where $(\mathbf{b}\mathbf{b}^\top)_{3,3}^\chi = \mathbf{E}[\tilde{\chi}\chi^2]/m_S^2 = p(1-p)/m_S^2$. Several assumptions can be made: fourth order closure, *i.e.* $\mathbf{E}[\tilde{\chi}^2\mathbf{X}\mathbf{X}^\top] = \mathbf{0}$ leads to sequential solution of the Lyapunov systems with rather stable results; separation in the form $\mathbf{E}[\tilde{\chi}^2\mathbf{X}\mathbf{X}^\top] = \mathbf{E}[\tilde{\chi}\mathbf{X}]\mathbf{E}[\tilde{\chi}\mathbf{X}]^\top$ would lead to nonlinear system of equations, nevertheless the unknowns are independent and solution eventually gives $\mathbf{E}[\tilde{\chi}\mathbf{X}] = \mathbf{0}$, hence higher order moment equations would be required for further information; attractive separation or local independence assumption in the form $\mathbf{E}[\tilde{\chi}^2\mathbf{X}\mathbf{X}^\top] = \mathbf{E}[\tilde{\chi}^2]\mathbf{c}_X$ gives

a coupled system, but with somewhat unstable and erroneous solution. Some of the results can be found in Fig. 6.2.

2. Algebraic approach

Stationary solution of our problem is written as

$$\mathbf{0} = \mathbf{a}(\boldsymbol{\chi}) \mathbf{c}_X(\boldsymbol{\chi}) + \mathbf{c}_X(\boldsymbol{\chi}) \mathbf{a}^\top(\boldsymbol{\chi}) + \mathbf{b}(\boldsymbol{\chi}) \mathbf{b}^\top(\boldsymbol{\chi}), \quad (6.13)$$

where $\mathbf{c}_X(\boldsymbol{\chi})$ is now a random matrix. Employing the Kronecker sum, we can rewrite Lyapunov Eq. (6.13) as a linear system of equations

$$[\mathbf{a} \oplus \mathbf{a}] \text{vec}(\mathbf{c}_X) = \text{vec}(\mathbf{b}\mathbf{b}^\top), \quad (6.14)$$

where the vectorization operator $\text{vec}(\bullet)$ transforms a matrix \bullet columnwise to a vector; the dependencies on $\boldsymbol{\chi}$ were skipped for brevity. For Kronecker sum the followings holds, cf [57]: $e^{\mathbf{A}} \otimes e^{\mathbf{B}} = e^{\mathbf{A} \oplus \mathbf{B}}$, $\mathbf{A} \oplus \mathbf{B} = \mathbf{A} \otimes \mathbf{I}_{n_B \times n_B} + \mathbf{I}_{n_A \times n_A} \otimes \mathbf{B}$, where n_A , n_B are sizes of the square matrices \mathbf{A} and \mathbf{B} . Together with the fact $\int_0^\infty e^{-\mathbf{L}t} dt = \mathbf{L}^{-1}$ for a regular \mathbf{L} , the resulting Lyapunov equation can be rewritten in the form of Eq. (6.14). The solution is a function of $\boldsymbol{\chi}$, which can be eliminated by averaging the result with respect to this random variable. Hence, only the mean solution $\mathbf{E}\mathbf{c}_X(\boldsymbol{\chi})$ is of our interest and can be obtained by appropriate methods, namely MC, Iteration method, *etc.*

3. Exact solution

Clearly, such an example can be easily solved with analytical tools employing the conditional analysis, since the situation is equivalent with probability p to the harmonic oscillator driven by Gaussian white noise of intensity $1 + \chi$; and with probability $1 - p$ to two-degrees-of-freedom system driven by the unit Gaussian white noise. Ergo, averaging among these two states leads to a linear interpolation in p between the two results. Nevertheless, contrary to approximation techniques introduced earlier, conditional analysis cannot be applied in general cases of many positions for spectators since too many combinations occur.

Graphs in Figs. 6.2a and 6.2b capture dependencies of $\text{var}Z_S$ and $\text{var}\dot{Z}_S$ as functions of $p \in [0, 1]$ for particular data $k_S = 170$ kN/m, $m_S = 2 \cdot 0.0862$ t, $c_S = 0.07 \cdot 2 \cdot \sqrt{k_S m_S}$ kNs/m, $f_1 = 5$ Hz, passive spectator according to Coermann used. Figures 6.2c and 6.2d capture dependencies of $L^2(0, 1)$ norms of relative errors on the empty structure eigenfrequency f_1 and on the mass ratio γ ,

$$\text{err}^2(f_1, \gamma) = \frac{\int_0^1 [\text{var}Z_S^e(p, f_1, \gamma) - \text{var}Z_S^\bullet(p, f_1, \gamma)]^2 dp}{\int_0^1 (\text{var}Z_S^e(p, f_1, \gamma))^2 dp}, \quad (6.15)$$

where $\text{var}Z_S^e$ stands for the exact analytical solution and $\text{var}Z_S^\bullet$ for an approximate one; \bullet denotes arbitrary one of the mentioned approximate methods. Graphs show quite poor agreement of the approximations in comparison with the exact solution even for high relative damping $\zeta_S = 0.07$, cf also Fig. 5.3.

Example 6.2. The last example will demonstrate on the structure in Appendix C.2 the performance of the Taylor series method when random distribution of a crowd is assumed.

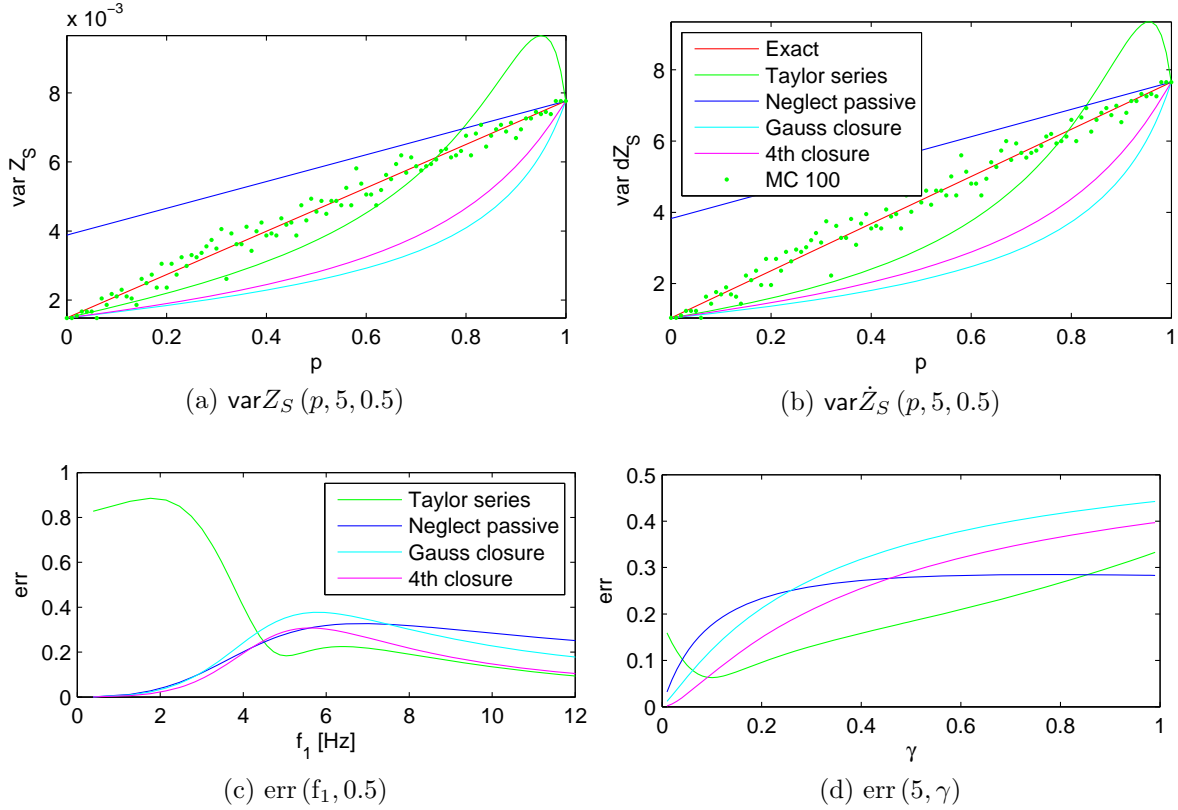


Figure 6.2: Dependencies of the structure displacement and acceleration variances on the probability p ; relative errors in Eq. (6.15) as functions of f_1 and γ ; MC based on algebraic approach in Eq. (6.14)

All spectators are treated as independent. Figures 6.3a and 6.3b show $\text{var} Z_{P_1}$ and $\text{var} \ddot{Z}_{P_1}$ as functions of p , and Figs. 6.3c and 6.3d compare the mean value solutions for $p = 0.5$. MC is based on 500 realizations of 160 s in length. It can be concluded from the results that the Taylor series method represents somewhat an upper estimate to the MC solution, and follows quite closely the overall evolution of the response variance along the probability p . Nevertheless, the computational burden was comparable with that of the MC solution for all realizations and hence, no computation times are listed.

6.3 Conclusion

In this chapter, it has been presented an approximation of the grandstand problem comprising random forcing and random distribution of both an active and a passive crowd in terms of Taylor series method. It has been shown, upon used complex example, that it is possible to approximate the resulting first two moments of the system response in acceptable bounds. Computational cost was, however, comparable with that one of the MC simulation, nevertheless further simplifications and reductions are possible in order to lower the computational burden. Some other approximate methods, namely Gaussian closure, higher order moment closure and algebraic approach were also briefly discussed and presented on a simple example.

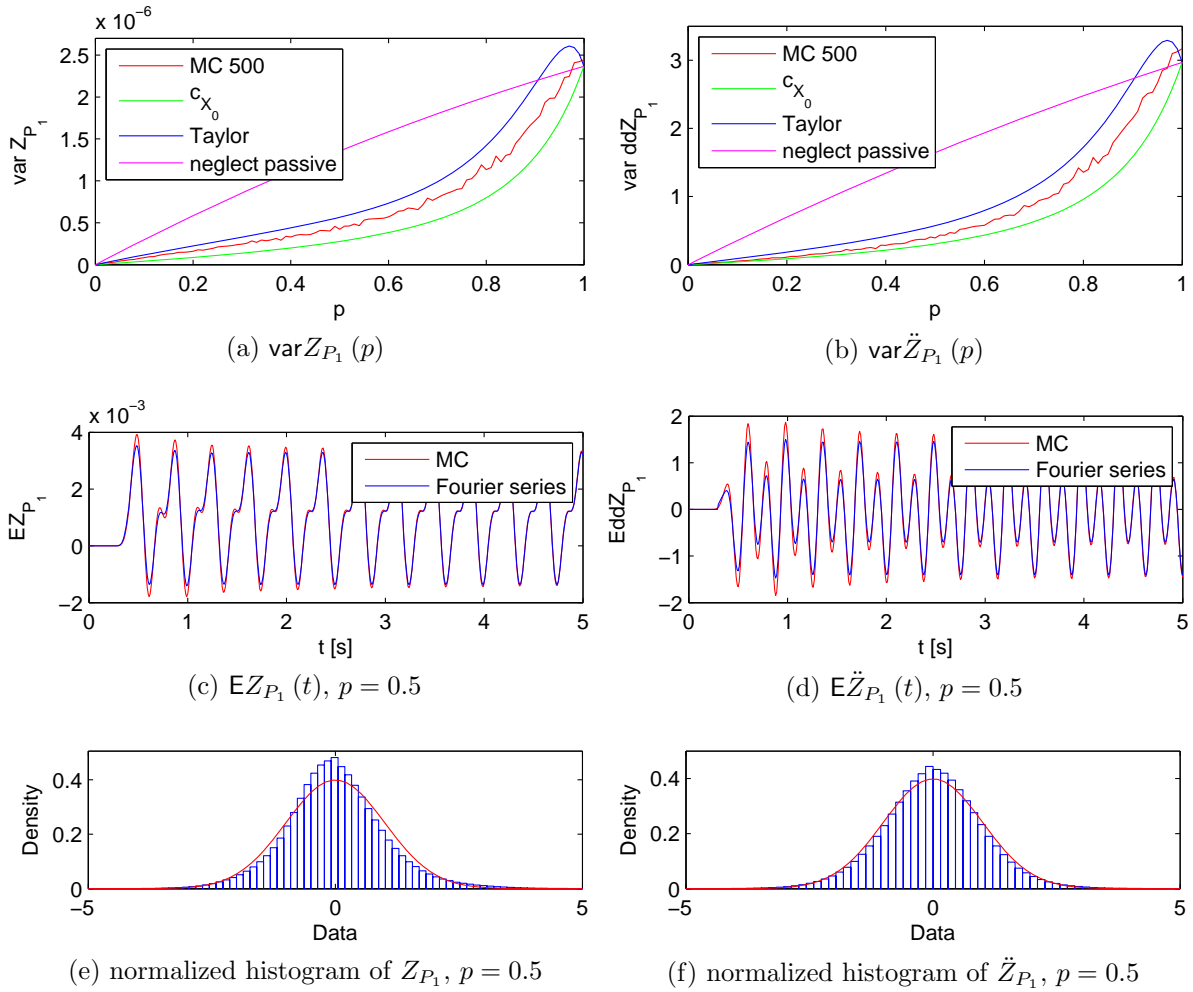


Figure 6.3: Dependencies of the structure displacement and acceleration variances on the probability p ; mean value solutions and normalized response histograms with standard normal density for $p = 0.5$, ergodicity in variance assumed

Chapter 7

Conclusion and future prospects

This thesis has provided, in its very beginning, a short overview of some generally accepted approaches in the field of grandstands. A brief inspection of Czech standards indicated a lack of systematic design methods available to engineers in the case of synchronized lively crowds. Other standards, such as Canadian or British, possess some instructions, nevertheless basically from the deterministic point of view. The model and the design procedures should take account of the evident randomness, especially the random forcing and the spatial distribution of a crowd.

After a short literature review and state of the art, submitted thesis has concentrated on the MC simulation with an emphasis on reduced order modelling. Analysis and examples carried out indicated that much richer projection basis is required than only one or two-dimensional unlike suggestions in some design procedures reducing the grandstand and passive crowd to simple two-degree-of-freedom systems; significant reduction can be, however, still achieved. Since many load models for active spectators are based on truncated Fourier series expansion—valid also for the approximation of the load mean value—the third chapter was concluded with the method for finding the worst crowd distribution or the mean-worst crowd distribution with respect to displacement or acceleration in some preselected node.

The first of the three main chapters, Chap. 4, pursued the approximation of the forcing terms, *i.e.* an active crowd. Under the simplifying assumptions, *e.g.* short contact time, the random forcing was approximated with nonstationary mean value by means of the truncated Fourier series with superposed zero mean weakly stationary ergodic Gaussian coloured noise. Subsequently, the theory of stochastic differential equations in terms of the Itô's calculus was briefly reviewed. Employing some heuristic arguments together with central limit and Rosenblatt theorems, the response was close to Gaussian, the result was supported with several examples. As a measure of the approximation quality, the mean upcrossing, distribution of maxima, stationary variances *etc* were employed; the convergence was improved for vanishing damping. On the basis of the overall time consumptions, though resulting only from a MATLAB implementation, the method proved to be quite efficient in comparison with the MC simulation. The forcing terms were then generalized to a random distribution of an active crowd introducing the random indicator variables which provide a switch between an active spectator and an empty seat. Introduced correlations between indicators correspond to some interaction between active spectators. A short digression concerning possibilities of the non-Gaussian processes was

then performed by means of the translation processes and bi-spectra. Other options were discussed providing also some hints for directions of further development.

The second main part reviewed the theory of random operator equations, namely in terms of the Taylor series method introducing randomness in biodynamic models; overall approach was nevertheless restricted only to the second order moments. Immediately, it was shown that the randomness in the biodynamic models yields up to 3.5 % of the total variance in the scope of the randomness caused by an active crowd, and the effect was neglected in further considerations; random distribution of a passive crowd yields much greater impact. So, the passive spectators were introduced in terms of the complementary indicator variables. Note that the Taylor series method is more stable and accurate for increasing damping which yields somewhat contradictory requirements: vanishing damping contributes to the improved Gaussianity of the response while increasing damping contributes to better convergence of the Taylor series method. Achieved approximation was, in the scope of examples used, found to be in quite satisfactory agreement with MC simulation.

Concluding chapter finally presented the most general approach within the scope of the thesis and the methods introduced herein. Active spectators were approximated by random forcing discussed previously with a random spatial distribution realized via indicator variables; remaining seats were filled with a passive spectators assuming fully occupied structure. Clearly, such a problem is a stochastic differential equation, moreover with the operator being fully correlated with the forcing. Again, the Taylor series method was employed performing quite satisfactorily for mass ratios small enough ($\gamma \leq 0.35$). The computational burden in this case was comparable with that of the MC simulation; in all approaches there is, however, a possibility of really efficient implementation which can change slightly the overall balance.

Developed approach proceeds inductively from simple models to complex ones and describes the possibilities of analytical methods in comparison with direct simulation. Nevertheless, it is not indicated which model should be employed for the best description of complex reality; certainly, knowing the distribution of a crowd leading to the extreme vertical displacement or acceleration in some preselected node is of some practical interest as well as knowing the response of the structure under stationary random spatial distribution of a crowd. But a model which can be described through a few variables reflecting the loading scenario and also capturing "typical" situation is much more sophisticated than the most complex one described in this thesis, *i.e.* in Chap. 6.

Introduced methods can be extended in many directions, the most important being the comparison of achieved results with the measurements on the real structures with indication which one suits best. All approximations, however fine or accounting of whichever area of randomness, are only stationary ones (up to the mean value), and hence cannot be realistic. All forcing processes are actually nonstationary; a crowd as a whole is evolving in time—active spectators become passive during the time and vice versa—and hence the models adopted cannot reflect such a phenomena in its full complexity. Spectral densities, being based on MC simulators available in the literature evaluated for discrete frequencies can be generalized to cover the whole frequency interval, preferably being fitted directly to measured data instead of artificial ones and also taking account of other types of loads such as bouncing and jouncing. Further generalization could be performed in terms of enlargement of the state space of the indicator variables in order to account for active

spectators, passive spectators and empty seats. Generalization of the forcing in terms of the discussion at the end of the Chap. 4 is also possible.

The main contributions of submitted thesis can be summarized as:

1. Development of systematic FEM-based approach for modelling a crowd-grandstand system in terms of semi-analytical solution avoiding direct MC simulation.
2. The method is capable to reflect major sources of system randomness, namely random forces induced by an active crowd, random distribution of a crowd and random parameters of biodynamic models representing a passive crowd.
3. Relative efficiency of the method in comparison with direct MC simulation method and transparency providing quantities required for serviceability (and possibly reliability) assessment of the crowd-grandstand system.

Among many possible options in continuation or generalization, the work can be extended mainly in following directions:

1. Comparison of introduced methods with measurements on real structures.
2. Spectral densities based on MC simulators available in the literature evaluated for discrete frequencies can be generalized to cover the whole frequency interval preferably being fitted directly to measured data and taking account also of other types of loads.
3. Reflect nonstationarity and non-Gaussianity of the forcing terms and the response in more detail.
4. Introduce wider state space of the random switch variables, *e.g.* to reflect an active spectator, a passive spectator and an empty seat; include the time evolution of a crowd – switching variables can be treated as random processes.

Apparently, the grandstand problem is quite complex and much work remains to be done to achieve a transparent, reliable and efficient design procedures. It is believed that this thesis will positively contribute to this endeavour and will provide some ideas how to improve or generalize present concepts.

Appendix A

Fractions of the probability theory

A brief overview of some basic notions from the probability theory and the theory of stochastic processes employed throughout the thesis is given below; for details and further discussions see [13, 17, 19, 39, 48, 50, 52, 53].

A.1 Basic concepts

The probability space is denoted $(\Omega, \mathcal{A}, \mathbf{P})$, where Ω is the sample space, \mathcal{A} the σ -field of events and $\mathbf{P} : \mathcal{A} \rightarrow [0, 1]$ is the probability measure.

A measurable function $X : (\Omega, \mathcal{A}) \rightarrow (\mathbb{R}, \mathcal{B})$, where \mathcal{B} is the Borel σ -field, is called a random variable; a function $\mathbf{X} : (\Omega, \mathcal{A}) \rightarrow (\mathbb{R}^d, \mathcal{B}^d)$ is called a d -valued random vector.

The distribution of X is the probability induced by the mapping $X : \Omega \rightarrow \mathbb{R}$, that is, $Q(B) = \mathbf{P}(X^{-1}(B))$, $B \in \mathcal{B}$; the distribution function of X is for $B = (-\infty, x]$, $x \in \mathbb{R}$, that is, $\mathbb{F}(x) = \mathbf{P}[X^{-1}((-\infty, x])] = \mathbf{P}\{\omega : X(\omega) \leq x\} = \mathbf{P}(X \leq x)$.

The expectation operator $\mathbf{E}[\bullet]$ of \bullet is defined as $\mathbf{E}[g(X)] = \int_{\Omega} g(X(\omega)) \mathbf{P}(d\omega) = \int_{\mathbb{R}} g(x) Q(dx) = \int_{\mathbb{R}} g(x) d\mathbb{F}(x)$. If the distribution function is absolutely continuous, then also $\mathbf{E}[g(X)] = \int_{\mathbb{R}} g(x) f(x) dx$ with $f(x) = \mathbb{F}'(x)$. If the random variable X is discrete, *i.e.* the distribution function is atomic, the integral degenerates into a sum over all atoms.

The conditional expectation $\mathbf{E}[X|\mathcal{G}]$ of X with respect to a σ -field \mathcal{G} is defined to be the class of \mathcal{G} -measurable functions satisfying $\int_{\Lambda} X d\mathbf{P} = \int_{\Lambda} \mathbf{E}[X|\mathcal{G}] d\mathbf{P}$, $\forall \Lambda \in \mathcal{G}$.

Moments of order p of a random variable X are computed according to $\mu_{(p)} = \mathbf{E}X^p$, the mean value is $\mu = \mu_{(1)} = \mathbf{E}X$, variance $\text{var}(X) = \sigma^2 = \mathbf{E}(X - \mu)^2$, coefficient of variation $c_v = \sigma/\mu$, coefficient of skewness $\gamma_3 = \mathbf{E}(X - \mu)^3/\sigma^3$ and the coefficient of kurtosis $\gamma_4 = \mathbf{E}(X - \mu)^4/\sigma^4$. In the case of random vectors, the mean $\boldsymbol{\mu} = \mathbf{E}\mathbf{X}$, covariance $\mathbf{c} = c_{ij} = \text{cov}(X_i, X_j) = \mathbf{E}[(\mathbf{X} - \boldsymbol{\mu})(\mathbf{X} - \boldsymbol{\mu})^{\top}]$, correlation $\mathbf{r} = \mathbf{c} + \boldsymbol{\mu}\boldsymbol{\mu}^{\top}$, and correlation coefficient $\rho_{ij} = c_{ij}/(\sigma_i\sigma_j)$.

A.2 Stochastic processes

A function $\mathbf{X} : T \times \Omega \rightarrow \mathbb{R}^d$ of two arguments, $t \in T$, $T \subset \mathbb{R}^+$, and $\omega \in \Omega$, $(\Omega, \mathcal{A}, \mathbf{P})$ being a probability space, is said to be an \mathbb{R}^d -valued random process, or vector process, if for each $t \in T$ it is an \mathbb{R}^d -valued random variable on $(\Omega, \mathcal{A}, \mathbf{P})$. $\mathbf{X}(\bullet, \omega)$ for fixed ω is called a realization, or a sample; for fixed t , $\mathbf{X}(t, \bullet)$ is a random variable. If T is an

interval, \mathbf{X} is a continuous time stochastic process, if T is discrete, it is called a discrete time stochastic process or time series.

A finite dimensional distributions of \mathbf{X} of order $p \in \mathbb{N}$ are the distributions of the random vector $[\mathbf{X}(t_1), \dots, \mathbf{X}(t_p)]$, that is,
 $\mathbb{F}_p(\mathbf{x}_1, \dots, \mathbf{x}_p; t_1, \dots, t_p) = \mathbb{P}(\bigcap_{i=1}^p \{\mathbf{X}(t_i) \in \mathbb{X}_{k=1}^d(-\infty, x_{i,k}]\})$, $\mathbf{x} = (x_{i,1}, \dots, x_{i,d}) \in \mathbb{R}^d$ and $p \geq 1$.

After Kolmogorov, upon satisfying consistency and symmetry conditions, the finite dimensional distributions \mathbb{F}_p , $p = 1, 2, \dots$ can be used to define a stochastic process. Usually, the information available is restricted to the first and second order distributions.

An \mathbb{R}^d -valued process \mathbf{X} is said to be stationary in the strict sense or stationary if $\mathbb{F}_p(\mathbf{x}_1, \dots, \mathbf{x}_p; t_1, \dots, t_p) = \mathbb{F}_p(\mathbf{x}_1, \dots, \mathbf{x}_p; t_1 + \tau, \dots, t_p + \tau)$, τ being a time shift.

A stochastic process \mathbf{X} is said to be ergodic if ensemble averages equal time averages, $\mathbb{E}[g(\mathbf{X}(t))] = \lim_{\tau \rightarrow \infty} \frac{1}{\tau} \int_{-\tau/2}^{\tau/2} g(\mathbf{X}(t)) dt$.

A stochastic process \mathbf{X} has independent or orthogonal increments if the random variables $\mathbf{X}(t) - \mathbf{X}(s)$ and $\mathbf{X}(v) - \mathbf{X}(u)$, $s < t \leq u < v$, are independent; moreover, if the distribution of $\mathbf{X}(t) - \mathbf{X}(s)$ depends only on the time lag $t - s$, the process is said to have stationary independent increments.

A process \mathbf{X} is called Gaussian if all its finite dimensional distributions are Gaussian.

In analogy to random variables, the mean value is $\boldsymbol{\mu}(t) = \mathbb{E}[\mathbf{X}(t)]$, the covariance function $\mathbf{c}(t, s) = \mathbb{E}[(\mathbf{X}(t) - \boldsymbol{\mu}(t))(\mathbf{X}(s) - \boldsymbol{\mu}(s))^\top]$, and the correlation function $\mathbf{r}(t, s) = \mathbf{c}(t, s) + \boldsymbol{\mu}(t)\boldsymbol{\mu}(s)^\top$. The second moment properties of the process \mathbf{X} are given by the pairs $\boldsymbol{\mu}, \mathbf{c}$ or $\boldsymbol{\mu}, \mathbf{r}$. In the case of a Gaussian process, this pair contains the complete information.

A process \mathbf{X} is said to be weakly stationary if the mean value $\boldsymbol{\mu}(t) = \boldsymbol{\mu}$ is constant and if the correlation and covariance functions depend only on the time lag, *i.e.* $\mathbf{c}(t, s) = \mathbf{c}(t - s)$, $\mathbf{r}(t, s) = \mathbf{r}(t - s)$.

The correlation function $r(\tau)$ of real, weakly stationary process $X(t)$ is a positive definite function; then, there exists a real, increasing and bounded function \mathcal{S} called spectral distribution function, such that $r(\tau) = \int_{-\infty}^{\infty} e^{i2\pi\xi\tau} d\mathcal{S}(\xi)$. If \mathcal{S} is absolutely continuous, then there exists a function $s(\xi) = d\mathcal{S}(\xi)/d\xi$, called spectral density or power spectral density. The correlation and spectral density functions are Fourier pairs.

A random variable X_n is said to converge in the mean square to X , notation $\text{l.i.m}_{n \rightarrow \infty} X_n = X$, if $\mathbb{E}[(X_n - X)^2] = 0$. Concept of mean square continuity, differentiation and integration is then developed. For example, a real valued process $X(t)$ is mean square differentiable at t if $\text{l.i.m}_{h \rightarrow 0} \frac{X(t+h) - X(t)}{h}$ exists.

For a complex, weakly stationary and mean square continuous process X with the spectral distribution function \mathcal{S} and the spectral density function s there exist a complex process U with orthogonal increments such that the mean square integral $X(t) = \int_{-\infty}^{\infty} e^{i2\pi\xi t} dU(\xi)$ exists for every t ; $\mathbb{E}U(\xi) = 0$, $\mathbb{E}|U(\xi)|^2 = \mathcal{S}(\xi)$ and $\mathbb{E}|dU(\xi)|^2 = d\mathcal{S}(\xi) = s(\xi) d\xi$, U is called spectral process associated with X .

For a mean square differentiable process $X(t)$, the mean x -upcrossing rate is expressed by means of the Rice's formula

$$\nu_x^+(t) = \int_0^\infty y f_{X, \dot{X}}(x, y) dy, \quad (\text{A.1})$$

where $f_{X,\dot{X}}(x, y)$ is the joint density of $[X(t), \dot{X}(t)]$.

A collection of increasing sub σ -fields $(\mathcal{F}_t)_{t \geq 0}$ of \mathcal{A} is called a filtration in (Ω, \mathcal{A}) and $(\Omega, \mathcal{A}, (\mathcal{F}_t)_{t \geq 0}, \mathbf{P})$ is called a filtered probability space. If a process X is \mathcal{F}_t -measurable function for all $t \geq 0$, then it is said to be \mathcal{F}_t -adapted.

A real stochastic process X defined on a filtered probability space is an \mathcal{F}_t -martingale if $\mathbf{E}|X(t)| < \infty$, X is \mathcal{F}_t -measurable and $\mathbf{E}[X(t) | \mathcal{F}_s] = X(s)$ almost surely for all $s \leq t$.

If $T : \Omega \rightarrow [0, +\infty]$ is a random variable defined on $(\Omega, \mathcal{A}, (\mathcal{F}_t)_{t \geq 0}, \mathbf{P})$ such that $\{\omega : T \leq t\} \in \mathcal{F}_t$ for all $t \geq 0$, then T is called an \mathcal{F}_t -stopping time.

A real process X is an \mathcal{F}_t -local martingale if there exists an increasing sequence T_k , $k = 1, 2, \dots$ of \mathcal{F}_t -stopping times, $T_k \leq T_{k+1}$, $\lim_{k \rightarrow \infty} T_k = \infty$ almost surely, and the stopped process $X^{T_k}(t)$ is an \mathcal{F}_t -martingale for each k .

If a process X is of the form $X(t) = X(0) + M(t) + A(t)$ where $M(0) = A(0) = 0$, M is a local martingale and A is a right continuous process with left limits and is of finite variation, then X is called a semimartingale.

For X and Y semimartingales, each $t \geq 0$ and each sequence of partitions $p_n = (0 = t_0^{(n)}, \dots, t_{m_n}^{(n)} = t)$ of $[0, t]$ and refining for $n \rightarrow \infty$ a quadratic covariation process $[X, Y]$ is defined as $\sum_{k=1}^{m_n} (X(t_k^{(n)}) - X(t_{k-1}^{(n)})) (Y(t_k^{(n)}) - Y(t_{k-1}^{(n)})) \xrightarrow{\text{ucp}} [X, Y](t)$, where ucp stands for uniformly on compacts in probability; $[X, X](t) = [X](t)$ is called a quadratic variation, $[X]$ is decomposed into continuous part $[X]^c$ and pure jump part.

A centered Gaussian random process B starting from 0 with almost surely continuous samples, with stationary independent Gaussian increments and covariance function $\mathbf{E}[B(t)B(s)] = \min(t, s)$ is called a Brownian motion or a Wiener process; quadratic variation is $[B] = [B]^c = t$, B is a semimartingale.

For T_k , $k = 1, 2, \dots$ strictly increasing sequence with $T_0 = 0$ almost surely, $N(t) = \sum_{k \geq 1} \mathbb{1}_{[t \geq T_k]}$ is called a counting process. Moreover, if the process is of stationary increments, *i.e.* $N(t) - N(s)$, $t > s$ has the same distribution as $N(t - s)$, it is called the Poisson counting process; $\mathbf{P}[N(t) = k] = e^{-\lambda t} \frac{(\lambda t)^k}{k!}$, with $\lambda > 0$ called an intensity.

The compound Poisson process C is of the form $C(t) = \sum_{k=1}^{N(t)} Y_k = \sum_{k=1}^{\infty} Y_k \mathbb{1}_{[t \geq T_k]}$, Y_k are *iid*, with $\mathbf{E}C(t) = \lambda t \mathbf{E}Y_1$, $c(t, s) = \lambda \min(t, s) \mathbf{E}[Y_1^2]$. The process $W_P(t) = \sum_{k=1}^{N(t)} Y_k \delta(t - T_k)$, where $\delta(\bullet)$ denotes the Dirac delta function, is called a Poisson white noise. $\mathcal{M}(t, dy)$ being a random measure which gives the number of jumps of C in $(y, y + dy)$ during the time interval $(0, t]$, an alternative definition is given in the form $C(t) = \int_{\mathbb{R}} y \mathcal{M}(t, dy)$, $\mathbf{E}\mathcal{M}(t, dy) = \lambda t d\mathbb{F}(y)$, \mathbb{F} denotes the distribution of Y_1 . The quadratic variation is $[C](t) = \sum_{k=1}^{N(t)} Y_k^2$ with $[C]^c = 0$, C is a pure jump semimartingale.

A.3 Itô's formula and stochastic differential equations

The Itô's formula is an extension of the change of variable formula of the classical calculus to integrals with integrands being adapted left continuous processes with right limits and semimartingale integrators.

For \mathbf{Y} an \mathbb{R}^d -valued semimartingale and $g : \mathbb{R}^d \rightarrow \mathbb{R}$ with continuous second order partial derivatives, $g(\mathbf{Y})$ is a semimartingale and the integral form of the Itô's formula

reads

$$\begin{aligned}
g(\mathbf{Y}(t)) - g(\mathbf{Y}(0)) &= \sum_{i=1}^d \int_{0+}^t \frac{\partial}{\partial y_i} g(\mathbf{Y}(s-)) dY_i(s) \\
&+ \frac{1}{2} \sum_{i,j=1}^d \int_{0+}^t \frac{\partial^2}{\partial y_i \partial y_j} g(\mathbf{Y}(s-)) d[Y_i, Y_j]^c(s) \\
&+ \sum_{0 < s \leq t} \left[g(\mathbf{Y}(s)) - g(\mathbf{Y}(s-)) - \sum_{i=1}^d \frac{\partial}{\partial y_i} g(\mathbf{Y}(s-)) \Delta Y(s) \right],
\end{aligned} \tag{A.2}$$

$Y(s-) = \lim_{u \uparrow s} Y(u)$ denotes the limit from the left and $\Delta Y(s) = Y(s) - Y(s-)$ denotes the jump discontinuity of Y at time s .

A random process \mathbf{X} is a solution to the stochastic differential equation

$$d\mathbf{X}(t) = \mathbf{a}(\mathbf{X}(t-), t) dt + \mathbf{b}(\mathbf{X}(t-), t) d\mathbf{Y}(t), \quad t \geq 0 \tag{A.3}$$

if

$$\mathbf{X}(t) = \mathbf{X}(0) + \int_0^t \mathbf{a}(\mathbf{X}(s-), s) ds + \int_0^t \mathbf{b}(\mathbf{X}(s-), s) d\mathbf{Y}(s), \quad t \geq 0, \tag{A.4}$$

where \mathbf{a} , \mathbf{b} are $\mathbb{R}^{d \times 1}$ and $\mathbb{R}^{d \times d'}$ matrices, \mathbf{Y} is an $\mathbb{R}^{d'}$ -valued semimartingale and \mathbf{X} is an \mathbb{R}^d -valued stochastic process; the integrals are interpreted in the mean square and in the Itô sense respectively.

Appendix B

MATLAB implementation

A short description of required procedures for the computation of the grandstand problem implemented in MATLAB[®] environment is listed below.

B.1 General overview

Geometry, material parameters, boundary conditions *etc* are given in the input file `*.m` comprising several key matrices and vectors:

1. `Lm`, the matrix of the structure geometry and corresponding code numbers. Columnwise, it stores a node number i , x_i , y_i and z_i -coordinates of the i -th node followed by the six code numbers.
2. `Con` denotes the matrix of connectivity, material and cross sections. Columnwise, it stores a label of the beam element j , number of starting and ending node m and n , identification of the cross-sectional and material parameters.
3. `rp` vector stores prescribed Dirichlet boundary conditions set to zero as default. DOFs with Dirichlet boundary conditions are situated at the end of the list.
4. `cond` matrix saves the information about elements having condensed some DOFs. Columnwise, it contains element number, twelve positions then comprise indicators; if 1 occupy an i -th position, $i = 1, \dots, 12$, then i -th local DOF is condensed.
5. `crosssect` and `matconst` carry information about the cross sectional properties and material constants; cross sectional area A , second moments of area I_y , I_z , polar moment I_k with respect to local coordinates of the beam, shear coefficients β_y and β_z . Material constants are Young modulus E , Poisson ratio ν , mass density ρ and relative damping coefficients $\zeta_{S,i}$ and $\zeta_{S,j}$ for two modes i and j according to Rayleigh model of proportional damping.
6. Vector `ns` stores the code numbers or DOFs which can be occupied either by active or passive spectators. Further data such as jumping frequency, type of biodynamic models are specified as single variables.

Subsequently, a `preprocessor` routine is called which creates a field `struct` comprising all elements with their particular data; `for` cycle spanning all the elements then assembles

required matrices $\mathbf{K}_S, \mathbf{M}_S$. The generalized eigenvalue problem is solved efficiently via MATLAB routine `eigs` for sparse matrices yielding necessary information for an assembly of the damping matrix \mathbf{C}_S .

Assembled matrices are then adjusted in `adjustMatrix` function such that to comprise also biodynamic models, *cf* Eq. (3.3). Then, using arbitrary one of the methods discussed in Sec. 3.4.2 and employing additional routines, the transformation basis \mathbf{V} is computed; MS is, however, preferred because of its simplicity and relative accuracy.

B.2 MC simulation

MC is mainly based on simulation of the artificial loading processes, which is described in detail in [51]. Random variables are generated employing wide variety of MATLAB tools capable to simulate a number of customary distributions. The core of the MC is the time integration of the system of deterministic second order differential equations in Eq. (2.1) or in Eq. (3.4) to obtain an output realizations. To this end, Newmark integration scheme was implemented.

Statistical processing of the output realizations is also readily carried out due to MATLAB functions such as `var`, `std`, `rms` evaluating variance, standard deviation, RMS values. Many other handy functions are available too.

B.3 Moment equations

After assembly of the drift and diffusion matrices, the main problems referred to many times are the Lyapunov and Sylvester equations. This matrix problem can, however, be solved efficiently calling the `lyap` routine, which is capable to solve both of the mentioned problems depending on the input data. Higher order moments are solved with the help of the external `*.mex` files written in C++ which supplement the basic code. These are employed to assemble the problems and to transform higher order tensor equations to the matrix-vector equations, *cf* Eqns. (4.71) – (4.78). Resulting systems of linear equations are solved via MATLAB resources, *e.g.* using `\` or `linsolve`. Finally, a brief diagram capturing the structure of the implementation is depicted in Fig. B.1.

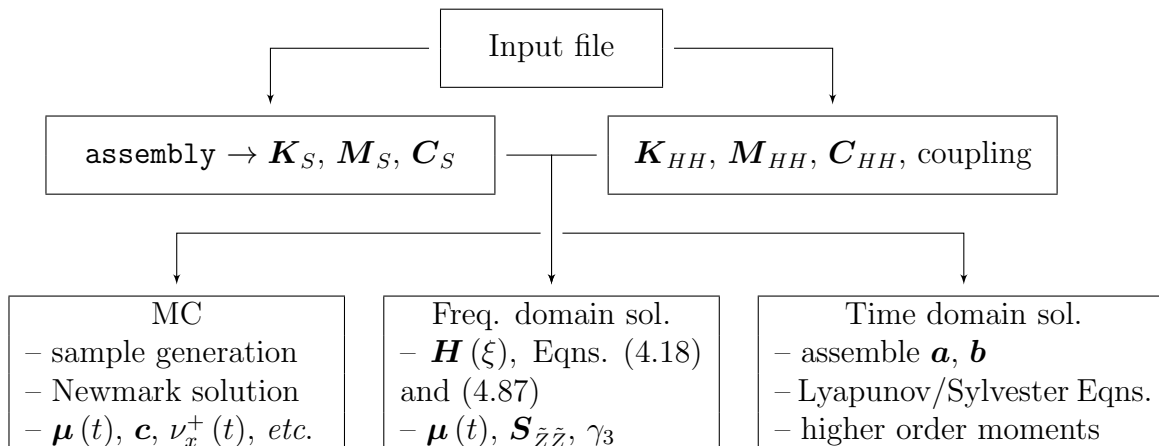


Figure B.1: Implementation diagram

Appendix C

Description of toy structures used

Test examples employed throughout the thesis in order to demonstrate introduced approaches and their performance are described below in this appendix in more detail.

C.1 Simply supported beam

Examples 4.3 and 4.9. The first, geometrically simplest structure is a straight, simply supported beam of 2 m length comprising four positions for spectators denoted with vertical red lines, *cf* Fig. C.1, where also three vertical eigenmodes are depicted together with the point of interest P_1 . Rayleigh damping with $\zeta_1 = 0.05$ and $\zeta_2 = 0.08$ for the first

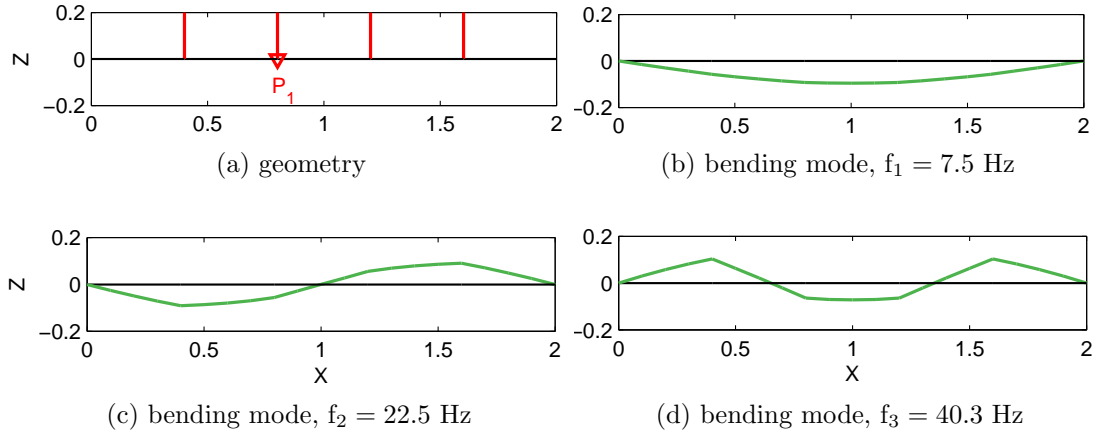


Figure C.1: Geometry, labelled point of interest, positions for spectators and the first three bending modes of simply supported beam

two vertical modes are used, total mass 1700 kg. Maximal mass ratio $\gamma = m_H/m_S = 0.20$, where m_H denotes the total mass of passive spectators and m_S denotes the total mass of the grandstand. Structure is discretized with 5 beam finite elements, has 6 nodes and 27 DOFs.

C.2 Cantilever grandstand

Examples 3.2, 3.5, 4.4, 4.7, 5.2, 5.4 and 6.2. This system is made of reinforced concrete and has total mass 18.2 t, possesses 72 positions for spectators of 0.5 m spacing in the row, Rayleigh damping with $\zeta_1 = 0.05$ and $\zeta_2 = 0.08$ is used for the first two vertical modes. See Fig. C.2 for geometry, cross-sections, spectator positions and the first two bending modes; Tab. C.1 contains the list of the first five vertical eigenfrequencies. Cantilever beams have rectangular cross-sections while simply supported cross-beams are L-shaped, *cf* Fig. C.2b. Points of interest are depicted in Fig. C.2c, maximal mass ratio $\gamma = 0.34$. Structure comprise 92 beam finite elements, 87 nodes and 504 DOFs.

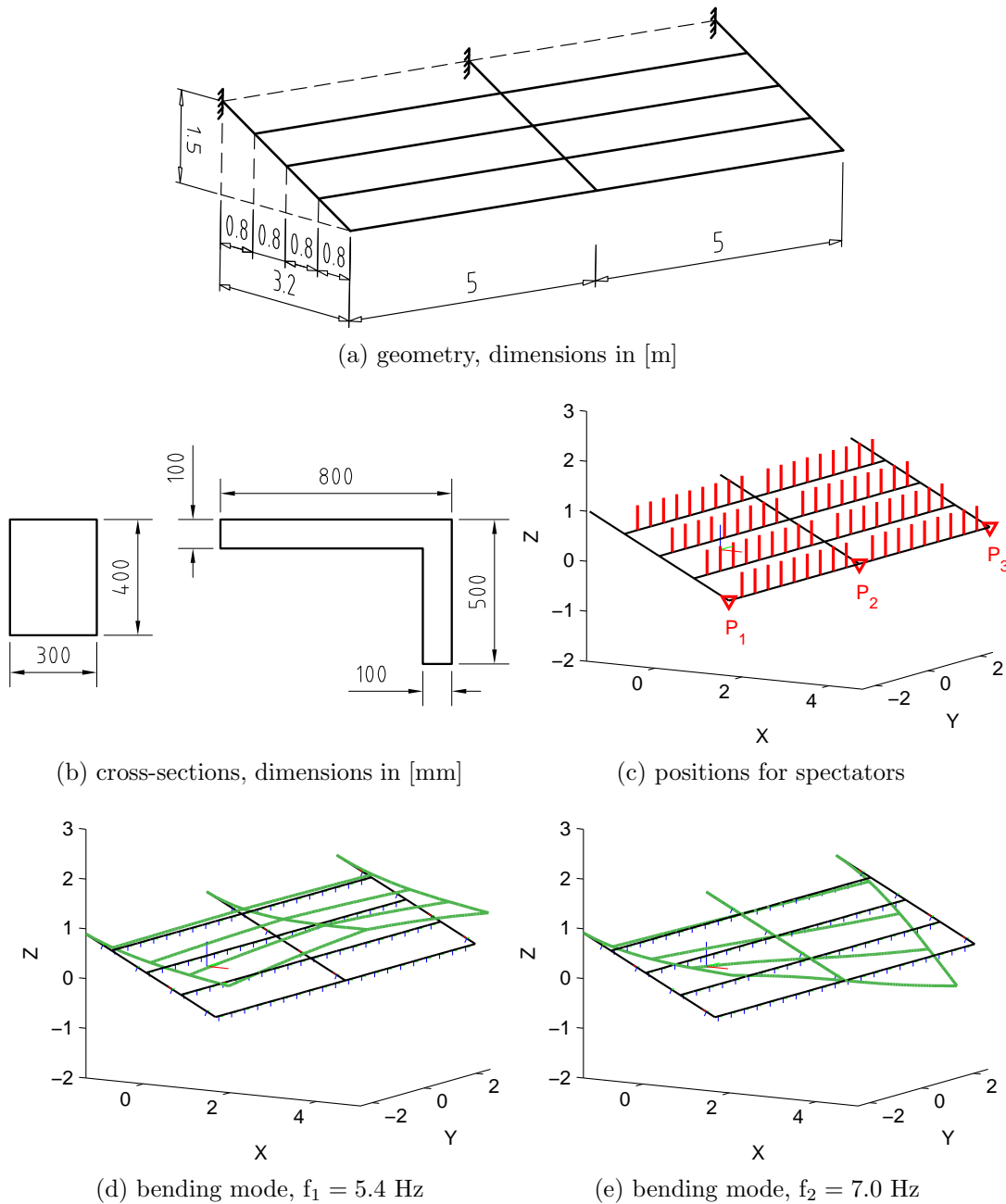


Figure C.2: Geometry, cross-sections, positions for spectators, labelled points of interest and the first two bending modes of cantilever grandstand

	f_1	f_2	f_3	f_4	f_5
f_i [Hz]	5.4	7.0	8.2	25.1	28.4

Table C.1: The first five eigenfrequencies of the cantilever grandstand corresponding to vertical bending modes [Hz]

C.3 Real grandstand

Examples 3.1, 3.2, 3.3, 3.4 and 4.5. This concluding structure represents a real grandstand depicted in Fig. C.3 with 630 positions for spectators of 0.5 m spacing in the row. For the points of interest and positions for spectators see Fig. C.4a and C.4b. The supporting structure is made of steel and consists of two outer and two inner bearing trusses all with curved upper edge, one lower edge horizontal and one sloping; geometrically are identical, but with different cross-sections of their bars. Structure is supported with eight columns and stiffen with a bracing. For cross sections of particular elements refer to Fig. C.3 and Tab. C.2. Grandstand deck girders are again L-shaped, simply supported and made of reinforced concrete, *cf* Fig. C.2b, but now with width 1,000 mm, height 400 mm and thickness 200 mm.

Dynamic properties of the structure are presented in Tab. C.3, where the first eight vertical eigenfrequencies are summarized, and in Fig. C.4c and C.4d, where two vertical bending modes are depicted. Rayleigh damping with $\zeta_1 = 0.01$ for the first and $\zeta_2 = 0.02$ for the sixth vertical mode is used. Total mass of the structure is 148.6 t, maximal mass ratio $\gamma = 0.37$, structure is discretized with 815 beam elements, 684 nodes and 4068 DOFs.

element of/ ID	outer bearing truss	inner bearing truss	bracing	columns
①	TR 245×6.3	TR 245×12.5	—	—
②	TR 168×5	TR 127×5	—	—
③	TR 89×3.6	TR 89×3.6	—	—
④	—	—	TR 127×5	—
⑤	—	—	TR 89×3.6	—
⑥	—	—	—	TR 245×6.3
⑦	—	—	—	TR 127×5

Table C.2: Table of cross-sections for the real grandstand, *cf* Fig. C.3; TR $A \times B$ represents a circular pipe with outer diameter A [mm] and wall thickness B [mm]

	f_1	f_2	f_3	f_4	f_5	f_6	f_7	f_8
f_i [Hz]	2.5	2.6	3.8	4.5	4.8	4.9	5.4	6.0

Table C.3: The first eigenfrequencies of the real grandstand corresponding to vertical bending modes [Hz]

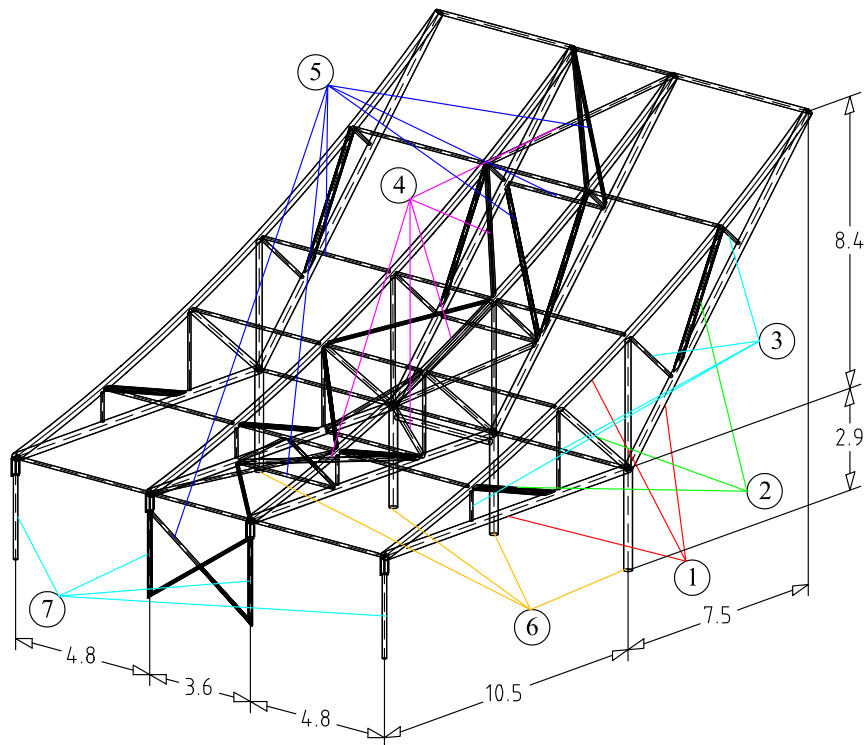


Figure C.3: Geometry of the real grandstand kindly provided by Ing. David Jermoljev from Excon company, identification of particular elements, dimensions in [m], for specification *cf* Tab. C.2; seating deck L-beams are not included contrary to Fig. C.4

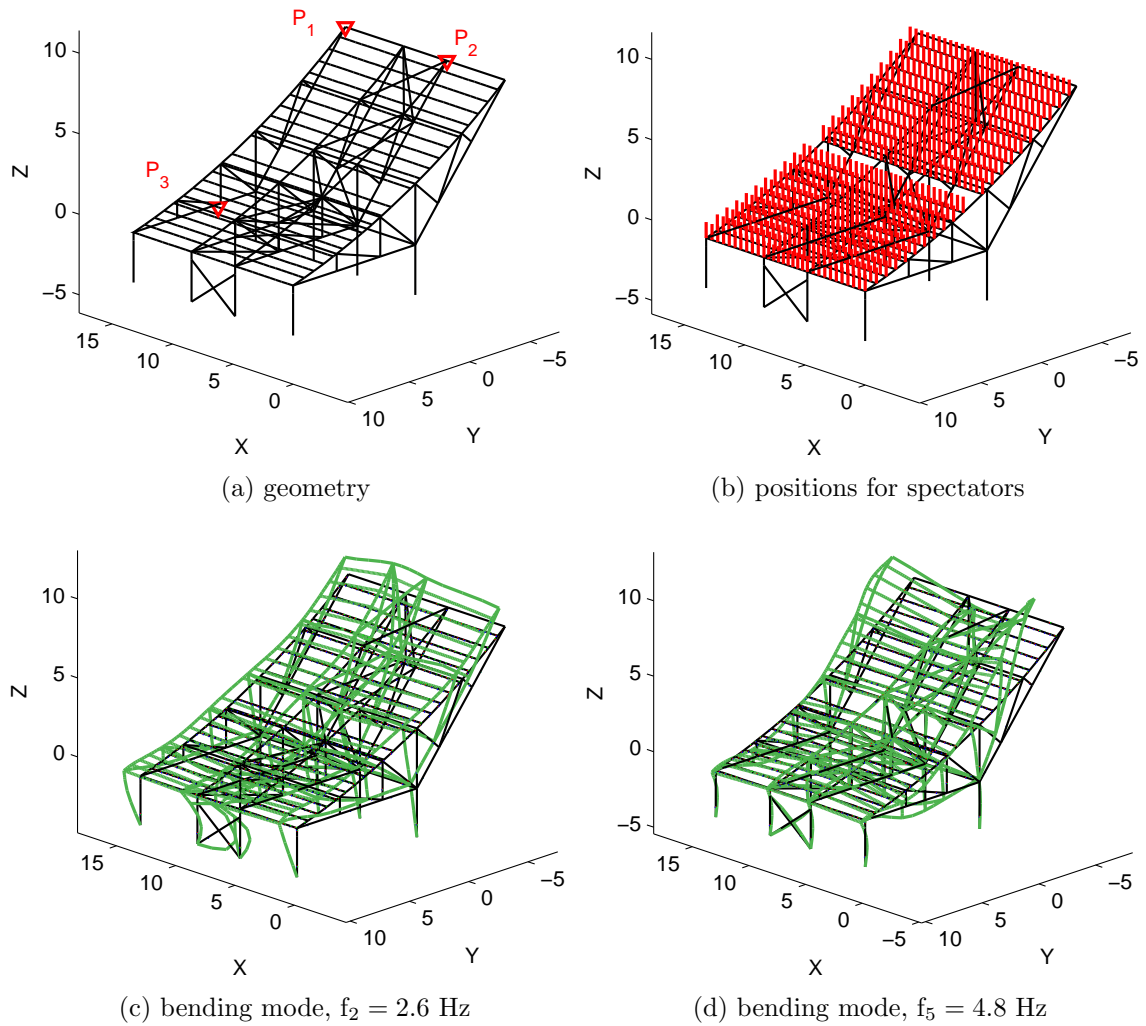


Figure C.4: Geometry, positions for spectators, labelled points of interest and the two bending modes of the real grandstand

Bibliography

- [1] J. Anděl. *Statistická analýza časových řad*. SNTL, 1976.
- [2] Z. Bai. Krylov subspace techniques for reduced-order modeling of large-scale dynamical systems. *Applied Numerical Mathematics*, 43:9–44, 2002.
- [3] Z. Bai and Y. Su. Soar: A second-order arnoldi method for the solution of the quadratic eigenvalue problem. *SIAM J. Matrix Anal. Appl.*, 26(3):640–659, 2005.
- [4] K.J. Bathe. *Finite Element Procedures*. Prentice-Hall Inc., 1996.
- [5] Z. Bittnar and J. Šejnoha. *Numerical Methods in Structural Mechanics*. Amer Society of Civil Engineers, 1996.
- [6] V.V. Bolotin. *Statistical Methods in Structural Mechanics*. Holden-Day, Inc., 1969.
- [7] V.V. Bolotin. *Random vibrations of elastic systems*. Martinus Nijhoff Publishers, 1969.
- [8] P.J. Brockwell, R.A. Davis, and Y. Yang. Continuous-time gaussian autoregression. *Statistica Sinica*, 17:63–80, 2007.
- [9] G.G. Browning. *Human Perception of Vibrations due to Synchronized Crowd Loading in Grandstands*. PhD thesis, University of Bath, 2011.
- [10] P.G. Ciarlet. *The Finite Element Method for Elliptic Problems*. Siam, 2002.
- [11] R.R. Coermann. The mechanical impedance of the human body in sitting and standing position at low frequencies. *Human Factors*, (4):227–253, 1962.
- [12] J.W. Dougill, J.R. Wright, J.G. Parkhouse, and R.E. Harrison. Human structure interaction during rhythmic bobbing. *The Structural Engineer*, 22:32–39, 2006.
- [13] V. Dupač and M. Hušková. *Pravděpodobnost a matematická statistika*. Karolinum, 2009.
- [14] B.R. Ellis and T. Ji. Floor vibration induced by dance-type loads: Verification. *The Structural Engineer*, 72(3):45–50, 1994.
- [15] B.R. Ellis, T. Ji, and J.D. Littler. The response of grandstands to dynamic crowd loads. *Proceedings of the Institution of Civil Engineers Structures and Buildings*, 140: 355–365, 2000.

- [16] CH. Farhat. Model reduction, 2011. URL http://www.stanford.edu/group/frg/course_work/CME345.html.
- [17] C. Fischer. *Numerické řešení úloh stochastické mechaniky*. PhD thesis, Charles University in Prague, 2002.
- [18] M. Grigoriu. *Applied Non-Gaussian Processes: Examples, Theory, Simulation, Linear Random Vibration, and MATLAB Solutions*. Prentice Hall, 1995.
- [19] M. Grigoriu. *Stochastic Calculus: Applications in Science and Engineering*. Birkhäuser, 2002.
- [20] V. Gusella and A.L. Materazzi. Non-gaussian along-wind response analysis in time and frequency domains. *Engineering Structures*, (22):49–57, 2000.
- [21] M. Hermanussen, H. Danker-Hopfe, and G.W. Weber. Body weight and the shape of the natural distribution of weight, in very large samples of german, austrian and norwegian conscripts. *International Journal of Obesity*, 25:1550–1553, 2001.
- [22] ISO 10137:2007. Bases for design of structures-serviceability of buildings and walkways against vibration, 2007.
- [23] ISO 2631-1:1997. Mechanical vibration and shock – evaluation of human exposure to whole body vibration – part 1: General requirements, 1997.
- [24] ISO 2631-2:1997. Mechanical vibration and shock – evaluation of human exposure to whole body vibration – part 2: Vibration in buildings (1 hz to 80 hz), 1997.
- [25] IStructE. Dynamic performance requirements for permanent grandstands: Recommendations for management design and assessment, 2008.
- [26] H. Jee, I. Lee, and S. Park. Analysis and comparison of step-by-step numerical integration methods. In *Twelfth KKNN Seminar/Workshop on Civil Engineering KAIST*, pages 120–126.
- [27] C.A. Jones, P. Reynolds, and A. Pavic. Vibration serviceability of stadia structures subjected to dynamic crowd loads: A literature review. *Journal of Sound and Vibration*, (330):1531–1566, 2011.
- [28] M. Kasperski. Actual problems with stand structures due to spectator induced vibrations. In *EURODYN 96*, pages 455–461.
- [29] H.U. Köylüoğlu, S.R.K. Nielsen, and A.Ş. Çakmak. Perturbation solutions for random linear structural systems subject to random excitation using stochastic differential equations. In *Proceedings of "Dynamics of Structures" : a workshop on dynamic loads and response of structures and soil dynamics, September 14-15, 1994, Aalborg University, Denmark*.
- [30] L.M. Lacoma and I. Romero. Error estimation for the hht method in non-linear solid dynamics. *Computers and Structures*, 85:158–169, 2007.

- [31] J.M. Mendel. Tutorial on higher-order statistics (spectra) in signal processing and system theory: Theoretical results and some applications. *IEEE*, 79(3):278–305, 1991.
- [32] N. Nawayseh and M.J. Griffin. A model of the vertical apparent mass and the for-and-aft cross-axis apparent mass of the human body during vertical whole-body vibration. *Journal of Sound and Vibration*, 319:719–730, 2008.
- [33] NBC 2005. User’s guide-nbc 2005: Structural commentaries, 2005.
- [34] S. Nhleko. *Human-induced Lateral Excitation of Public Assembly structures*. PhD thesis, University of Oxford, 2011.
- [35] S. Nhleko, A. Zingoni, and P. Moyo. A variable mass model for describing load impulses due to periodic jumping. *Engineering Structures*, 30:1760–1769, 2008.
- [36] S. Nhleko, M.S. Williams, A. Blakeborough, and J. Stebbins. Horizontal dynamic forces generated by swaying and jumping. *Journal of Sound and Vibration*, 332:2856–2871, 2013.
- [37] J.G. Parkhouse and D.J. Ewins. Vertical dynamic loading produced by people moving to beat. In *ISMA 2004*, pages 821–835.
- [38] A. Pavic, C.H. Yu, J. Brownjohn, and P. Reynolds. Verification of the existence of human-induced horizontal forces due to vertical jumping. In *IMAC-XX: Conference & Exposition on Structural Dynamics*, pages 120–126.
- [39] Z. Prášková. *Základy náhodných procesů II*. Karolinum, 2007.
- [40] V. Racic and A. Pavic. Stochastic approach to modelling of near-periodic jumping loads. *Mechanical Systems and Signal Processing*, 8:3037–3059, 2009.
- [41] V. Racic and A. Pavic. Mathematical model to generate near-periodic human jumping force signals. *Mechanical Systems and Signal Processing*, 24:138–152, 2010.
- [42] T.S. Rao and M.M. Gabr. *An Introduction to Bispectra Analysis and Bilinear Time Series Models, Lecture Notes in Statistics*. Springer-Verlag, 1984.
- [43] M. Rathinam and L.R. Petzold. A new look at proper orthogonal decomposition. *SIAM Journal of Numerical Analysis*, 41:1893–1925, 2003.
- [44] K. Rektorys. *Variational Methods in Mathematics, Science and Engineering*. Springer, 2001.
- [45] O. Rokoš and J. Máca. The response of grandstands driven by filtered gaussian white noise processes. *Advances in Engineering Software*, 72(0):85 – 94, 2014. Special Issue dedicated to Professor Zdeněk Bittnar on the occasion of his Seventieth Birthday: Part 2.
- [46] S. Rützel, B. Hinz, and H.P. Wolfel. Modal description — a better way of characterizing human vibration behavior. *Journal of Sound and Vibration*, 298:810–823, 2006.

- [47] R. Sachse, A. Pavic, and P. Reynolds. Human-structure dynamic interaction in civil engineering dynamics: A literature review. *The Shock and Vibration Digest*, 35:3–18, 2003.
- [48] J. Seidler. *Vybrané kapitoly ze stochastické analýsy*. Matfyzpress, 2011.
- [49] Ch. Seung-Bok and H. Young-Min. Vibration control of electrorheological seat suspension with human-body model using sliding mode control. *Journal of Sound and Vibration*, 303:391–404, 2006.
- [50] A.N. Shiryaev. *Probability*. Springer, 1995.
- [51] J.H. Sim. *Human structure interaction in cantilever grandstands*. PhD thesis, University of Oxford, 2006.
- [52] T.T. Soong. *Random Differential Equations in Science and Engineering*. Academic Press, 1973.
- [53] T.T. Soong and M. Grigoriu. *Random Vibration of Mechanical and Structural Systems*. Prentice Hall, New Jersey, 1993.
- [54] A. Swami, J.M. Mendel, and C.L. Nikias. *Higher-Order Spectral Analysis Toolbox For Use With MATLAB*. User’s Guide, 1998.
- [55] C. Tuan. Symphatetic vibration due to co-ordinated crowd jumping. *Journal of Sound and Vibration*, 269:1083–1098, 2004.
- [56] L. Wei and M.J. Griffin. Mathematical models for the apparent mass of the seated human body exposed to vertical vibrations. *Journal of Sound and Vibration*, 212: 855–874, 1998.
- [57] E.W. Weisstein. Kronecker sum, 2013. URL <http://mathworld.wolfram.com/KroneckerSum.html>.
- [58] H. Ya and M.J. Griffin. Nonlinear dual-axis biodynamic response of the semi-supine human body during longitudinal horizontal whole-body vibration. *Journal of Sound and Vibration*, 312:273–295, 2008.
- [59] O.C. Zienkiewicz and R.L. Taylor. *The Finite Element Method Volume 1: The Basis*. McGraw-Hill, 2000.
- [60] O.C. Zienkiewicz and R.L. Taylor. *The Finite Element Method Volume 2: Solid Mechanics*. McGraw-Hill, 2000.

Index

- Actuator, 7
- Apparent mass, 16
- Approximation
 - Gaussian, 10, 29, 30, 38, 62
 - Padé, 21
 - translation, 56, 58, 62
- Conditional analysis, 72, 78
- Contact time, 6, 81
- Decomposition
 - balanced proper orthogonal, 21
 - Karhunen-Loève, 21, 61
 - proper orthogonal, 21, 33
 - singular value, 20
- Dirac delta distribution, 24
- Distribution
 - Erlang, 59
 - normal, 62
- Equation
 - Lyapunov, 31, 33, 48, 71, 76–78
 - stochastic differential, 10, 13, 30, 55, 69, 71, 75, 77, 81, 82, 88
 - Sylvester, 33, 69, 71
- Factor
 - coordination, 7
 - crest, 5
 - dynamic load, 7
 - generated load, 7
 - impact, 6
 - sensitivity, 65, 66, 69, 76
- Finite element method, 1, 9, 10, 16, 19
- Formula
 - Itô's, 31, 45, 55, 59, 69, 75, 77, 87
 - Rice, 33, 56, 86
- Frequency response function, 24, 25, 32, 37, 60
- Frequency weight, 5
- Green function, 30
- Hadamard product, 25, 46
- Hermite polynomial, 19, 52, 53, 57, 62
- Hermitian transpose, 32
- Integration method
 - Central difference, 18
 - Hilber-Hughes-Taylor, 18
 - Newmark, 18, 42, 90
- Kronecker sum, 78
- Krylov subspace, 20
- Loading scenario, 7, 23, 43
- Maximum transient vibration value, 5
- Mechanical impedance, 16
- Method
 - Adomian, 65
 - decomposition, 77
 - iteration, 78
 - least squares, 35
 - nonlinear least squares, 38
 - perturbation, 65, 68, 77
 - state augmentation, 31
 - Taylor series, 11, 65, 68, 74, 75, 77–79, 82
- Modal
 - superposition, 20
 - synthesis, 21, 42, 49, 69
- Moving average, 5
- Noise
 - coloured
 - Gaussian, 29, 36, 62, 81
 - non-Gaussian, 35, 50
 - white

- Gaussian, 30, 31, 47, 71, 76, 78
- Poisson, 11, 50, 58, 59, 62, 63
- Norm
 - L^2 , 21, 38, 67, 68, 78
 - Frobenius, 56, 70
- Parzen window, 34, 62
- Periodogram, 32, 62
 - bi-, 61
- Process
 - autoregression, 10, 30, 33, 37–39, 44, 50, 54, 55, 58, 62, 65, 68, 75
 - Brownian motion, 31
 - Gaussian, 33, 36, 38, 50, 55, 57, 86
 - local martingale, 87
 - martingale, 87
 - non-Gaussian, 29, 50, 61, 62, 81
 - Ornstein-Uhlenbeck, 31
 - Poisson, 58, 59, 61
 - semimartingale, 87
 - translation, 11, 29, 50, 51, 57, 58, 62, 82
- Projection
 - Galerkin, 20
 - Petrov-Galerkin, 20
- Quasimoments, 57
- Ratio
 - contact, 6, 7, 15
 - mass, 67, 68, 72, 78, 82, 91–93
- Rayleigh damping, 16
- Reduced-order model, 19, 21, 22, 32, 42, 47, 49, 56, 61, 62, 69, 81
- Second order Arnoldi Algorithm, 21
- Series
 - Fourier, 1, 6, 24, 30, 61, 62, 81
 - Gram-Charlier, 56, 58, 62
 - Taylor, 65
 - time, 14, 15, 61
- Simulated annealing, 38
- Snapshots, 21
- Spectra
 - bi-, 60, 61, 82
 - poly-, 11, 60, 63
- Spectral
 - density, 15, 32, 34, 35, 37–39, 50, 54, 61, 82, 86
 - distribution function, 38, 86
 - moments, 32
- Subspace
 - Invariant, 21
 - Krylov, 22, 33
- Theorem
 - Central limit, 29, 36, 81
 - Isserli's, 53
 - Price, 52
 - Rosenblatt, 29, 36, 81
- Third order cumulant, 61
- Transform
 - Fourier, 24, 30, 61
 - Laplace, 21
- Tuned mass damper, 9
- Upcrossing rate, 26, 29, 33, 50, 56–58, 86
- Vibration dose value, 5